

**GAMMA SCAN MEASUREMENTS
AT
ZION STATION UNIT 2
FOLLOWING CYCLE 1**

**EPRI NP-509
(Research Project 130)**

Final Report

✓
October 1977

Prepared by

**Nuclear Energy Systems Division
GENERAL ELECTRIC COMPANY
175 Curtner Avenue
San Jose, California 95125**

PRINCIPAL INVESTIGATORS

**G. R. Parkos
G. F. Valby**

Prepared for

**Electric Power Research Institute
3412 Hillview Avenue
Palo Alto, California 94304**

**EPRI Project Manager
Robert N. Whitesel**

DISTRIBUTION OF THIS DOCUMENT IS UNLIMITED

DISCLAIMER

This report was prepared as an account of work sponsored by an agency of the United States Government. Neither the United States Government nor any agency thereof, nor any of their employees, makes any warranty, express or implied, or assumes any legal liability or responsibility for the accuracy, completeness, or usefulness of any information, apparatus, product, or process disclosed, or represents that its use would not infringe privately owned rights. Reference herein to any specific commercial product, process, or service by trade name, trademark, manufacturer, or otherwise does not necessarily constitute or imply its endorsement, recommendation, or favoring by the United States Government or any agency thereof. The views and opinions of authors expressed herein do not necessarily state or reflect those of the United States Government or any agency thereof.

DISCLAIMER

Portions of this document may be illegible in electronic image products. Images are produced from the best available original document.

LEGAL NOTICE

This report was prepared by General Electric (GE), as an account of work sponsored by the Electric Power Research Institute, Inc. (EPRI), and in conjunction with Commonwealth Edison Company (CECO). Neither EPRI, members of EPRI, CECO, GE, nor any person acting on behalf of either: (a) makes any warranty or representation, express or implied, with respect to the accuracy, completeness, or usefulness of the information contained in this report, or that the use of any information, apparatus, method, or process disclosed in this report may not infringe privately owned rights; or (b) assumes any liabilities with respect to the use of, or for damages resulting from the use of, any information, apparatus, method, or process disclosed in this report.

FOREWORD

This report is the second in a series of three compilations of reactor power distribution data coming from measurement campaigns at operating power reactors. The purpose of the project is to provide reference quality power distribution information for use in the qualification of reactor core analysis methods.

The measurements described in this report were performed at the Zion Unit 2 PWR, owned and operated by Commonwealth Edison Company. Similar measurements (EPRI Report NP-214) were performed in January 1976 at the Quad Cities Unit 1 BWR, another Commonwealth Edison plant. The final report in the series will document measurements made at the Hatch Unit 1 BWR, owned and operated by Georgia Power Company.

This work is part of the EPRI Reactor Core Performance program. The objective of this program is to provide for the development and application of computational capabilities used for assessing nuclear reactor core performance characteristics. One particular goal is concerned with the neutronic and thermal-hydraulic analysis required for effective operational evaluations. The results of this project will provide part of the data base against which the various reactor core simulator codes can be qualified.

*Robert N. Whitesel
EPRI Project Manager*

ACKNOWLEDGMENTS

The success of this project is due to the efforts of the following General Electric staff members:

<i>L. M. Shiraishi</i>	<i>R. E. Gest</i>
<i>G. W. Tunnell</i>	<i>O. Raza</i>
<i>A. L. Myrabo</i>	<i>F. K. Porter</i>
<i>B. F. Rider</i>	<i>P. G. Aline</i>
<i>C. P. Ruiz</i>	<i>J. E. Wood</i>
<i>C. H. Ballard</i>	<i>W. H. Reas</i>
<i>L. W. Hengf</i>	

It is with pleasure that we acknowledge the warm cooperative support of the Commonwealth Edison Company staffs at Zion Station and Chicago. In particular we thank:

<i>J. S. Bitel</i>
<i>J. Baker</i>
<i>V. Mathews</i>
<i>D. Walden</i>
<i>J. LaFontaine</i>
<i>W. M. Kiefer</i>
<i>A. Veras</i>
<i>W. F. Naughton</i>
<i>W. J. Dean</i>
<i>C. Grier</i>

The support and encouragement of EPRI staff members R. N. Whitesel and B. Zolotar is appreciated.

TABLE OF CONTENTS

	Page
1. INTRODUCTION AND SUMMARY.....	1-1
2. MEASUREMENT SPECIFICATION.....	2-1
2.1 Program Objectives	2-1
2.2 Detailed Assembly Selections	2-1
2.3 Measurement Locations.....	2-1
2.4 System Performance	2-6
2.5 Special Measurements	2-6
3. MEASUREMENT TECHNIQUE.....	3-1
3.1 Detection System.....	3-1
3.2 Hardware System	3-4
3.3 Data Acquisition.....	3-10
3.4 Data Reduction	3-10
4. ACCURACY.....	4-1
4.1 Measurement Uncertainty.....	4-1
4.2 Attenuation Coefficient Measurements.....	4-1
4.3 Method Biases and Limitations.....	4-1
4.4 Summary of Limitations	4-2
5. RESULTS	5-1
5.1 Nodal Measurements.....	5-1
5.2 Averaged and Integrated Measurements	5-1
5.3 Depression in the Region of a Grid Strap.....	5-1
6. UTILIZATION OF THE DATA FOR POWER DISTRIBUTION BENCHMARK.....	6-1
7. CONCLUSIONS.....	7-1

APPENDICES

A. PLANAR MAPS OF 25 ASSEMBLIES MEASURED DEFINING THE La-140 DISTRIBUTION IN ONE OCTANT OF THE CORE (13 pages)	A-1
B. PLANAR DISPLAYS OF THE OTHER 12 ASSEMBLIES MEASURED (13 pages)	B-1
C. AXIAL PLOTS OF THE La-140 INTENSITY FOR THE 37 ASSEMBLIES MEASURED (39 pages).....	C-1
D. DATA LISTINGS OF THE La-140 INTENSITIES FOR THE 37 ASSEMBLIES MEASURED (11 pages).....	D-1

LIST OF ILLUSTRATIONS

Figure	Title	Page
2-1	Assemblies Selected for La-140 Gamma Scan at Zion 2 Following Cycle 1.....	2-4
2-2	Fuel Loading Pattern for Zion 2, Cycle 1 (Octant Symmetric).....	2-5
3-1	Exploded View of NaI(Tl) Detector Assembly.....	3-2
3-2	NaI Detection System.....	3-3
3-3	Canal Hardware.....	3-5
3-4	Collimator.....	3-7
3-5	Front Snout of Collimator.....	3-9
3-6	Typical Gamma Ray Energy Spectrum.....	3-11
4-1	Percent Count Rate Contribution from Each Rod, Equal Source Strength for All Fuel Rods (Water Holes in 21 Locations).....	4-3
5-1	Radial La-140 Distribution (Assembly Average) Edge Assembly Correction Applied	5-2
5-2	Core Average Axial La-140 Distribution	5-3
5-3	Radial La-140 Distribution (Assembly Average) Edge Assembly Correction Applied	5-4
5-4	Radial La-140 Distribution (Assembly Average) No Edge Assembly Correction.....	5-5
5-5	Radial La-140 Distribution (Assembly Average) No Edge Assembly Correction.....	5-6
5-6	Depression in La-140 Intensity Near Grid Strap	5-7
6-1	Ratio of La-140 Atom Density to Ba-140 Atom Density after Shutdown, Following Long Irradiation.....	6-1
6-2	Flow Chart of Ba-140 Calculation.....	6-2

1. INTRODUCTION AND SUMMARY

An extensive gamma scan measurement of irradiated fuel was performed following Cycle 1 at Zion Station Unit 2 as part of EPRI Project RP-130, "Nuclear Reactor Core Benchmark Data." The objective of these measurements was to provide power distribution benchmark data for verification of those methods used for predictive calculations and in-core monitoring of core power distributions. Combination of the benchmark data reported here and the design details and operating history of the core allows evaluation of the accuracy of power distribution calculations. These measurements constitute a detailed benchmark for power distribution in a PWR, addressing the questions of gross core shape, detailed axial shape, core symmetry, and power sharing among assemblies of differing enrichments. Successful completion of a program of this magnitude is a result of excellent cooperation between Commonwealth Edison, EPRI, and General Electric. EPRI-sponsored programs such as this will provide the users and manufacturers of nuclear supply systems with valuable benchmark data to improve performance and availability, and increase margin, by reducing uncertainties in the design and operation of plants.

Relative La-140 activity, reflective of recent power history, was measured for 37 fuel assemblies at 12 to 24 elevations. A sodium iodide gamma ray detector, mounted inside a 3000-lb moveable collimator, was used to sequentially measure the relative intensity of the 1596 keV La-140 gamma ray at each elevation on the fuel. A minicomputer-based data acquisition system controlled the sequencing and reduced the data. From consideration of the accuracy of the measured intensities, small inherent biases in the technique, and the process by which calculated power distributions can be converted to La-140 distributions, it is concluded that benchmarking of power distribution methods within 4% is reasonably achievable from the data resulting from this program.

2. MEASUREMENT SPECIFICATION

2.1 PROGRAM OBJECTIVES

The objectives of the gamma scan program reported here are specified in the contract under which the work was performed. Detailed selection of assemblies to be measured was made by Commonwealth Edison.

The following areas of investigation are included in RP-130 for the PWR phase of the work.

1. **Gross Core Power Shape** by measuring the relative La-140 distribution, at up to 12 elevations for assemblies comprising up to one octant of the core, plus one to seven assemblies in each of the remaining octants.
2. **Axial Power Shape** by gamma scanning up to 4 assemblies at no fewer than 24 elevations, to determine the effects of core location, control, enrichment, and exposure on axial shape.

2.2 DETAILED ASSEMBLY SELECTIONS

2.2.1 Gross Core Power Shape

Gross Core Power Shape was determined by measurement of the relative La-140 1596 keV gamma ray intensity of 37 selected assemblies. Measurements were made at 12 elevations for 30 assemblies and 24 elevations for the remaining 7 assemblies. The assemblies selected are shown in Figure 2-1. Figure 2-2 shows the fuel type loading pattern and burnable poison rod assembly locations during operation. Table 2-1 lists the assemblies in the order they were measured. Because of fuel shuffle constraints, it was necessary to measure some assemblies with rod cluster control or burnable poison rod assemblies in place. See Section 3.4.5 for further discussion.

2.2.1.1 Choice of Octant

Most of the measured assemblies (24) were chosen from one octant, which has a large number of instrumented assemblies (9). This region of the core coincided with that section removed for in-service inspection of lower core internals, affording some efficiency in the fuel shuffle. Assemblies at core locations G-1, E-1, and E-2 were returned to the core prior to the beginning of gamma scan measurements. The assembly at H-3 was not brought out of the containment during the fuel shuffle.

2.2.1.2 Choice of Assemblies from Other Octants

To test core symmetry, a set of four symmetric assemblies was chosen (at core locations L-5, L-11, E-11, and E-5). Ten more assemblies were chosen to gain additional core-wide power distribution information.

2.2.2 Axial Power Shape

Seven assemblies were scanned at 24 elevations to determine detailed axial power shape. Included were:

- a. the four symmetric assemblies specified in 2.2.1.2 above;
- b. an edge assembly (C50 at core location F-1);
- c. an assembly near the core center (A26 at core location H-6);
- d. a medium-enrichment assembly midway out from the center (B44 at core location G-12).

2.3 MEASUREMENT LOCATIONS

La-140 fission product intensity was determined at the core elevations specified in Table 2-2. Note that 4 of the 24 locations are slightly displaced (1 to 2 inches) from their even-mesh positions. This was done to avoid grid strap elevations within assemblies.

Table 2-1
ASSEMBLIES GAMMA SCANNED

	Assembly Identification	Core Location	Computer Assembly Identification	Number of Axial Locations	Internals Present at Time of Measurement
1	C04	G-2	304	12	—
2	B13	G-6	213	12	—
3	C02	D-2	302	12	RCC ^a
4	B21	D-3	221	12	20BP ^b
5	C06	R-5	306	12	—
6	C50	F-1	350	24	—
7	C63	C-2	363	12	—
8	B55	H-7	255	12	—
9	B44	G-12	244	24	—
10	B59	F-3	259	12	—
11	B18	N-6	218	12	—
12	C22	R-8	322	12	—
13	C43	K-1	343	12	—
14	B34	F-7	234	12	—
15	C46	B-13	346	12	—
16	B15	E-4	215	12	20BP
17	B48	H-5	248	12	16BP
18	C12	H-1	312	12	9BP
19	B41	L-10	241	12	—
20	B45	G-4	245	12	16BP
21	B03	F-5	203	12	16BP
22	A29	H-8	129	12	RCC
23	A42	G-3	142	12	16BP
24	A14	E-5	114	24	—
25	A59	E-11	159	24	—
26	A51	L-5	151	24	20BP
27	A50	L-11	150	24	8BP
28	A26	H-6	126	24	20BP
29	A29 ^c	H-8	129	12	—
30	A33	E-3	133	12	12BP
31	A16	F-2	116	12	—
32	A52	H-4	152	12	8BP
33	A03	G-7	103	12	8BP
34	A23	G-5	123	12	—
35	A01	F-4	101	12	20BP
36	A22	H-2	122	12	—
37	A31	K-12	131	12	—
38	A43	K-4	143	12	—

^a Control rod assembly

^b Burnable poison assembly (prefix is the number of burnable poison rods)

^c Repeat, without control rod (RCC) present

Table 2-2
MEASUREMENT LOCATIONS

Position Number	Inches Above Bottom of Active Fuel	24-Point Scan	12-Point Scan	Grid Strap Centers (Inches Above Bottom of Active Fuel)
				2.24
1 ^a	4	X		
2	9	X	X	
3	15	X		
4	21	X	X	
				26.44
5 ^a	29	X		
6	33	X	X	
7	39	X		
8	45	X	X	
9 ^a	50	X		
				52.63
10	57	X	X	
11	63	X		
12	69	X	X	
13	75	X		
				78.82
14	81	X	X	
15	87	X		
16	93	X	X	
17	99	X		
18 ^a	103	X	X	
				105.01
19	111	X		
20	117	X	X	
21	123	X		
22	129	X	X	
				131.20
23	135	X		
24	141	X	X	
				149.88

^a Moved from even mesh locations to avoid grid straps.

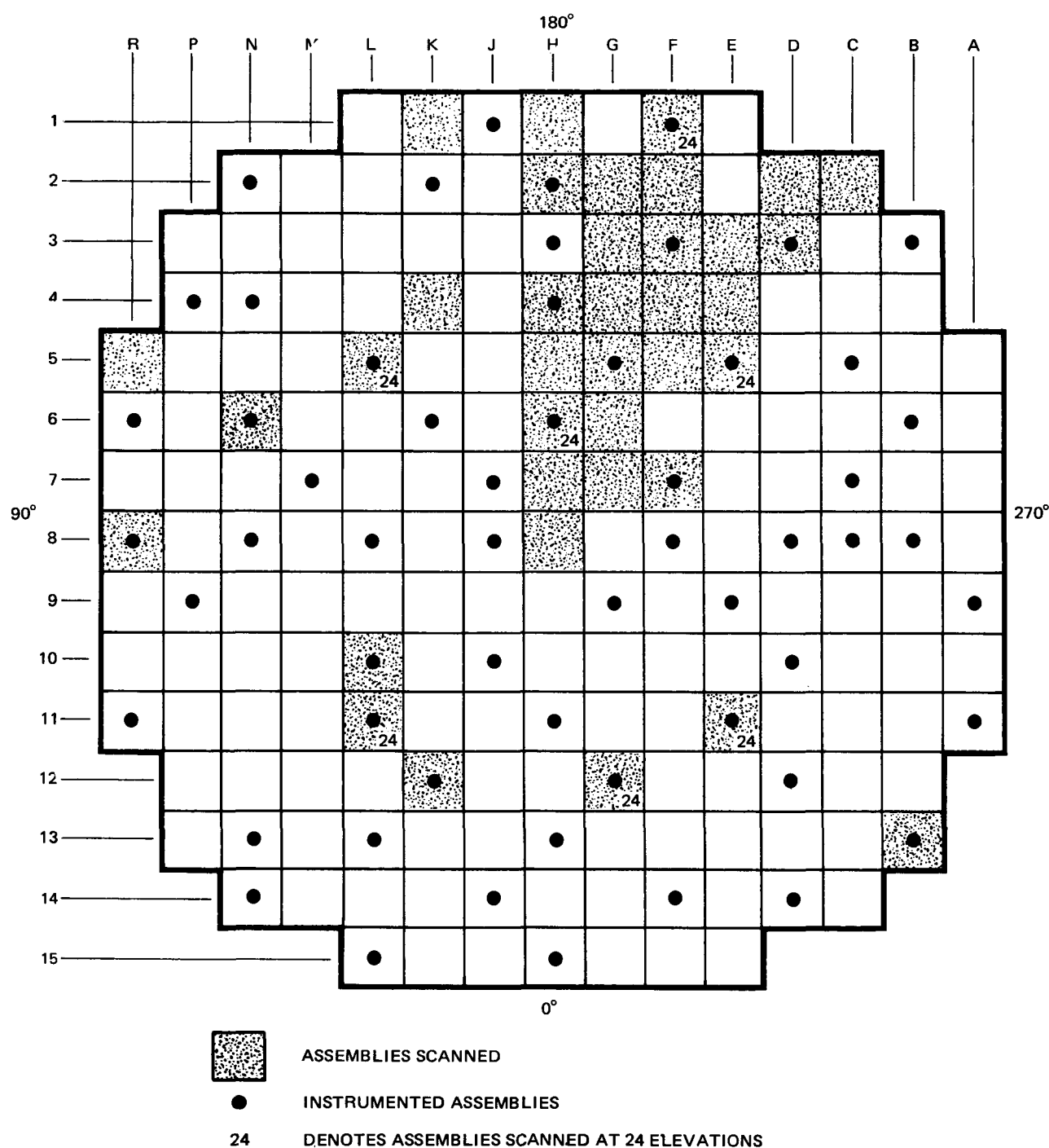


Figure 2-1. Assemblies Selected for La-140 Gamma Scan at Zion 2 Following Cycle 1

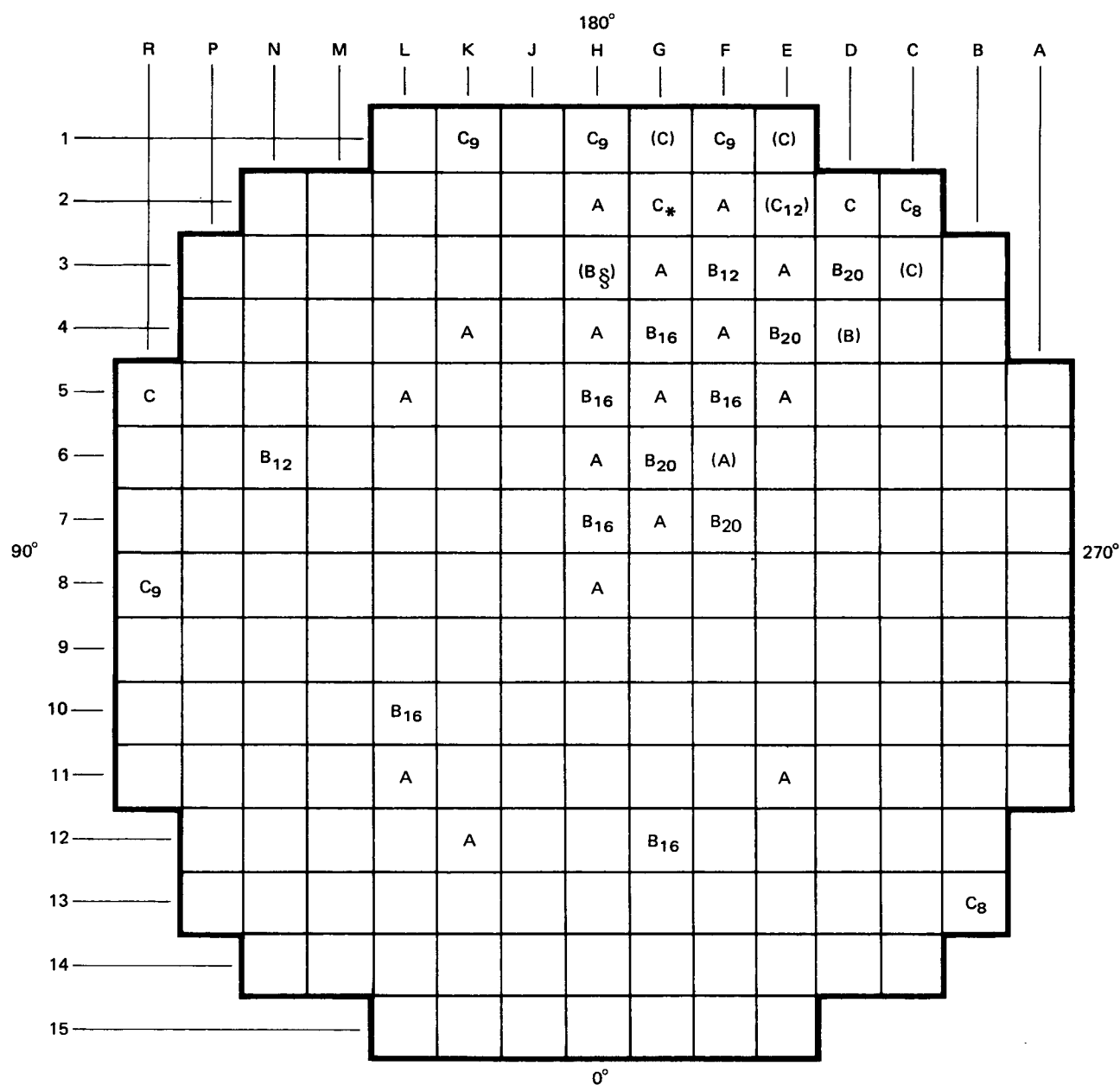


Figure 2-2. Fuel Loading Pattern for Zion 2, Cycle 1 (Octant Symmetric)

2.4 SYSTEM PERFORMANCE

Gamma scan system performance was monitored by periodically rescanning one corner of assembly A14, chosen as the reference standard. Reproducibility of these standard measurements was one of the key inputs to determining overall measurement uncertainty. In addition, measurements of the attenuation coefficient for lead were made to verify unbiased measurement of relative La-140 intensities.

2.5 SPECIAL MEASUREMENTS

One assembly (A29) was measured both with and without a control rod assembly in place, to allow correction for gamma ray attenuation due to the control rod assembly based on experimental data. In addition, the depression in the region of a grid strap was measured.

3. MEASUREMENT TECHNIQUE

3.1 DETECTION SYSTEM

3.1.1 General

The gamma ray detection system used was a thallium-activated sodium iodide [NaI(Tl)] crystal detector with associated electronics. This detector, with its high efficiency and count rate capability, was chosen to simplify the hardware for the stationary fuel/moving collimator configuration. The energy resolution of this detector was adequate for this application since only the energetically well isolated (1596 keV) gamma ray from La-140 was being measured.

3.1.2 NaI(Tl) Detector System

Figure 3-1 is an exploded view of the NaI(Tl) detector assembly. The crystal detector is a cylindrically shaped NaI(Tl) crystal of density 3.67. It is mounted to a 0.635 cm thick lucite disc in which two Monsanto MV-5253 light-emitting diodes (LED's) are embedded. Electrical leads to the LED's are routed through the detector base. The crystal and lucite disc are optically coupled to an RCA 8575 photomultiplier tube which is connected to a voltage divider network and tube base.

The electronic configuration is shown in Figure 3-2. The anode signal from the detector goes to a fast discriminator which is set to trigger on input pulses whose amplitudes are greater than a predetermined voltage level. The discriminator provides an external trigger to the linear gate. The dynode signal from the detector is amplified and differentiated in the fast side of the linear amplifier, then routed to the linear gate where the pulses of amplitude greater than the discriminator setting are selected. These pulses are then routed to the slow side of the linear amplifier where they are further shaped for presentation to a spectrum stabilizer and the analog-to-digital converter (ADC) of a 1024-channel multi-channel analyzer (MCA). The memory of the MCA is read out to the HP2100 computer after each accumulation period, and the data stored on magnetic tape.

The fast discriminator and linear gate eliminate the low energy component of the fission product spectrum (energy cutoff approximately 900 keV), leaving only the 1596 keV and higher energy gammas. Thus a much lower pulse rate is presented to the linear amplifier, reducing the pileup. This detection system can be used with detector count rates up to 250 kHz.

A pulse generator, which is triggered randomly, provides the drive pulse for the LED. The LED/pulser provides a standard energy peak by which the total system gain can be stabilized against changing conditions of count rate, temperature, or high voltage. It also provides a peak of known input count rate from which pile-up losses in the system can be determined.

Counting losses occur because of the need to operate the system at high rates to maximize fuel measurement throughput. The losses which occur in the linear amplifier, the ADC, and the memory of the MCA are a result of electronic dead times which prohibit the analysis of more than one event at a time. In the memory of the MCA, the losses are due to the fixed time required to fetch a particular channel from memory, increment it, then return the value to memory. The MCA live-time clock automatically compensates for this loss due to processing time.

Losses in the ADC arise from the timing circuitry necessary to detect (time-to-peak) and to digitize (digitizing time) the incoming pulse peak height. As with the memory processing time, these time losses are automatically accounted for by the MCA live-time clock. Additional "losses" can occur in the time-to-peak circuitry because of a spectral biasing toward higher energy pulses. If, during the time-to-peak period after the input discriminator is triggered, a second pulse appears at the ADC input, the larger pulse will be digitized and the smaller one will be "lost."

Losses in the linear amplifier are governed by the Poisson statistics; these occur if two or more pulses arrive during the amplifier resolving time. The amplifier integrates the charge in all of the pulses and produces a single output pulse of larger amplitude and width than any of the individual input pulses. These electronic losses are accounted for by comparing the integrated LED/pulser peak intensity in the gamma spectrum to the average rate of the pulse generator.

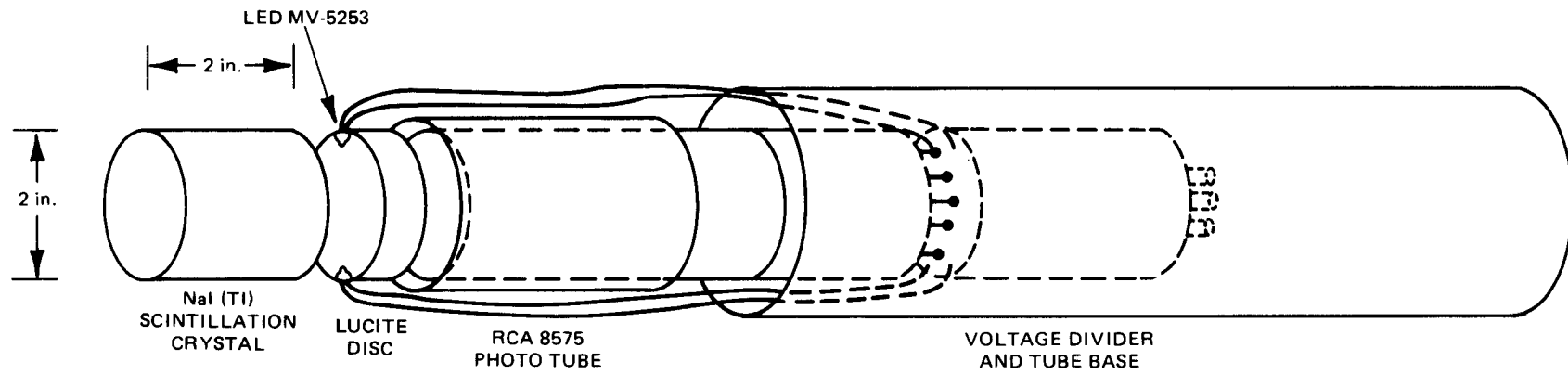
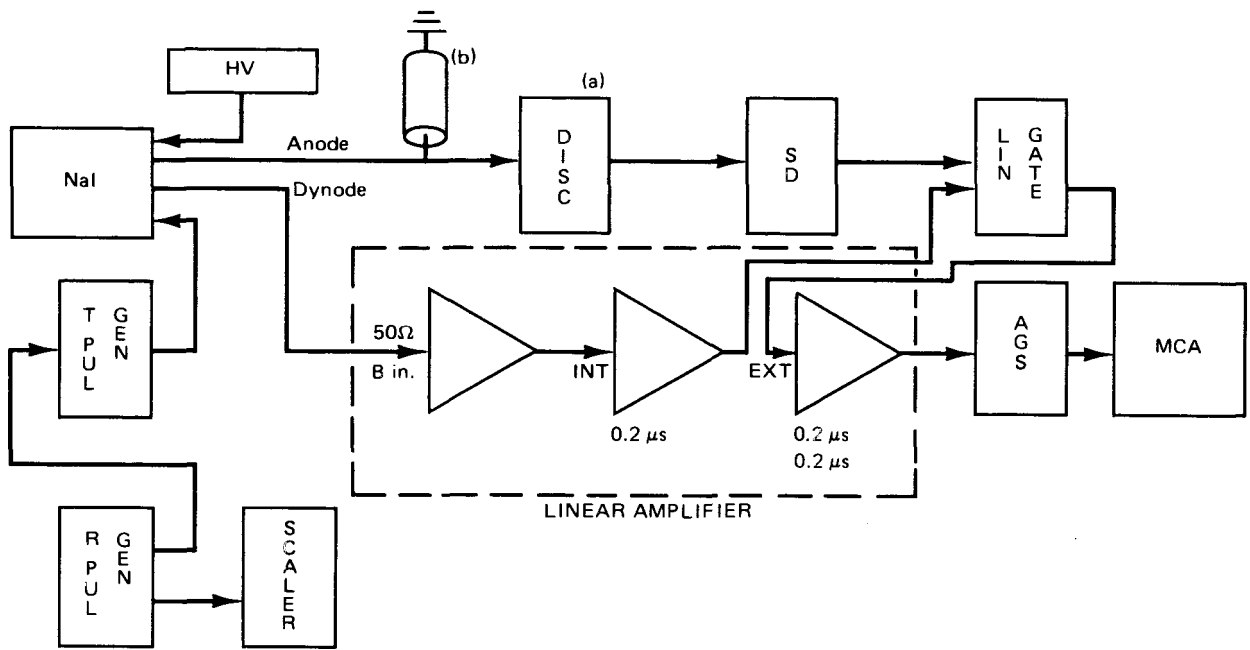


Figure 3-1. Exploded View of NaI(Tl) Detector Assembly



EQUIPMENT LIST

1. 5.08 cm X 5.08 cm NaI(Tl) DETECTOR ASSEMBLY, NUCLEAR ENTERPRISES, INC (NaI)
2. HIGH VOLTAGE POWER SUPPLY, AEC315, POWER DESIGNS, INC (HV)
3. TAIL PULSE GENERATOR, BH-1, BERKELEY NUCLEONICS CORPORATION. (T PUL GEN)
4. RANDOM PULSE GENERATOR, DB-2, BERKELEY NUCLEONICS CORPORATION. (R PUL GEN)
5. FAST DISCRIMINATOR, #4680, NUCLEAR ENTERPRISES, INC (DISC)
6. SCALER DRIVER, DS104/N, E.G.&G. (SD)
7. LINEAR GATE, TC304, TENNELEC, INC
8. LINEAR AMPLIFIER, TC220BLR, TENNELEC, INC
9. AUTOMATIC GAIN STABILIZER, M1720 CANBERRA INDUSTRIES. (AGS)
10. MULTI-CHANNEL ANALYZER, HP5401B, HEWLETT PACKARD. (MCA)
11. SCALER/PRINTER, MODEL 4660, KINETIC SYSTEMS, INC

NOTES

- a) DISCRIMINATOR LEVEL SET AT ~ 0.9 MeV
- b) CLIPPING LENGTH IS 122 cm

Figure 3-2. NaI Detection System

3.2 HARDWARE SYSTEM

The measurements were performed in the transfer canal with the fuel assemblies in a stationary vertical position. By use of a 2 ton hoist, the collimator was raised or lowered under computer control until the desired elevation of fuel was viewed by the collimator. Alignment was maintained by a guide frame. The fuel holder permitted rotation of the assembly about its axis to allow each of the four corners to be oriented toward the collimator. Corners rather than sides were oriented toward the collimator to reduce sensitivity to exact angular positioning. Figure 3-3 shows the general layout of this underwater hardware.

The sequence of operations was as follows: A fuel assembly was placed in the positioning fixture and oriented so that the desired corner pointed toward the collimator. The collimator was then positioned sequentially to each measurement elevation and a measurement made. The fuel assembly was then rotated 90 degrees and the process repeated until all four corners of the fuel assembly were measured.

3.2.1 Collimator

The collimator, shown in Figure 3-4, served the following principal functions: provided a shielded environment for the detector, provided a path for the gamma beam of interest to reach the detector, and defined the geometry of the gamma beam. The collimator was pressurized with N₂ to prevent any possible in-leakage of water.

At the fuel end of the collimator, the lead filter box was located about 10 inches away from the corner of the fuel assembly. This filter box allowed the total count rate to be adjusted with variable lead thickness, preferentially filtering out the lower energy gammas. Directly behind the filter box was the slit box, containing two tungsten alloy plates separated to form a 0.200 inch high by 12.62 inch wide beam-defining slit. (The fuel assembly has a diagonal width of about 11.7 inches.) The angular alignment of the slit was remotely adjustable to optimize collimation. Behind the beam-defining slit was a 6 inch thick lead shield, with a 1.5 inch high by 12.75 inch wide (nonlimiting) slit through the center. A tapered hole surrounded by high-density concrete led to aperture pieces of lead and tungsten alloy; directly behind the tungsten aperture piece was the NaI(Tl) detector. Lead and high-density concrete surround the NaI(Tl) crystal and photomultiplier tube to provide shielding from background radiation. A cadmium/copper cover was placed around the aluminum crystal housing to shield against x-rays.

During the system tests at the beginning of the program, it was found that the low energy scattered component of the spectrum was higher in relation to the La-140 peak than previously experienced. Therefore, additional lead shielding was placed near the front tungsten slits, as shown in Figure 3-5, to reduce the low energy scattered gamma ray background in the spectrum. Three lead bricks, 2 x 4 x 6 inches, were strapped to the top of the slit box, and 1/4 inch lead sheet was used to partially fill open regions inside the slit box. This field modification improved the ratio of La-140 to low energy background sufficiently to allow accurate data reduction using the methods discussed in Subsection 3.4.

3.2.2 Guide Frame

The collimator weighed approximately 3000 pounds and was suspended on a chain hoist so that it could be positioned at any point along the active fuel region. A guide frame ensured that the collimator was always properly positioned in the horizontal plane. This guide frame consisted of a pair of straight, vertical rails, and a carriage which travelled up and down on the rails. The carriage had a total of 10 wheels which forced it to accurately follow the vertical rails, and had bosses which allowed remote removal or attachment of the collimator.

3.2.3 Fuel Assembly Positioning Fixture

The fuel assembly positioning fixture, supplied by Nuclear Assurance Corp., was a free-standing inspection stand modified to fit in the transfer canal and to allow an unobstructed view of the diagonal of a fuel assembly for the full fuel length. The assembly was held in an open basket, whose position was constrained only at the upper end. The basket could be rotated from above with a 25 foot long tool. Angular positioning was obtained by visual alignment of marks on the basket and frame, at about a 15 inch radius from the center of rotation.

Although the fuel holder and collimator guide frame were aligned to the vertical during installation, it became evident during the program that the fuel was not held exactly vertical by the holder. The reason for the apparent change in alignment

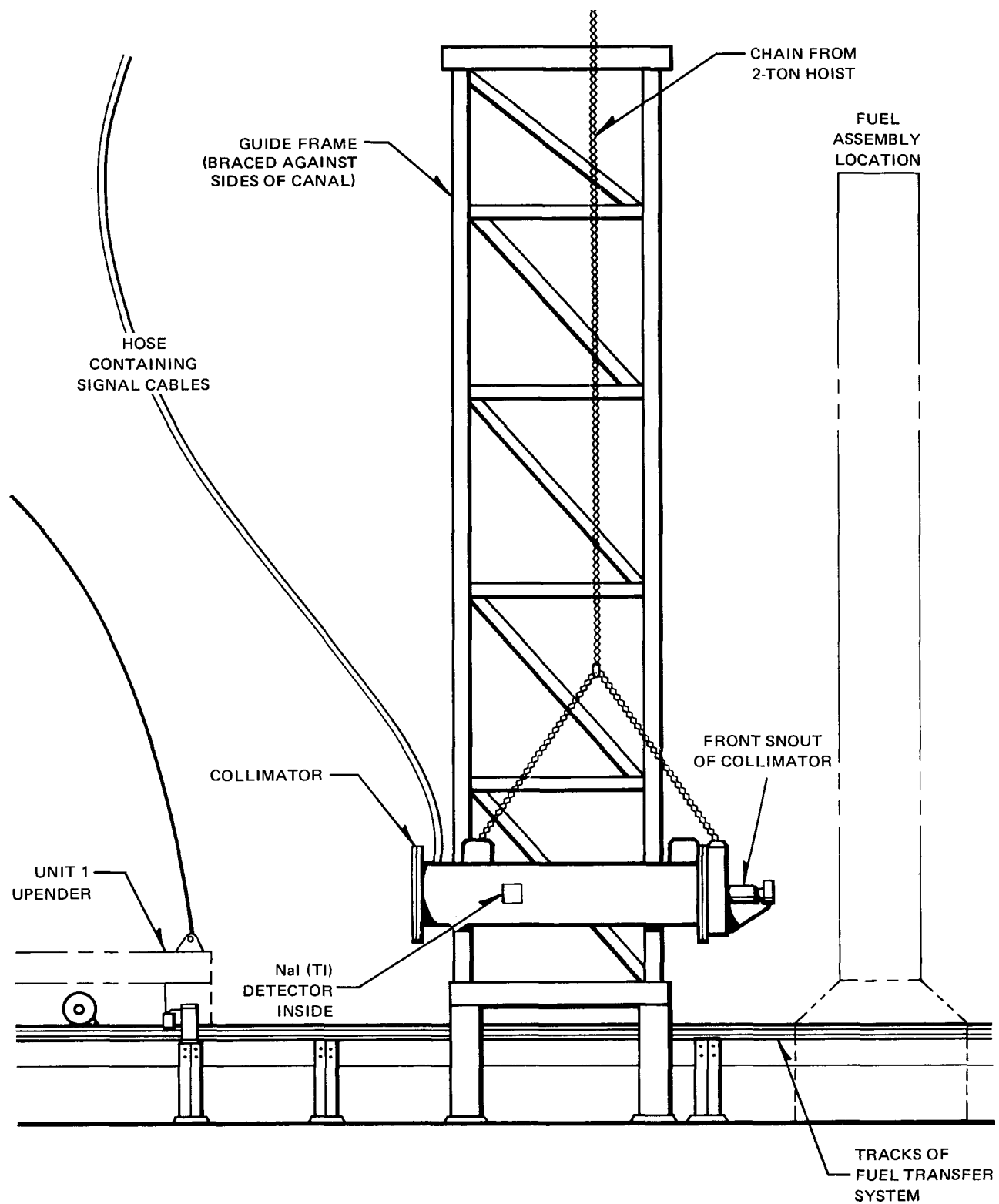
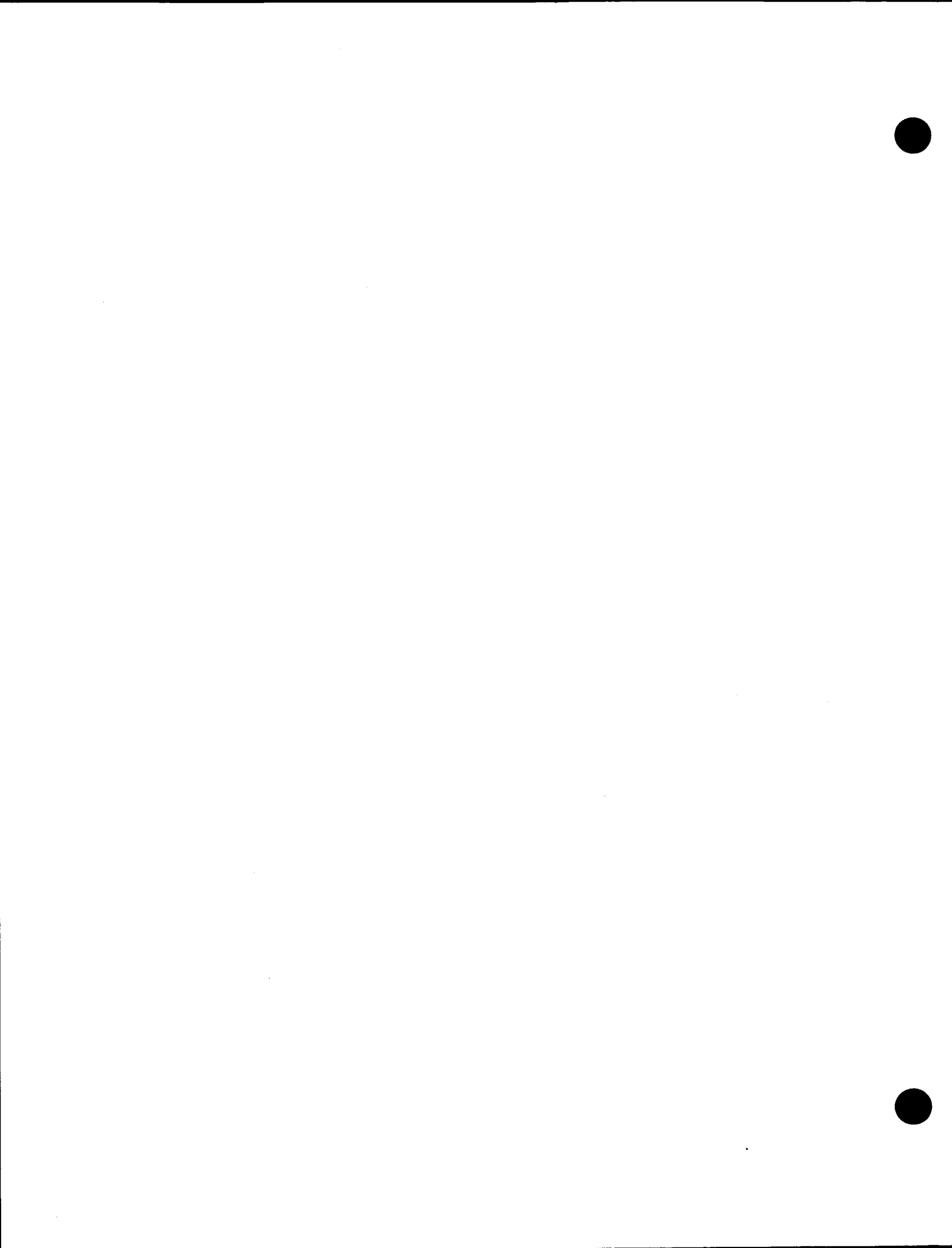
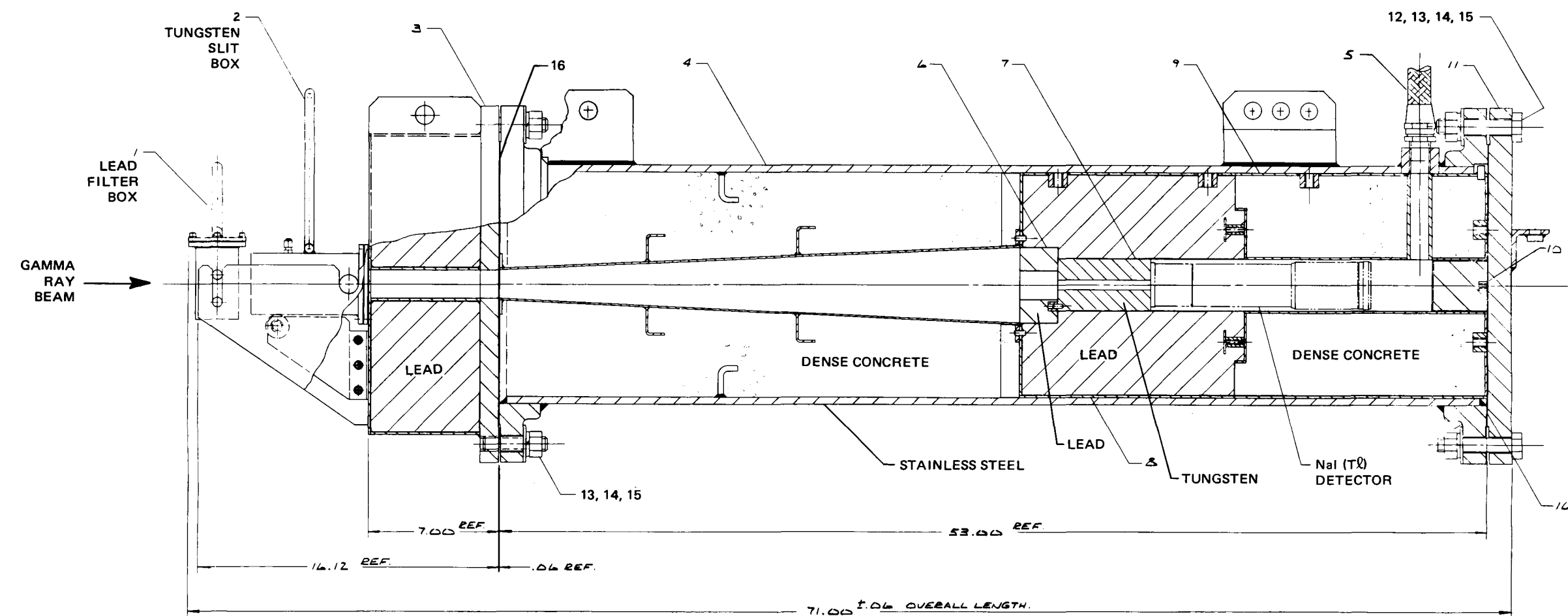


Figure 3-3. Canal Hardware





PT NO.	NAME
1	FILTER BOX
2	SLIT BOX
3	NOSE ASS'Y
4	COLLIMATOR PIPE
5	FLEX HOSE
6	SHIELD
7	PLUG
8	SHIELD

PT NO.	NAME
9	SHIELD
10	PLUG
11	BLIND FLANGE
12	BOLT
13	NUT
14	LOCK WASHER
15	PLAIN WASHER
16	GASKET

Figure 3-4. Collimator



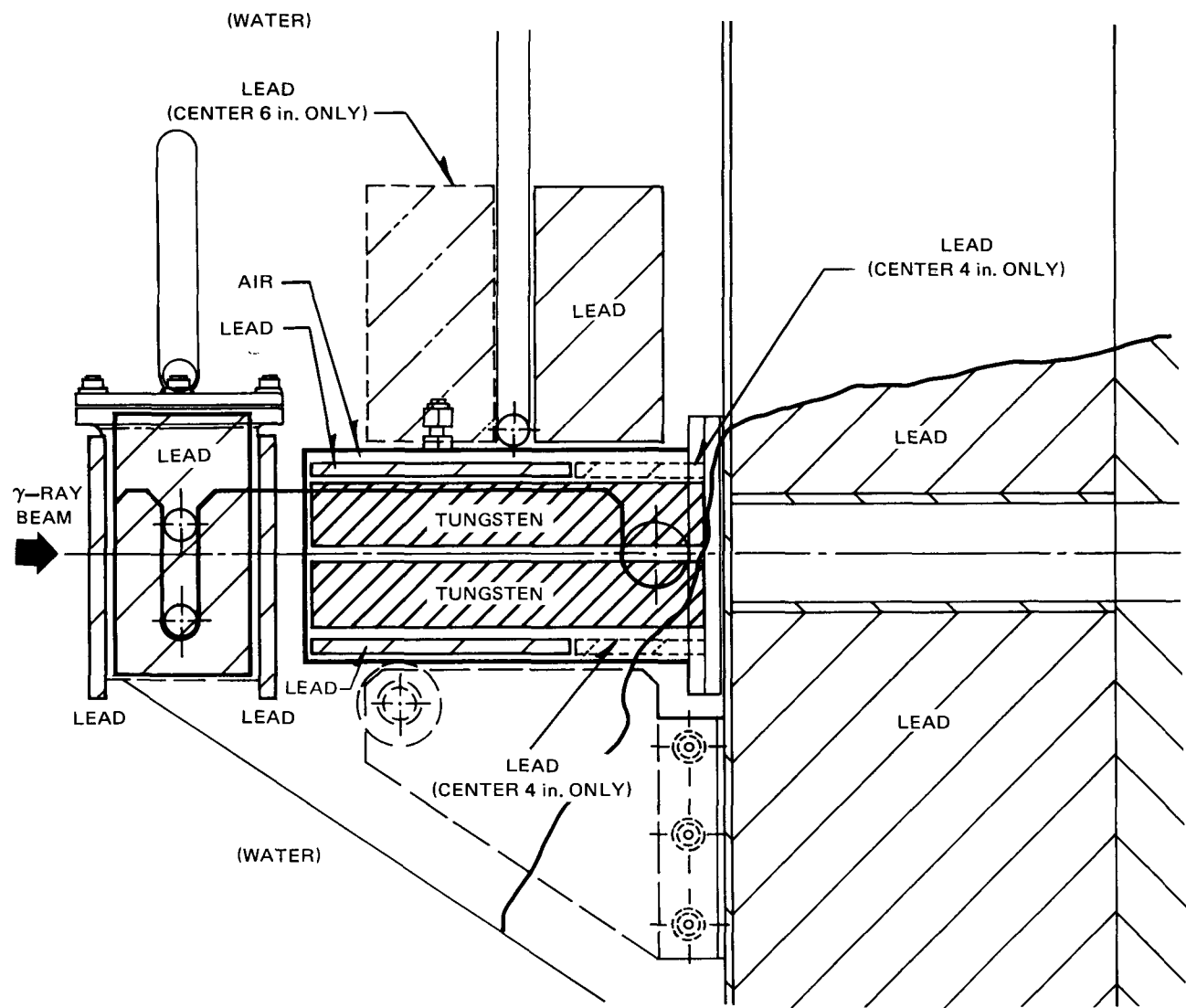


Figure 3-5. Front Snout of Collimator

is not known at this time. This caused the individual corner measurements near the bottom of the fuel to be biased with respect to each other, because of a difference, apparently reproducible, in the thickness of water between the fuel and the collimator for each of the four corners. By averaging the four individual corner nodal intensities, however, this bias is virtually removed from the assembly nodal intensities reported here.

In summary, although the fuel holder is judged adequate for the purpose intended, it is recommended that tighter geometry constraints be incorporated into future fuel holder designs for gamma scan programs.

3.2.4 Support Hardware

In addition to the underwater hardware described previously, several items of support equipment were used. The collimator hoist was a 2 ton, electrically operated chain hoist attached to a special bracket which spanned the transfer canal and allowed the refueling bridge free passage. A hoist control box allowed either computer controlled or manual operation. The automatic positioner worked well and typically positioned the collimator to within a few tenths of an inch of the desired location. The collimator position was sensed by a cable reel and potentiometer, the signal from which was digitized and sent to the computer. Other equipment included a portable winch for raising the slit and filter boxes, underwater tools and lights, and personnel work platforms.

3.3 DATA ACQUISITION

The data acquisition system was located on the mezzanine level of the fuel building in a radioactively clean area. The system consisted of NIM (Nuclear Instrument Module) electronics, a 1024 channel multichannel analyzer and a digital computer (HP2100). Automatic collimator positioning was accomplished by computer controlled relays and a digital voltmeter. Input-output devices peripheral to the computer included a CRT terminal, moving head disc drive, magnetic tape unit, teletype, paper tape reader, high speed punch, and electrostatic printer/plotter. The HP2100 has a 16-bit word, 1.6 microsecond memory cycle time and 32K memory size.

After an assembly was placed in the holder and rotated to point the desired corner at the collimation system, the computer positioned the collimator axially and started the MCA data collection cycle. After 1 minute of data collection the spectrum was transferred to both disc and magnetic tape. Each spectrum was stored with a 128 word identification block. This sequence was repeated for a predetermined set of axial measurement positions. Operator control was necessary only when the assembly was rotated to the next corner or a new assembly was inserted in the holder.

System software permitted fast on-line evaluation of the data stored on disc. Preliminary spectrum analysis results were output to the printer/plotter for immediate use and stored on a disc file for future detailed analyses. Highly automated, on-line, data handling procedures were essential due to the large volume of data accumulated (3000 gamma ray energy spectra).

Figure 3-6 shows a typical NaI spectrum from the measurements. The La-140 photopeak is located at channel 250 and the LED peak at channel 646. No La-140 intensity was observed except when fuel was placed in front of the collimator.

3.4 DATA REDUCTION

The process of converting gamma energy spectra to relative La-140 distributions involves several stages of data reduction which are described below.

3.4.1 Calculation of Peak Intensity

Gross photopeak areas were found by summing the counts in each channel of the peak region. Net peak areas were calculated by subtracting a background determined from a linear least-squares fit through two regions of data points, one on each side of the photopeak, which best represented the background under the photopeak. Peak and background regions for the La-140 and the pulser peaks were chosen after examining several spectra spanning the intensity range encountered in the measurement. The regions used were automatically shifted by any small amount that the peak drifted.

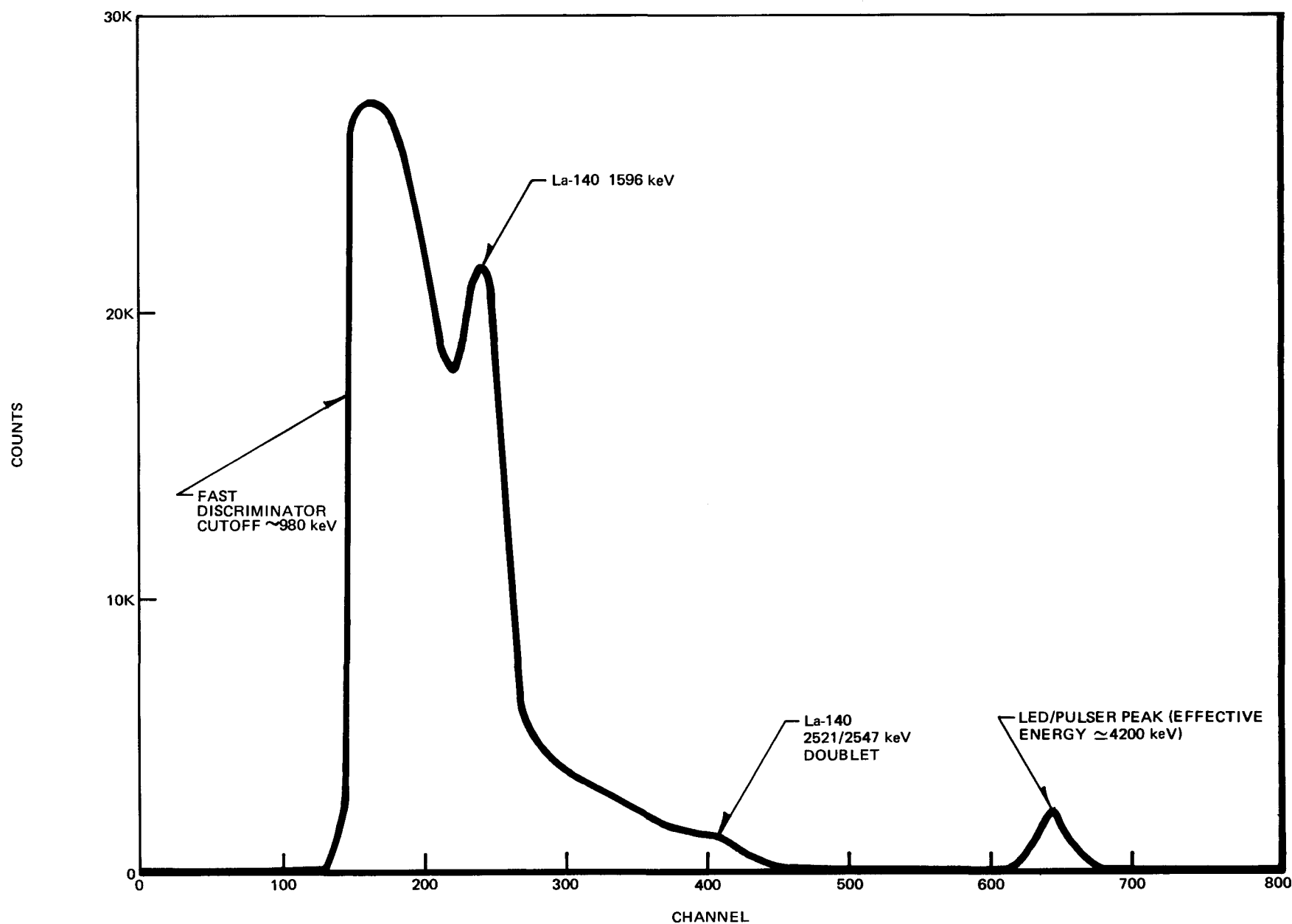


Figure 3-6. Typical Gamma Ray Energy Spectrum

3.4.2 Correction for Counting Losses

Photopeak intensities were corrected for counting losses by monitoring losses of a pulser peak introduced at a known rate. The magnitude of this factor ranged from 1.15 for the least intense points to 1.92 for the most intense points. This technique has become standard to high-count-rate gamma ray spectroscopy.

3.4.3 Counting Time and Decay Time Corrections

Measured La-140 intensities were normalized with respect to the MCA live time. Decay of the La-140 activity was taken into account by multiplying measured intensities by a decay correction factor $e^{-\lambda T}$ where $\lambda = 0.05419 \text{ day}^{-1}$ (corresponding to the 12.79 day Ba-140 parent half-life) and T is the time interval between 0000 hr, January 8, 1977, and the time of measurement.

3.4.4 Averaging

The corrected La-140 intensities were averaged over the four corners measured at each elevation for each assembly. Further averaging and normalization are discussed in Section 5.

3.4.5 Attenuation Due to Presence of Control Rod Cluster During Measurement

Measurements were made on one assembly with and without a control rod cluster (RCC) in place to allow experimental determination of the attenuating effect of the Ag/In/Cd rods. The 4.3% correction factor so determined was applied to measurements on Assembly C02, which was measured with an RCC in place. The measured intensities with and without the RCC in place are shown in Table 3-1 along with the percent difference. Analogous corrections for assemblies with burnable poison rod clusters in place are judged unnecessary because of the much lower density of the boron silicate glass relative to the Ag/In/Cd alloy.

Table 3-1
RCC ATTENUATION EFFECT

Measurement Location	La-140 Counts		% Difference
	with RCC	without RCC	Relative to Inserted Case
2	852164	917972	7.7
4	955598	986577	3.2
6	890181	920459	3.4
8	819342	869214	6.1
10	813784	859360	5.6
12	835840	859973	2.9
14	820468	871237	6.2
16	924000	926057	0.2
18	963063	980412	1.8
20	1148093	1223452	6.6
22	1222939	1277386	4.5
24	626770	647232	3.3
	Average		4.3

3.4.6 Special Calibration Factor

System changes were made early in the program following measurements on Assembly C63. These changes included adjustment of the electronics to lower the fast discriminator level. A 15.2% step change in system response at this point was determined by repeat measurements on the reference assembly. Thus, measured intensities on Assemblies C04, B13, C02, B21, C06, C50, and C63, which were scanned prior to the change, have been multiplied by 1.152 to make all reported measurements directly comparable.

3.4.7 Missing Points

Of the 2112 individual corner measurements, 4 were inadvertently skipped. Intensities for these points were estimated from axially adjacent locations on all four corners by linear interpolation. The estimated value was then averaged with the three measured corner intensities; the resulting four-corner average is reported. This procedure should not introduce more than 0.2% more uncertainty into the data for these points. Points affected are shown below.

Assembly	Position Number (See Table 2-2)
C22	24
A50	22
A59	22
A59	23

3.4.8 Edge Assembly Correction

As will be discussed in Subsection 4.3.1, a correction factor of 1.03 has been applied to the edge assembly intensities shown in Figures 5-1 and 5-3 and Appendices A and B to account for differing local power distributions. The uncorrected intensities are available in Appendix D, Data Listing, and were used in Appendix C, Axial Plots.

4. ACCURACY

4.1 MEASUREMENT UNCERTAINTY

Uncertainties were estimated from individual measurement reproducibility (determined by periodic scanning of one corner of the reference assembly). The reference measurement reproducibility of 2.9% (1σ) for a single point represents a quadratic combination of the statistical uncertainty of the individual standard measurements and other random measurement errors. Unfolding of the random error by inserting an average statistical error for the standard of 1.3% (1σ) yields 2.6% (1σ) for other random errors. These random errors include such effects as angular and axial positioning of the assembly. The repeat measurements on the reference assembly demonstrated proper decay characteristics of Ba-140 (12.79 day half-life) within the above uncertainty and with no overall trend. Counting statistics for all points measured fell in the range 1.0 to 1.4% (1σ). Thus, the uncertainty of every measured point can be taken as 2.9% (1σ). All intensities reported here are averages of four such individual measurements, one for each corner; thus the measurement uncertainty for intensities reported here is $2.9\% \div \sqrt{4} = 1.5\%$. An additional 0.2% systematic error should be added for the interpolated points (see Subsection 3.5.8).

As-built physical and nuclear manufacturing tolerances are an additional source of random error not explicitly included in the above analysis.

4.2 ATTENUATION COEFFICIENT MEASUREMENTS

Confirmation that accurate relative La-140 intensities were being measured was obtained by measuring the attenuation of 1596 keV gammas through lead. Different thicknesses of lead were placed in the beam line and the intensities measured. From this data the mass attenuation coefficient for lead was found to be $0.0509 \pm 0.0016 \text{ cm}^2/\text{gm}$, which agrees with the expected value of $0.0492 \pm 0.0005 \text{ cm}^2/\text{gm}$ within measurement uncertainty.

4.3 METHOD BIASES AND LIMITATIONS

Although the La-140 gamma scan technique is the most accurate method for independent verification of power distribution, there are some inherent biases which must be recognized in evaluating the accuracy and usefulness of the data.

4.3.1 Gamma Ray Attenuation in Fuel Assemblies

The gamma scan system does not measure all fuel pins in an assembly with equal efficiency, because of attenuation due to the fuel, cladding, and water. Edge pins have a substantially higher contribution to the total observed intensity than interior pins; the effect increases with decreasing gamma ray energy. Even for the relatively high energy (1596 keV) gamma ray of La-140, the intensities of the centermost pins are attenuated by about a factor of 14.7 compared to the corner pins. Insofar as the local (pin-to-pin) power distribution may vary due to design, control state, presence of burnable poison, exposure, or position in the core, biases in the nodal La-140 intensities reported here are inherent.

To examine the magnitude of these biases, calculations were made using two-dimensional gamma ray transport methods to determine the relative contribution from each pin in the assembly, with the collimator pointing toward a corner of the assembly. Figure 4-1 gives these results for equal source strength in each pin. No control rods or burnable poison rods were present. Typical local pin-to-pin distributions from PDQ-7 calculations were combined with Figure 4-1 to estimate the magnitude of biases that would result by using the four-corner-average method for determining relative nodal average intensities. The types of pin-to-pin power distributions available for the calculations are represented by enrichments, locations, and exposures shown in Table 4-1.

The higher exposure cases are more typical of conditions for Zion 2 at the end of Cycle 1. For these exposures, all three distributions cause lower measured intensities relative to a uniform distribution as seen by the gamma scan system; a, by 1.1%; b, by 0.7%; and c, by 3.7%. Thus, the relative bias is $\leq 3\%$ for these distributions. At the lower exposures the corresponding values are 3.1, -0.6, and 3.9%, respectively, for a relative bias of $\leq 4.5\%$. Note that at the beginning of life the assembly with burnable poison rods has a distribution skewed slightly to the exterior, causing an enhanced intensity relative to a uniform distribution.

Table 4-1
CHARACTERIZATION OF PIN-TO-PIN POWER DISTRIBUTIONS CONSIDERED

	Enrichment (wt %)	Core Location	Exposures (Mwd/t)	Comments
a.	1.85	Center	173 and 14760	
b.	2.55	Next to Center	187 and 16119	12 burnable poison rods
c.	3.1	Edge	131 and 10000	

Based on this small sample of distributions, it is estimated that biases $\leq 3\%$ could be expected in intensities uncorrected for differing local power distribution. The major bias is between edge assemblies and central assemblies. To compensate for this bias the edge assembly intensities in Figures 5-2 and 5-3 and Appendices A and B have been multiplied by 1.03. The estimated uncertainty in this correction factor is ± 0.015 . The effect of burnable poison at the end of cycle is small, based on distributions a. and b. above, and no correction has been applied. After this correction to the edge assemblies, biases of $\leq 2\%$ are expected. Detailed knowledge of pin-to-pin distributions for each assembly measured, would, when combined with Figure 4-1, allow more accurate correction for this effect, but in the absence of such information, it is felt that correction of only the edge assemblies is warranted. The uncorrected data are available in Appendix D.

A rough estimate of the attenuation caused by the presence of a control rod cluster during measurement was made based on Figure 4-1 and estimated attenuation for the Ag/In/Cd alloy. (This effect was measured during the program by a repeat measurement of the same assembly following removal of the RCC.) The estimate was 3.7%, compared to the measured value of $4.3 \pm 0.7\%$. The measured value was used to correct measurements of one assembly, C02.

4.3.2 Physical Positioning Biases

The assembly tilt relative to the direction of motion of the collimator, mentioned in Subsection 3.4, caused a slight misweighting of the four corners during the four-corner averaging for the bottom of the fuel. Even in the most severe case, on edge bundles where the four corners are most different from each other, the effect on the four-corner average is $\leq 1.6\%$. This would cause a bias in the axial shape of $\leq 1\%$.

4.4 SUMMARY OF LIMITATIONS

The combined considerations of measurement uncertainty and method biases imply a practical accuracy of approximately 3% in the reported relative La-140 intensities. It should be noted that no single value applies to all possible specific comparisons of the data, and that the appropriate uncertainty to apply in specific comparisons might be slightly higher or lower. The basis for estimating the 3% was quadratic combination of uncertainties and biases, treating them as additional random sources (1.5% from measurement uncertainty, Subsection 4.1; 2.0% from local distribution bias, Subsection 4.3.1; 1.6% from physical positioning bias, Subsection 4.3.2).

1.02	0.603	0.360	0.221	0.172	0.081	0.057	0.050	0.024	0.014	0.014	0.0085	0.0034	0.0018	0.0047
1.09	0.645	0.386	0.324	0.144	0.096	0.094	0.045	0.023	0.025	0.014	0.056	0.030	0.0082	
1.16	0.692		0.253	0.160		0.081	0.039	0.044		0.094	0.0051			
1.24	0.740	0.446	0.272	0.223	0.146	0.066		0.031	0.015	0.0086	0.018			
1.33	0.786	0.477	0.406		0.112	0.093	0.055	0.026	0.014					
1.42	0.841		0.313	0.192	0.162	0.096	0.044	0.025	0.040					
1.51	0.906	0.547	0.333	0.285	0.169	0.076	0.044	0.072						
1.62	0.968	0.584		0.298	0.131	0.076								
1.73	1.03	0.622	0.530	0.228	0.136	0.161								
1.84	1.10		0.400	0.240	0.285									
1.96	1.17	0.707	0.424											
2.10	1.25	0.753	0.637											
2.24	1.34	0.818												
2.38	1.43													
2.55														

DETECTOR

(SYMMETRIC ACROSS DIAGONAL)

Figure 4-1. Percent Count Rate Contribution from Each Rod, Equal Source Strength for All Fuel Rods (Water Holes in 21 Locations)

5. RESULTS

5.1 NODAL MEASUREMENTS

A total of 37 assemblies were scanned over a period of 8 days. The measured relative La-140 intensity distributions are presented in several different formats to facilitate review and evaluation.

5.1.1 Planar Maps of 25 Assemblies Measured Defining the La-140 Distribution in One Octant of the Core (See Appendix A)

Planar maps at 12 measurement locations are included as Appendix A. The normalization approximates the core average at each plane and is performed as follows: The average of the 24 assemblies measured that are part of the octant (Figure 5-1 with B34 deleted, since it is outside the octant), plus approximations for the four holes at G1, E1, E2, and H3, was set equal to one. Assembly C06 at core location R5 is a symmetric counterpart of core location E1 and was substituted for this hole. Assembly B59 at F3 was used for the hole at H3. Assembly C43 at K1 was used for the hole at G1. It is expected that this method of normalization to the "core average" is accurate to within 1%. Note that the edge assemblies are corrected as discussed in Subsection 4.3.1. To remove this correction from the normalized values, multiple the values for the edge assemblies by 0.97 and all others by 1.006.

5.1.2 Planar Displays of the Other Twelve Assemblies (See Appendix B)

Planar displays at 12 measurement locations are shown in Appendix B. The same normalization factor as above is used at each plane.

5.1.3 Axial Plots of the La-140 Intensity of 37 Assemblies (See Appendix C)

Of the 37 assemblies shown, 30 were measured at 12 nodes and 7 were measured at 24 nodes. The plots are not normalized, but the scales are the same for all 37 plots. Note that the 3% edge assembly correction (see Subsection 4.3.1) has not been applied to these plots.

5.1.4 Listing of the Data (See Appendix D)

The La-140 intensities of the 37 assemblies measured are listed at each elevation. The axially integrated intensity for each assembly is also given. Integrals were formed as described in Subsection 5.2. Note that the 3% edge assembly correction (see Subsection 4.3.1) has not been applied to these data listings. Normalized intensities are also given; each assembly is normalized separately to an average nodal intensity of one.

5.2 AVERAGED AND INTEGRATED MEASUREMENTS

For the 37 assemblies measured two methods have been used to collapse the data and display general trends. The normalization factors determined in Subsection 5.1.1 were used to plot a "core averaged" axial distribution. This distribution is plotted in Figure 5-2).

Core average radial trends are displayed in Figures 5-1 and 5-3, in which the nodal intensities have been integrated axially for each assembly. Since the elevations were not evenly spaced, this was done by weighting the intensity at each axial elevation by the length of fuel represented by that point. This length was determined from the midpoints between adjacent measurement locations. Only the even-numbered measurement locations were used since most assemblies were measured only at these points. In Figures 5-1 and 5-3 the 3% correction for the edge bundle bias discussed in Subsection 4.3.1 has been applied. Figures 5-4 and 5-5 show similar displays, but without the correction applied.

5.3 DEPRESSION IN THE REGION OF A GRID STRAP

The depression in the measured La-140 intensity near a grid strap is shown in Figure 5-6. The depression, about 13% at the center, is due to both flux depression and gamma ray attenuation (in the immediate region only).

ZION-2 EOC1 BENCHMARK GAMMA SCAN
FEBRUARY 1977

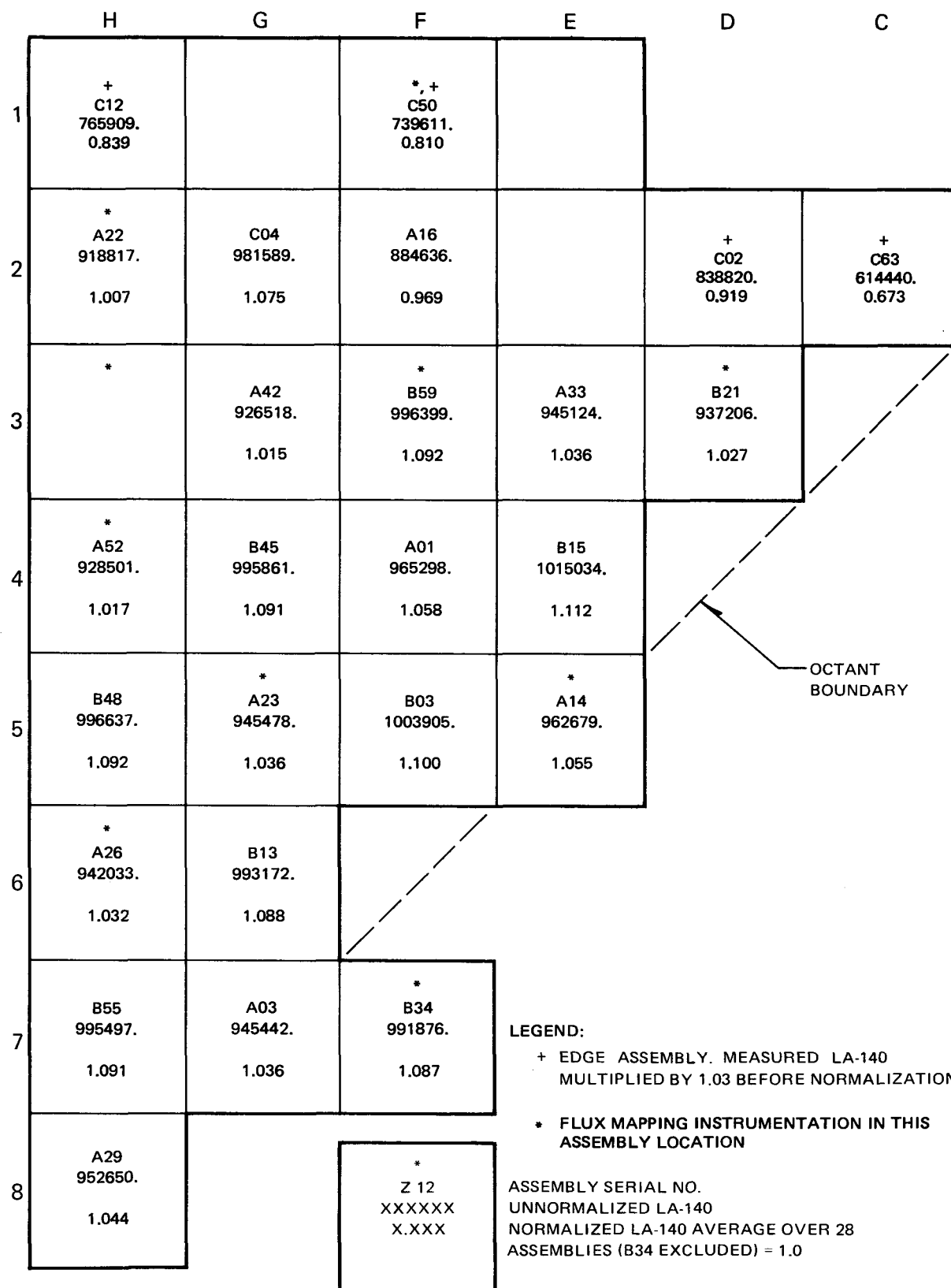
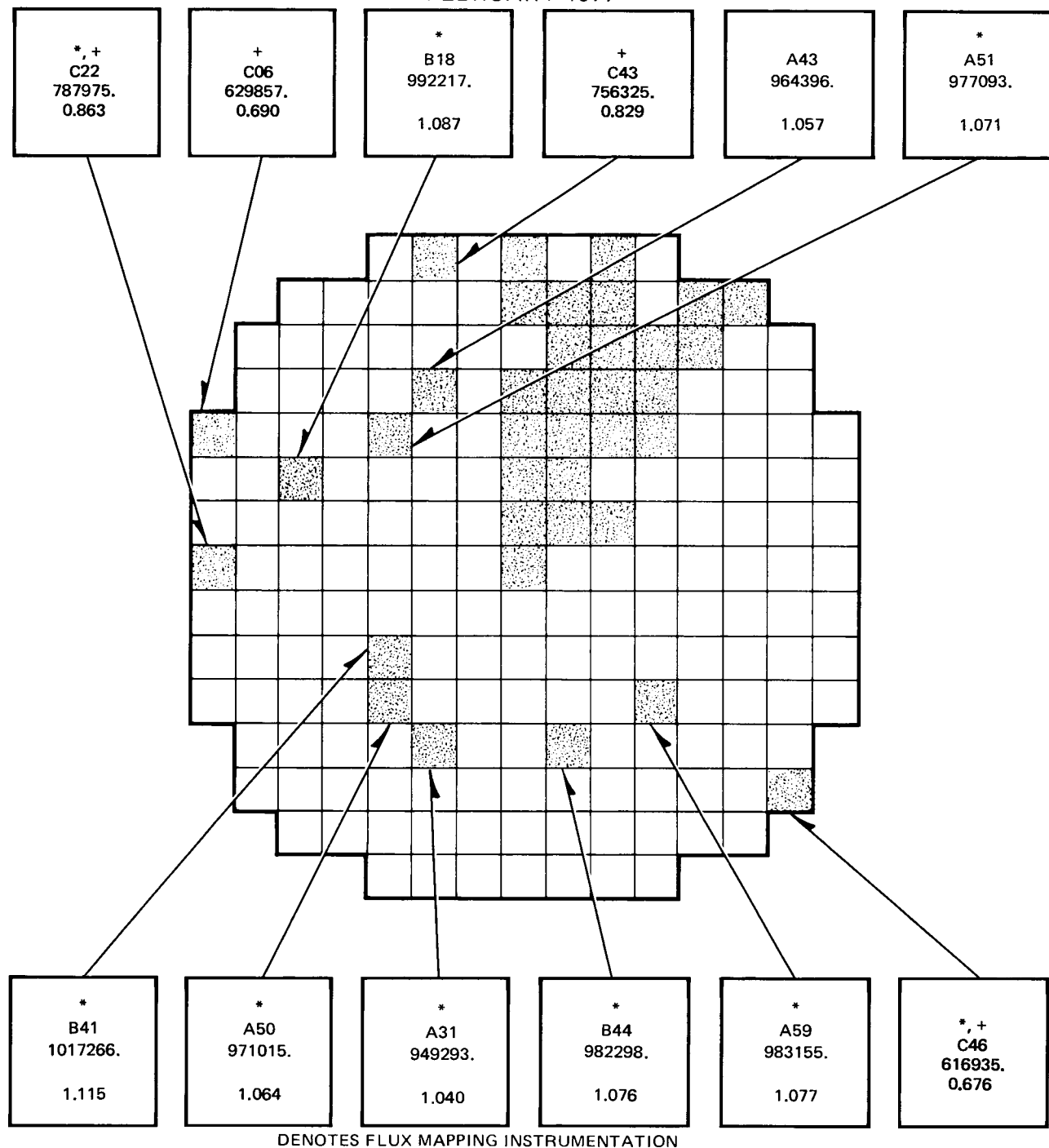


Figure 5-1. Radial La-140 Distribution (Assembly Average) Edge Assembly Correction Applied

ZION-2 EOC1 BENCHMARK GAMMA SCAN
FEBRUARY 1977



*

Z 12

XXXXXX

X.XXX

ASSEMBLY SERIAL NO.
UNNORMALIZED LA-140
NORMALIZED LA-140 AVERAGE OVER 28
ASSEMBLIES (B34 EXCLUDED) = 1.0

LEGEND:

- + EDGE ASSEMBLY, MEASURED LA-140 MULTIPLIED BY 1.03
- * FLUX MAPPING INSTRUMENTATION IN THIS ASSEMBLY LOCATION

Figure 5-3. Radial La-140 Distribution (Assembly Average) Edge Assembly Correction Applied

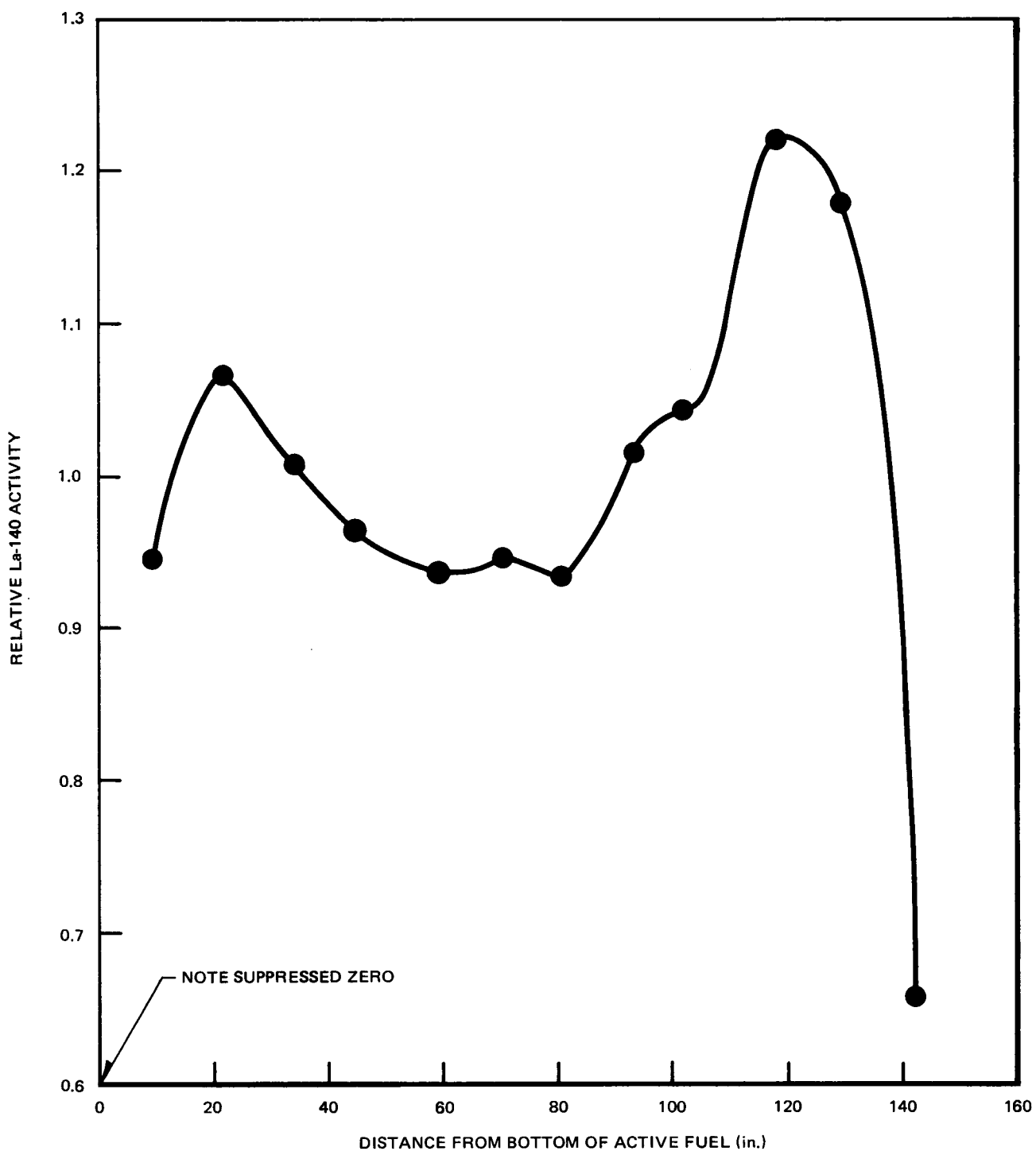


Figure 5-2. Core Average Axial La-140 Distribution

ZION-2 EOC1 BENCHMARK GAMMA SCAN
FEBRUARY 1977

H	G	F	E	D	C
1	C12 743601. 0.819		*	C50 718069. 0.791	
2	*	A22 918817. 1.012	C04 981589. 1.081	A16 884636. 0.974	
3	*	A42 926518. 1.020	*	B59 996399. 1.097	A33 945124. 1.041
4	*	A52 928501. 1.022	B45 995861. 1.097	A01 965298. 1.063	B15 1015034. 1.118
5	B48 996637. 1.097	*	A23 945478. 1.041	B03 1003905. 1.105	*
6	*	A26 942033. 1.037	B13 993172. 1.094		
7	B55 995497. 1.096	A03 945442. 1.041	*	B34 991876. 1.092	
8	A29 952650. 1.049		Z 12 XXXXXX X.XXX		

LEGEND:

* FLUX MAPPING INSTRUMENTATION IN THIS ASSEMBLY LOCATION

ASSEMBLY SERIAL NO.
UNNORMALIZED LA-140
NORMALIZED LA-140 AVERAGE OVER 28
ASSEMBLIES (B34 EXCLUDED) = 1.0

Figure 5-4. Radial La-140 Distribution (Assembly Average) No Edge Assembly Correction

ZION-2 EOC1 BENCHMARK GAMMA SCAN
FEBRUARY 1977

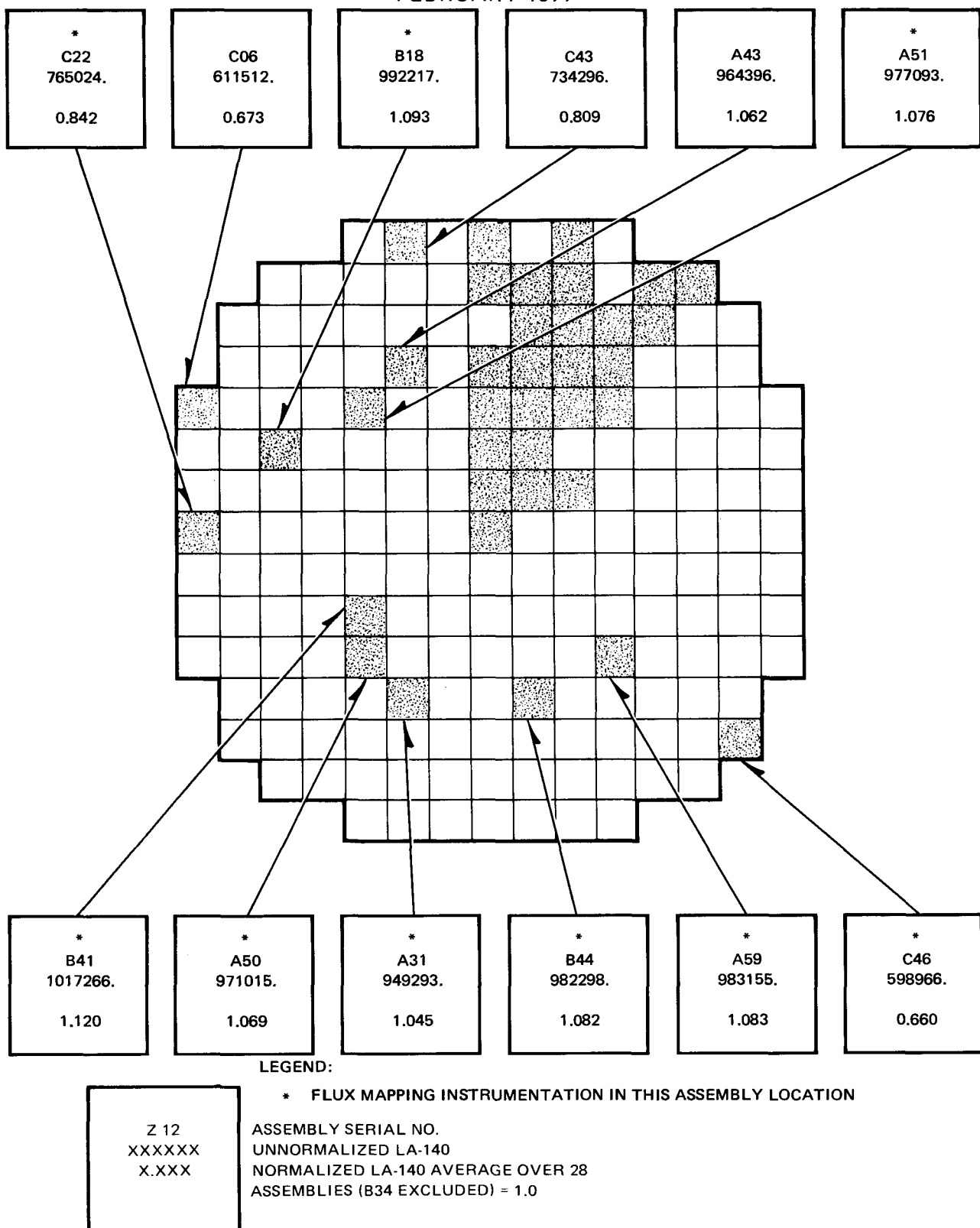


Figure 5-5. Radial La-140 Distribution (Assembly Average) No Edge Assembly Correction

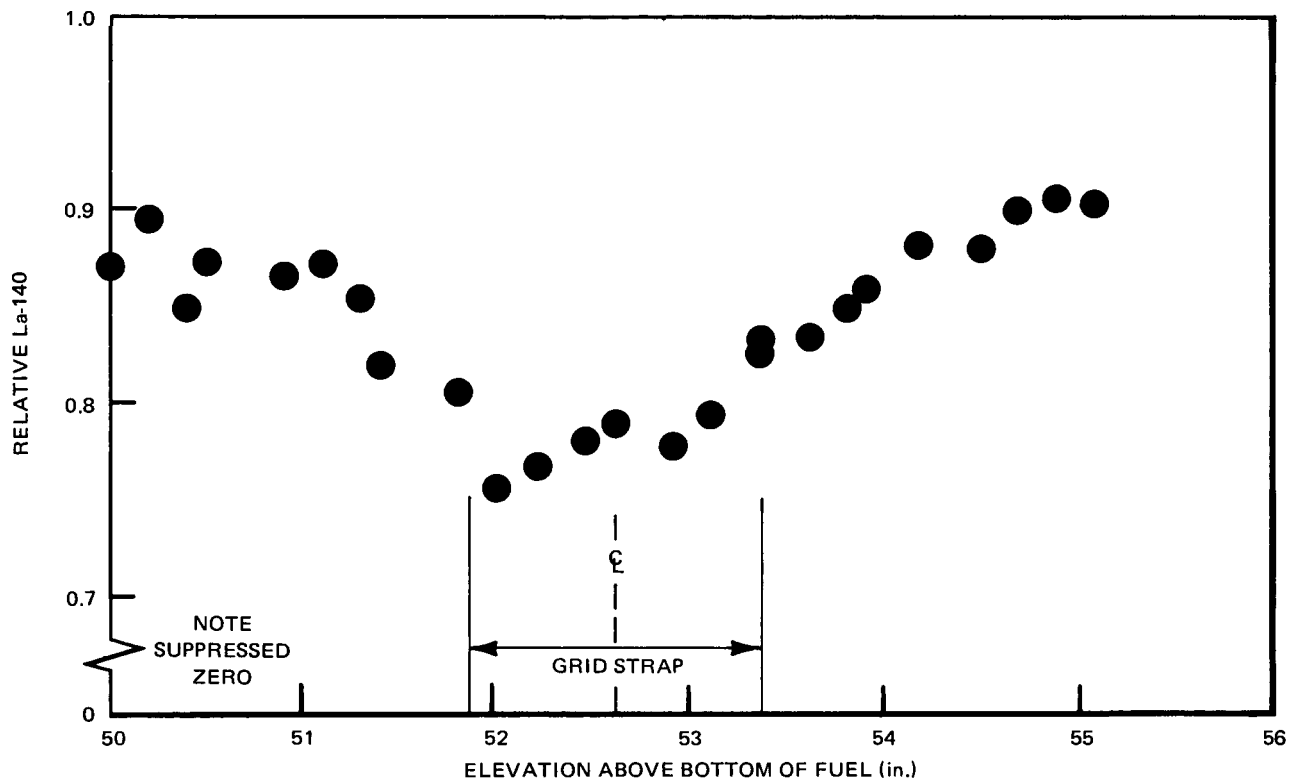


Figure 5-6. Depression in La-140 Intensity Near Grid Strap

6. UTILIZATION OF THE DATA FOR POWER DISTRIBUTION BENCHMARK

The gamma scanning technique described in this report measures the 1596 keV gamma which accompanies the beta decay of La-140. The primary mechanism for the accumulation of La-140 in exposed fuel is the beta decay of the fission product Ba-140 with a half-life of 12.79 days. Because of this equilibration time constant, the Ba-140 distribution is characteristic of the integrated power history of the core during the last 2 to 3 months before shutdown. Following a period of approximately 10 days after the reactor shutdown, the La-140 activity is decaying at a rate determined by the half-life of Ba-140 and is proportional to the Ba-140 atom density (see Figure 6-1).

In general, proper utilization of the measured La-140 intensities for benchmarking power distribution methods requires the predicted end of cycle Ba-140 distribution to be calculated. By far the most sensitive input to this calculation is the power distribution history, so that a valid benchmark results. Figure 6-2 gives a flow chart of the process.

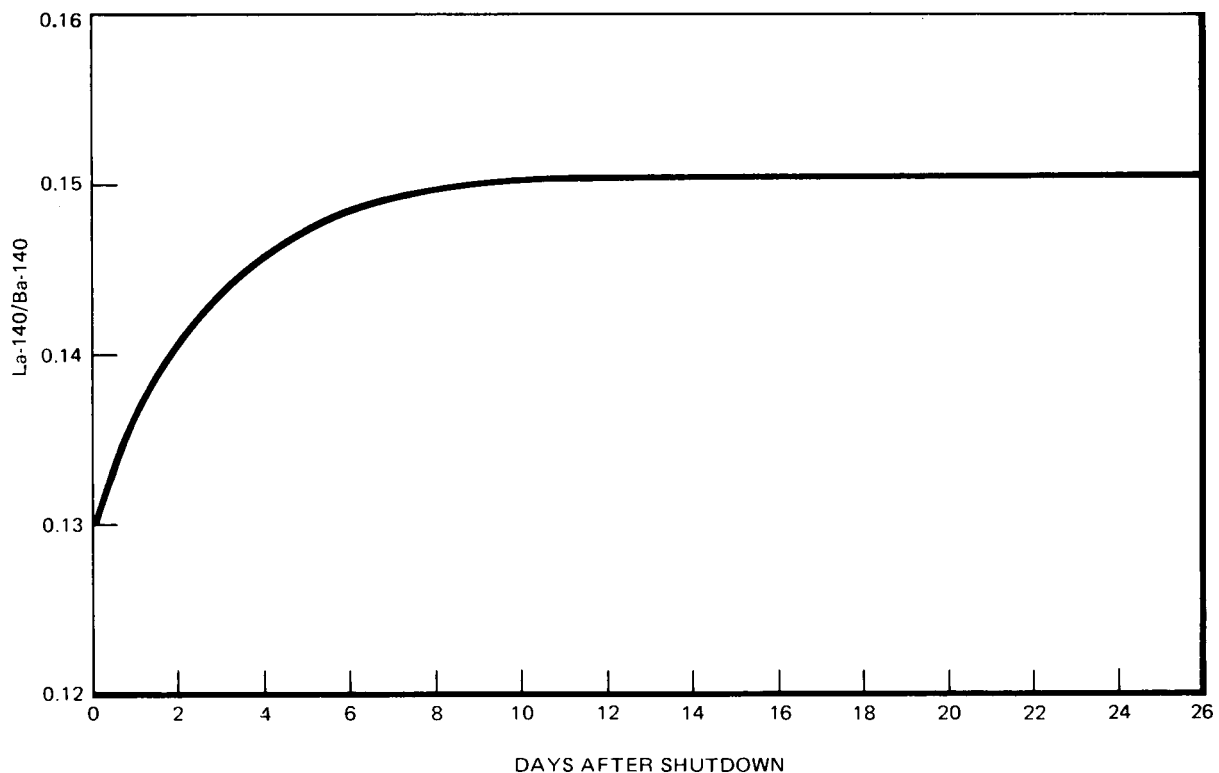


Figure 6-1. Ratio of La-140 Atom Density to Ba-140 Atom Density after Shutdown, Following Long Irradiation

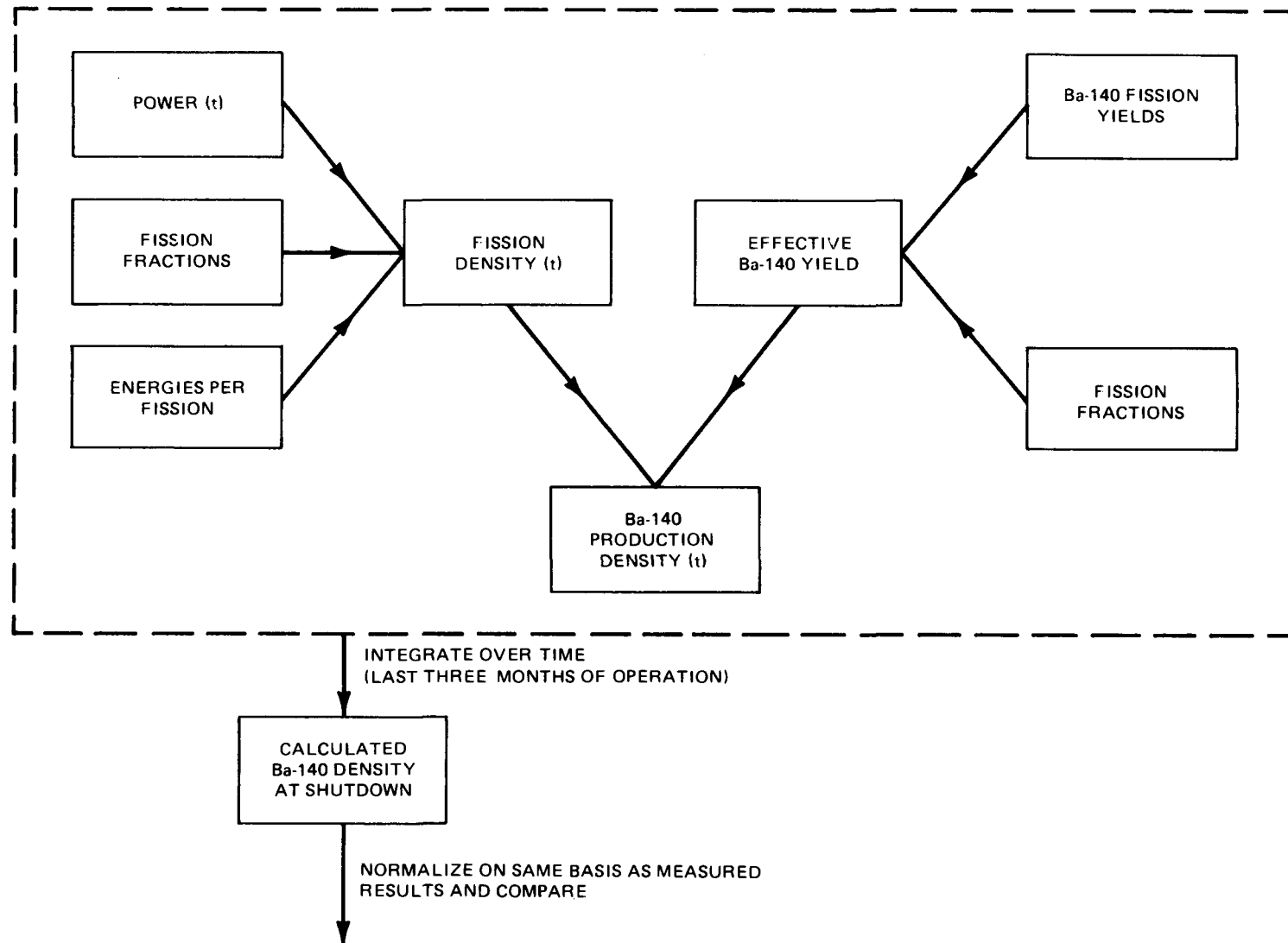


Figure 6-2. Flow Chart of Ba-140 Calculation

The relationship between the fission rate (F) at time t , at a point \vec{r} , and the power (P) at that point, is given by

$$F = \frac{KP}{\langle E \rangle} \text{ fissions/sec-cm}^3$$

where K is a proportionality constant with the value

$$K = 6.2383 \times 10^{18} \text{ MeV/sec/MW}$$

and

$$P = \text{power density at } \vec{r}, \text{ MW/cm}^3$$

and

$$\langle E \rangle = \frac{\sum_k (\Sigma_{fk} \phi) E_k}{\sum_k (\Sigma_{fk} \phi)} = \sum_k f_k E_k = \text{the average energy per fission}$$

ϕ = neutron flux at position \vec{r} ,

Σ_{fk} = macroscopic fission cross-section for fissile nuclide k at position \vec{r} , cm^{-1}

E_k = energy per fission of the k^{th} fission cross-section, MeV

f_k = fission fraction of nuclide k at \vec{r}

Then the relationship between the production rate of Ba-140 (S_B) and power, at a time t , is given as

$$S_B = \left\{ \sum_k X_{Bk} f_k \right\} F = \left\{ \sum_k X_{Bk} f_k \right\} \frac{KP}{\langle E \rangle} \frac{\text{Barium atoms}}{\text{cm}^3 \text{ sec}}$$

where

X_{Bk} = cumulative fission yield of Ba-140 from fissile nuclide k

To determine the total accumulation of Ba-140, then, requires solving the equation

$$N_B(t) = \int_{t_0}^{t_f} [S_B(t) - \lambda N_B(t)] dt$$

where

N_B = Ba-140 atom density, atoms/cm³

λ = Ba-140 decay constant = 0.05419 day⁻¹

and the interval of integration is the entire irradiation period. Neutron absorption by Ba-140 is negligible relative to decay. Since Ba-140 may not be one of the fission products normally followed by the core simulator it may be necessary to determine it by independent calculation. Some simplifying assumptions can generally be made to assist in the solution of this problem. In most cases the number of fissile nuclides, k , which contribute significantly to the fission rate, is small. An "effective Ba-140

fission yield," dependent only on exposure, can be calculated by weighting the yields shown in Table 6-1 by the fission fractions for each fissile species at several exposures. An additional assumption that can be made is to assume that P and $\langle E \rangle$ are stepwise constant over the interval $\Delta t = t_n - t_{n-1}$, therefore replacing the time integral with successive substitution, as

$$N_B(t_n) = \frac{S_B(t_n)}{\lambda} + \left[N_B(t_{n-1}) - \frac{S_B(t_n)}{\lambda} \right] \exp(-\lambda \Delta T)$$

where

$$n = 1, 2, \dots m$$

$N_B(t_m)$ = end of cycle Ba-140 atom density

Table 6-1
Ba-140 CUMULATIVE FISSION YIELDS*

Species	Fission Yield (%)
U-235	6.32
Pu-239	5.57
Pu-241	5.90
U-238	6.02

* M. E. Meek and B. F. Rider, "Compilation of Fission Product Yields, Vallecitos Nuclear Center — 1974," NEDO-12154-1, January 26, 1974.

The production term, S_B , can be further simplified. $\langle E \rangle$ can be approximated as constant. To determine the *relative* distribution of Ba-140 rather than absolute atom densities, power and effective yield are the only inputs, K and $\langle E \rangle$ being eliminated by normalization. This consideration is very useful in gamma scan and power comparisons, since only relative Ba-140 distributions are measured. The resulting formulation, using $S_B(t_n) = Y_e P(t_n)$, is

$$N_B(t_n) = \frac{Y_e P(t_n)}{\lambda} + \left[N_B(t_{n-1}) - \frac{Y_e P(t_n)}{\lambda} \right] \exp(-\lambda \Delta T)$$

where

$$Y_e = \text{effective yield} = \sum_{i=1}^4 Y_i F_i, \text{ i = U-235, U-238, Pu-239, and Pu-241}$$

Y_i = cumulative yield for fissile nuclide i

F_i = fraction of fissions for fissile nuclide i

The term $P(t_n)$ is the power distribution (one, two, or three dimensional), taken from the core simulator or process computer. Thus, in this mode of calculation, the gamma scan can serve as a benchmark for computer programs which calculate power distributions. The power distribution should be calculated for as many power levels and control configurations as is necessary to adequately represent the operating history of the reactor. Each distribution is then input in turn as $P(t_n)$. Minor control rod changes late in the cycle, which have little effect on the total power history of the core, can significantly affect the Ba-140 distribution for specific assemblies. Therefore, it is desirable that the power level and control configuration

remain constant near shutdown, such that the Ba-140 distribution of every assembly is allowed to equilibrate with a single power distribution.

The uncertainty in determining the relative barium distribution from the relative assembly powers, is dependent upon the power and $\langle E \rangle$ remaining constant over the period ΔT , and the accuracy of determining Y_e , the effective yield for Ba-140 for that period. Naturally, finer ΔT steps will improve the accuracy of the calculation. The minor uncertainties in the calculation of Ba-140 from process computer power calculations or core simulators, combined with the consideration of Section 4 indicate that benchmarking of power distribution methods within 4% is reasonably achievable from the data resulting from this program. In specific comparisons, even more accurate benchmarking is possible, or the calculation necessary can be simplified, or both.

In particular cases where the power distributions have not appreciably changed over the equilibrium period, such as assembly power sharing at one elevation, it is generally adequate to only apply the consideration of differing fission yields, and not to calculate Ba-140 using time steps in operating history. In these cases, knowing an effective yield allows the calculation of an *approximate* power distribution *from* the La-140 distribution. This is only accurate in cases where the power distribution is stable.

In a few instances the La-140 distribution can be used directly for power distribution questions. For instance, core power *symmetry* in symmetrically loaded and operated cores can be examined without direct application of either the time integral or differing fission yield considerations.

7. CONCLUSIONS

The extensive set of gamma scan La-140 intensities determined in this project constitute an accurate data base against which power distribution calculations and on-line power measurement systems can be benchmarked. It is the hope of the participants that these data will be useful in reducing uncertainties in the design and operation of nuclear power plants, resulting in improved performance and increased operating margins.



APPENDIX A

**PLANAR MAPS OF 25 ASSEMBLIES MEASURED
DEFINING THE La-140 DISTRIBUTION
IN ONE OCTANT OF THE CORE**

ZION-2 EOC1 BENCHMARK GAMMA SCAN
FEBRUARY 1977

H	G	F	E	D	C
1	+ C12 709286. 0.823		* C50 663922. 0.771		
2	* A22 872343. 1.013	C04 892632. 1.036	A16 833759. 0.968		+ C02 783309. 0.909
3	*	A42 891436. 1.035	* B59 968442. 1.124	A33 895354. 1.039	* B21 838511. 0.973
4	*	A52 911575. 1.058	B45 969190. 1.125	A01 952032. 1.105	B15 955069. 1.109
5	B48 946013. 1.098	*	A23 913394. 1.060	B03 957657. 1.112	*
6	*	A26 917166. 1.065	B13 917792. 1.065		OCTANT BOUNDARY
7	B55 937202. 1.088	A03 910286. 1.057	*	B34 949519. 1.102	LEGEND:
8	A29 917972. 1.065		Z 12 XXXXXX X.XXX		+ EDGE ASSEMBLY. MEASURED LA-140 MULTIPLIED BY 1.03 BEFORE NORMALIZATION
					* FLUX MAPPING INSTRUMENTATION IN THIS ASSEMBLY LOCATION
					ASSEMBLY SERIAL NO. UNNORMALIZED LA-140 NORMALIZED LA-140 AVERAGE OVER 28 ASSEMBLIES (B34 EXCLUDED) = 1.0

Figure A-1. Planar La-140 Distribution at 9 Inches Above Bottom of Active Fuel

ZION-2 EOC1 BENCHMARK GAMMA SCAN
FEBRUARY 1977

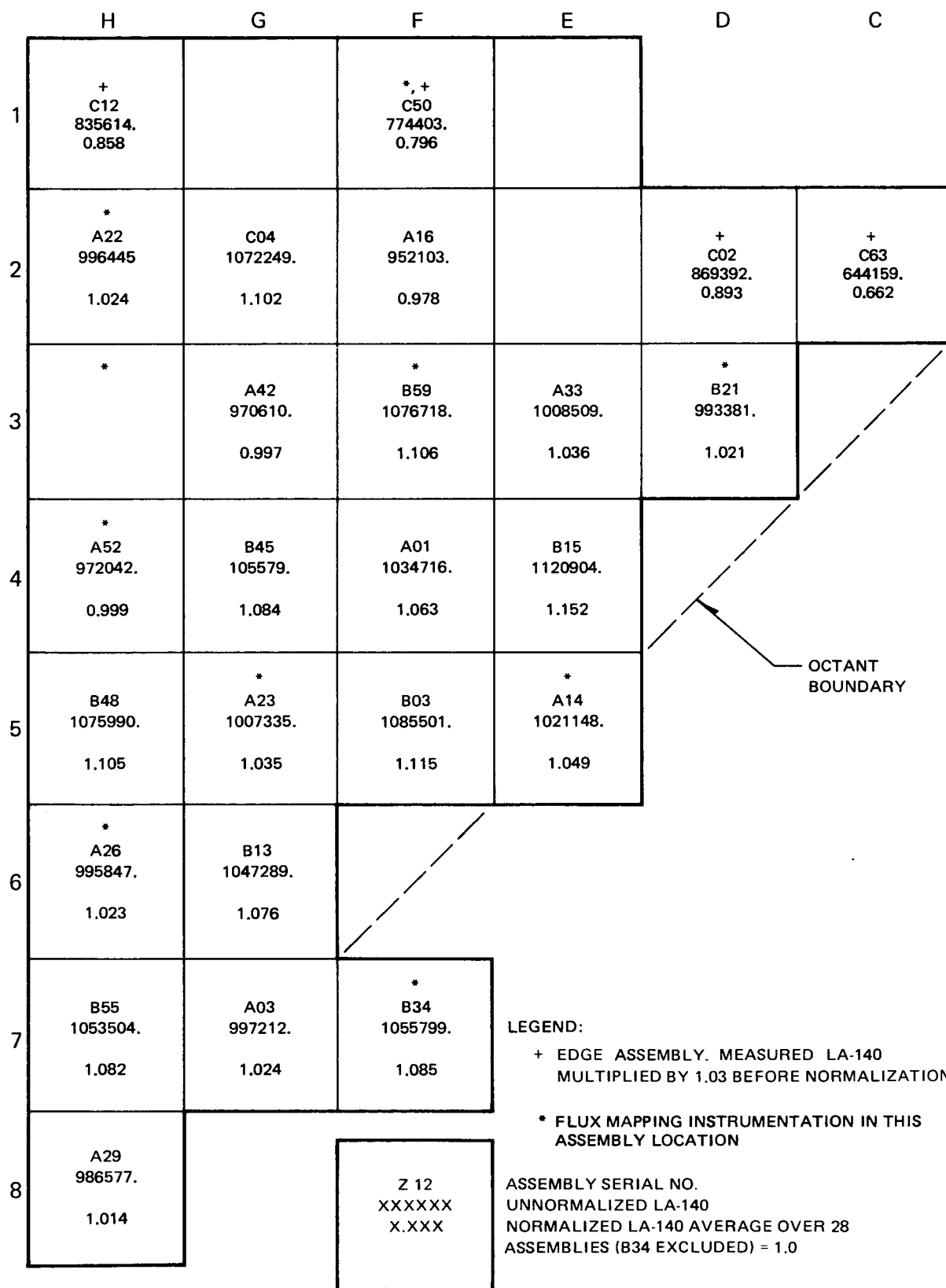


Figure A-2. Planar La-140 Distribution at 21 Inches Above Bottom of Active Fuel

ZION-2 EOC1 BENCHMARK GAMMA SCAN
FEBRUARY 1977

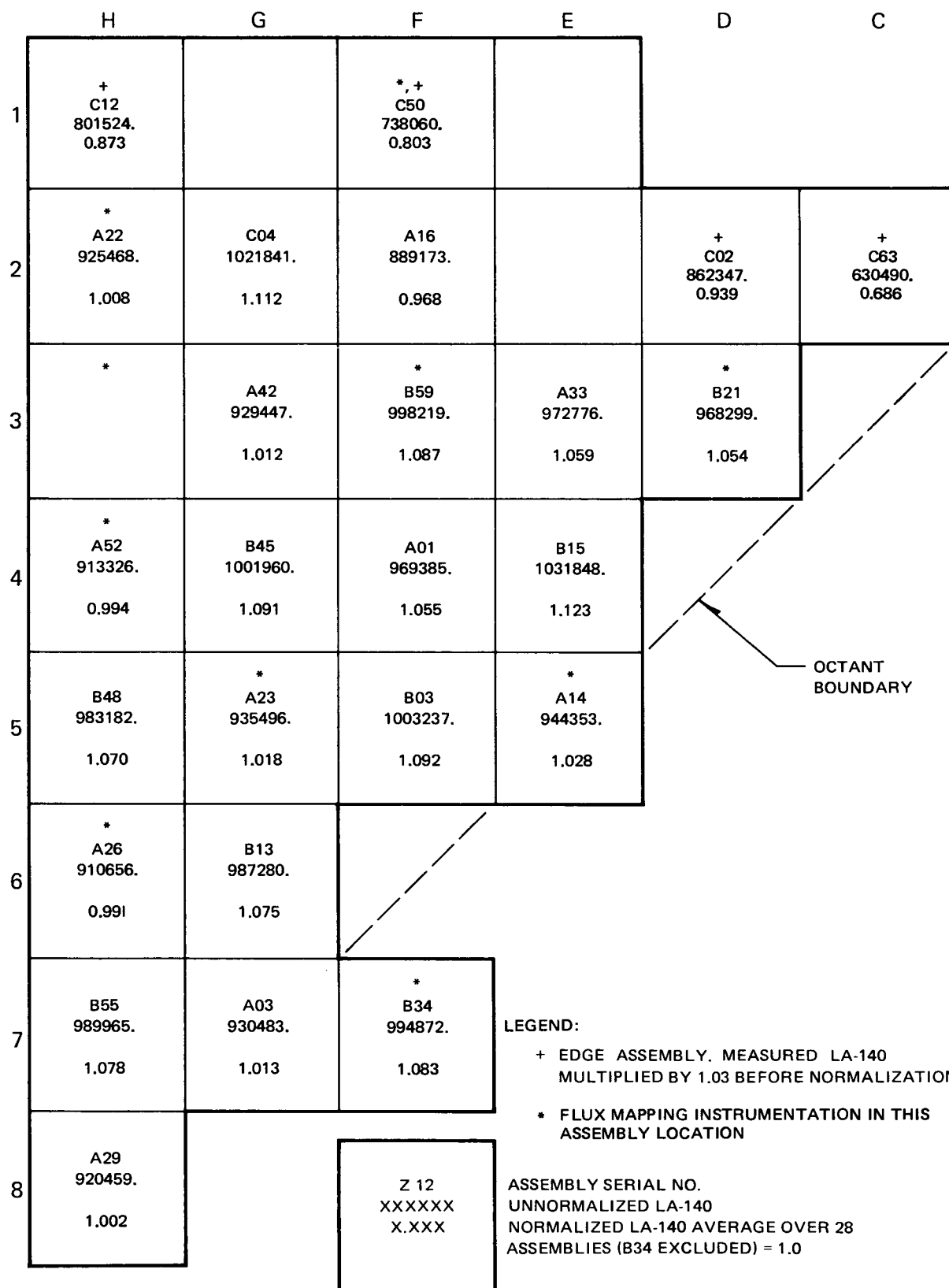


Figure A-3. Planar La-140 Distribution at 33 Inches Above Bottom of Active Fuel

ZION-2 EOC1 BENCHMARK GAMMA SCAN
FEBRUARY 1977

H	G	F	E	D	C
1	+ C12 773708. 0.881		* C50 766663. 0.873		
2	* A22 892947. 1.016	C04 978006. 1.113	A16 861601. 1.095		+ C02 819466. 0.933
3	*	A42 880206. 1.002	* B59 933767. 1.063	A33 910752. 1.037	* B21 930330. 1.059
4	* A52 864272. 0.984	B45 929088. 1.058	A01 914233. 1.041	B15 973953. 1.109	
5	B48 928878. 1.057	*	A23 892299. 1.016	B03 928562. 1.057	* A14 907131. 1.033
6	* A26 872684. 0.993	B13 952295. 1.084			OCTANT BOUNDARY
7	B55 913960. 1.040	A03 900807. 1.025	*	B34 917365. 1.044	LEGEND: + EDGE ASSEMBLY. MEASURED LA-140 MULTIPLIED BY 1.03 BEFORE NORMALIZATION * FLUX MAPPING INSTRUMENTATION IN THIS ASSEMBLY LOCATION
8	A29 869214. 0.989		Z 12 XXXXXX X.XXX		ASSEMBLY SERIAL NO. UNNORMALIZED LA-140 NORMALIZED LA-140 AVERAGE OVER 28 ASSEMBLIES (B34 EXCLUDED) = 1.0

Figure A-4. Planar La-140 Distribution at 45 Inches Above Bottom of Active Fuel

ZION-2 EOC1 BENCHMARK GAMMA SCAN
FEBRUARY 1977

	H	G	F	E	D	C
1	+ C12 737637. 0.863		*, + C50 757264. 0.886			
2	* A22 870923. 1.019	C04 946368. 1.107	A16 858338. 1.004		+ C02 800374. 0.937	+ C63 616701. 0.722
3	*	A42 842847. 0.986	*	B59 946889. 1.108	A33 873661. 1.022	B21 915415. 1.071
4	* A52 836344. 0.979	B45 892530. 1.044	A01 898981. 1.052	B15 933580. 1.092		
5	B48 896794. 1.049	*	A23 861466. 1.008	B03 919701. 1.076	*	A14 875291. 1.024
6	*	A26 847066. 0.991	B13 926580. 1.084			
7	B55 919457. 1.076	A03 850410. 0.995	*	B34 906090. 1.060	LEGEND:	+ EDGE ASSEMBLY. MEASURED LA-140 MULTIPLIED BY 1.03 BEFORE NORMALIZATION
8	A29 859360. 1.006		Z 12 XXXXXX X.XXX			* FLUX MAPPING INSTRUMENTATION IN THIS ASSEMBLY LOCATION
						ASSEMBLY SERIAL NO. UNNORMALIZED LA-140 NORMALIZED LA-140 AVERAGE OVER 28 ASSEMBLIES (B34 EXCLUDED) = 1.0

OCTANT BOUNDARY

Figure A-5. Planar La-140 Distribution at 57 Inches Above Bottom of Active Fuel

ZION-2 EOC1 BENCHMARK GAMMA SCAN
FEBRUARY 1977

H	G	F	E	D	C
1	+ C12 755380. 0.873		* + C50 752335. 0.870		
2	* A22 887117. 1.025	C04 968848. 1.120	A16 849601. 0.982		* C02 818367. 0.946
3	*	A42 855377 0.989	* B59 926268. 1.071	A33 893628. 1.033	* B21 913171. 1.056
4	* A52 876350. 1.013	B45 940261. 1.087	A01 896275. 1.036	B15 946607. 1.094	
5	B48 930724. 1.076	*	A23 882610. 1.020	B03 933564. 1.079	* A14 892294. 1.031
6	* A26 864408. 0.999	B13 919571. 1.063			OCTANT BOUNDARY
7	B55 911991. 1.054	A03 863926. 0.999	*	B34 918460. 1.062	LEGEND: + EDGE ASSEMBLY. MEASURED LA-140 MULTIPLIED BY 1.03 BEFORE NORMALIZATION * FLUX MAPPING INSTRUMENTATION IN THIS ASSEMBLY LOCATION
8	A29 859973. 0.994		Z 12 XXXXXX X.XXX		ASSEMBLY SERIAL NO. UNNORMALIZED LA-140 NORMALIZED LA-140 AVERAGE OVER 28 ASSEMBLIES (B34 EXCLUDED) = 1.0

Figure A-6. Planar La-140 Distribution at 69 Inches Above Bottom of Active Fuel

ZION-2 EOC1 BENCHMARK GAMMA SCAN
FEBRUARY 1977

H	G	F	E	D	C
1	+ C12 739737. 0.868		* + C50 723737. 0.850		
2	* A22 853991. 1.002	C04 943651. 1.108	A16 826908. 0.971		+ C02 798408. 0.937 + C63 605297. 0.711
3	*	A42 849079. 0.997	* B59 922556. 1.083	A33 871764. 1.023	* B21 887075. 1.041
4	* A52 855890. 1.005	B45 904037. 1.061	A01 894313. 1.050	B15 935800. 1.098	
5	B48 898048. 1.054	*	A23 867851. 1.019	B03 909822. 1.068	*
6	*	A26 866897. 1.018	B13 922456. 1.083		OCTANT BOUNDARY
7	B55 897363. 1.053	A03 875930. 1.028	*	B34 907332. 1.065	LEGEND: + EDGE ASSEMBLY. MEASURED LA-140 MULTIPLIED BY 1.03 BEFORE NORMALIZATION * FLUX MAPPING INSTRUMENTATION IN THIS ASSEMBLY LOCATION
8	A29 871237. 1.023		Z 12 XXXXXX X.XXX		ASSEMBLY SERIAL NO. UNNORMALIZED LA-140 NORMALIZED LA-140 AVERAGE OVER 28 ASSEMBLIES (B34 EXCLUDED) = 1.0

Figure A-7. Planar La-140 Distribution at 81 Inches Above Bottom of Active Fuel

ZION-2 EOC1 BENCHMARK GAMMA SCAN
FEBRUARY 1977

	H	G	F	E	D	C
1	+ C12 807106. 0.869		* C50 773479. 0.833			
2	* A22 942456. 1.015	C04 1037705. 1.118	A16 895119. 0.964		+ C02 86724. 0.934	+ C63 661588. 0.713
3	*	A42 953682. 1.027	* B59 1016530. 1.095	A33 975093. 1.050	*	B21 980575. 1.056
4	* A52 923075. 0.994	B45 1002276. 1.079	A01 965766. 1.040	B15 1036846. 1.117		
5	B48 982009. 1.058	* A23 932367. 1.004	B03 999489. 1.076	*	A14 970782. 1.046	
6	* A26 935513. 1.008	B13 1004253. 1.082				OCTANT BOUNDARY
7	B55 971962. 1.047	A03 919944. 0.991	* B34 997889. 1.075			
8	A29 926057. 0.997		Z 12 XXXXXX X.XXX			

LEGEND:

+ EDGE ASSEMBLY. MEASURED LA-140
MULTIPLIED BY 1.03 BEFORE NORMALIZATION

* FLUX MAPPING INSTRUMENTATION IN THIS
ASSEMBLY LOCATION

ASSEMBLY SERIAL NO.
UNNORMALIZED LA-140
NORMALIZED LA-140 AVERAGE OVER 28
ASSEMBLIES (B34 EXCLUDED) = 1.0

Figure A-8. Planar La-140 Distribution at 93 Inches Above Bottom of Active Fuel

ZION-2 EOC1 BENCHMARK GAMMA SCAN
FEBRUARY 1977

	H	G	F	E	D	C
1	+ C12 790065. 0.831		* + C50 779357. 0.820			
2	* A22 947673. 0.997	C04 1033423. 1.087	A16 928713. 0.977		+ C02 892165. 0.938	+ C63 662368. 0.697
3	*	A42 969578. 1.020	* B59 1039399. 1.093	A33 972998. 1.023	*	B21 983384. 1.034
4	*	A52 955093. 1.005	B45 1012463. 1.065	A01 1004258. 1.056	B15 1050639. 1.105	
5	B48 1035486. 1.089	*	A23 966626. 1.017	B03 1046688. 1.101	*	A14 1004024. 1.056
6	*	A26 978880. 1.030	B13 1054690. 1.109			OCTANT BOUNDARY
7	B55 1039776. 1.094	A03 952508. 1.002	*	B34 1035428. 1.089	LEGEND:	
8	A29 980412. 1.031		Z 12 XXXXXX X.XXX		+ EDGE ASSEMBLY. MEASURED LA-140 MULTIPLIED BY 1.03 BEFORE NORMALIZATION	
					* FLUX MAPPING INSTRUMENTATION IN THIS ASSEMBLY LOCATION	
					ASSEMBLY SERIAL NO. UNNORMALIZED LA-140 NORMALIZED LA-140 AVERAGE OVER 28 ASSEMBLIES (B34 EXCLUDED) = 1.0	

Figure A-9. Planar La-140 Distribution at 103 Inches Above Bottom of Active Fuel

ZION-2 EOC1 BENCHMARK GAMMA SCAN
FEBRUARY 1977

	H	G	F	E	D	C
1	+ C12 906036. 0.814		* C50 852026. 0.765			
2	* A22 1105386. 0.993	C04 1147365. 1.031	A16 1058315. 0.951		+ C02 1007745. 0.905	+ C63 733879. 0.659
3	*	A42 1131842. 1.017	* B59 1192944. 1.072	A33 1156916. 1.039	*	B21 1158393. 1.041
4	* A52 1142024. 1.026	B45 1232437. 1.107	* A01 1163218. 1.045	B15 1281292. 1.151		
5	B48 1255489. 1.128	* A23 1145581. 1.029	B03 1245999. 1.119	* A14 1173962. 1.055		OCTANT BOUNDARY
6	* A26 1162138. 1.044	B13 1255566. 1.128				
7	B55 1260154. 1.132	A03 1179248. 1.059	* B34 1230516. 1.106			
8	A29 1223452. 1.099		Z 12 XXXXXX X.XXX			

LEGEND:

- + EDGE ASSEMBLY. MEASURED LA-140
MULTIPLIED BY 1.03 BEFORE NORMALIZATION
- * FLUX MAPPING INSTRUMENTATION IN THIS
ASSEMBLY LOCATION

ASSEMBLY SERIAL NO.
UNNORMALIZED LA-140
NORMALIZED LA-140 AVERAGE OVER 28
ASSEMBLIES (B34 EXCLUDED) = 1.0

Figure A-10. Planar La-140 Distribution at 117 Inches Above Bottom of Active Fuel

ZION-2 EOC1 BENCHMARK GAMMA SCAN
FEBRUARY 1977

H	G	F	E	D	C
1	+ C12 814571. 0.757		* + C50 793371. 0.737		
2	* A22 1033031. 0.960	C04 1059256. 0.984	A16 998730. 0.928		+ C02 945308. 0.878
3	*	A42 1100218. 1.022	* B59 1195200. 1.110	A33 1094294. 1.017	* B21 1055654. 0.981
4	*	A52 1201197. 1.116	B45 1230375. 1.143	A01 1163434. 1.081	B15 1200845. 1.116
5	B48 1231617. 1.144	*	A23 1162015. 1.079	B03 1227355. 1.140	*
6	*	A26 1172839. 1.089	B13 1167960. 1.085		OCTANT BOUNDARY
7	B55 1267480. 1.177	A03 1172597. 1.089	*	B34 1210665. 1.125	LEGEND: + EDGE ASSEMBLY. MEASURED LA-140 MULTIPLIED BY 1.03 BEFORE NORMALIZATION * FLUX MAPPING INSTRUMENTATION IN THIS ASSEMBLY LOCATION
8	A29 1277386. 1.187		Z 12 XXXXXX X.XXX		ASSEMBLY SERIAL NO. UNNORMALIZED LA-140 NORMALIZED LA-140 AVERAGE OVER 28 ASSEMBLIES (B34 EXCLUDED) = 1.0

Figure A-11. Planar La-140 Distribution at 129 Inches Above Bottom of Active Fuel

ZION-2 EOC1 BENCHMARK GAMMA SCAN
FEBRUARY 1977

H	G	F	E	D	C
1 + C12 446249. 0.740		* + C50 437584. 0.725			
2 * A22 617142. 1.023	C04 593910. 0.984	A16 588320. 0.975		+ C02 525108. 0.870	+ C63 339361. 0.562
3 * A42 674924. 1.119		* B59 644059. 1.068	A33 635674. 1.054	* B21 530450. 0.879.	
4 * A52 592912. 0.983	B45 687978. 1.140	A01 629996. 1.044	B15 605189. 1.003		
5 B48 714830. 1.185	* A23 710128. 1.177	B03 705766. 1.170	* A14 691048. 1.145		OCTANT BOUNDARY
6 * A26 709499. 1.176	B13 682592. 1.131				
7 B55 699784. 1.160	A03 723697. 1.200	* B34 695751. 1.153			
8 A29 647232. 1.073		Z 12 XXXXXX X.XXX			

LEGEND:

+ EDGE ASSEMBLY. MEASURED LA-140
MULTIPLIED BY 1.03 BEFORE NORMALIZATION

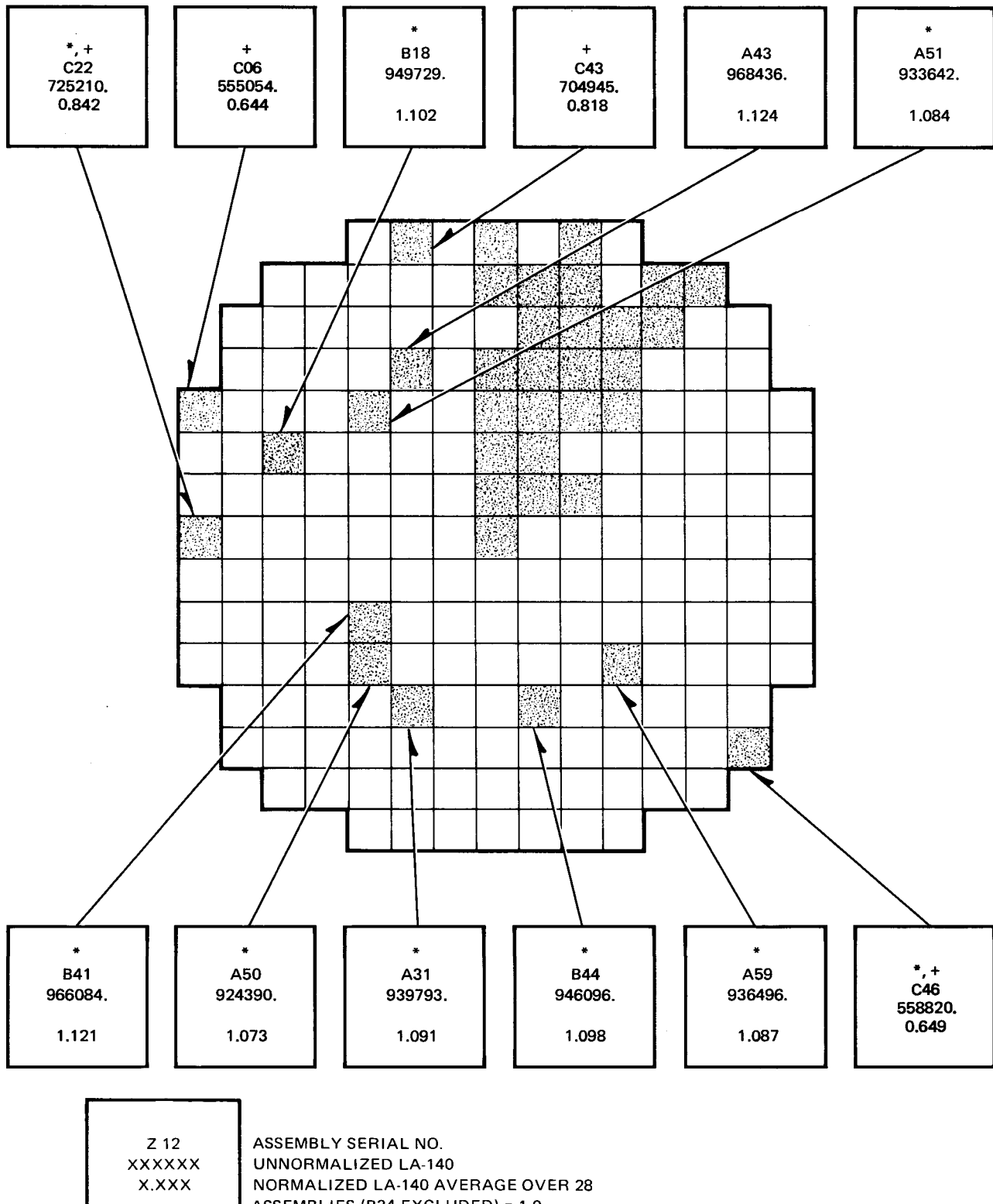
* FLUX MAPPING INSTRUMENTATION IN THIS
ASSEMBLY LOCATION

ASSEMBLY SERIAL NO.
UNNORMALIZED LA-140
NORMALIZED LA-140 AVERAGE OVER 28
ASSEMBLIES (B34 EXCLUDED) = 1.0

Figure A-12. Planar La-140 Distribution at 141 Inches Above Bottom of Active Fuel

APPENDIX B
PLANAR DISPLAYS OF THE OTHER
12 ASSEMBLIES MEASURED

ZION-2 EOC1 BENCHMARK GAMMA SCAN
FEBRUARY 1977



Z 12
XXXXXX
X.XXX

ASSEMBLY SERIAL NO.
UNNORMALIZED LA-140
NORMALIZED LA-140 AVERAGE OVER 28
ASSEMBLIES (B34 EXCLUDED) = 1.0

LEGEND:

- + EDGE ASSEMBLY. MEASURED LA-140 MULTIPLIED BY 1.03 BEFORE NORMALIZATION
- * FLUX MAPPING INSTRUMENTATION IN THIS ASSEMBLY LOCATION

Figure B-1. Planar La-140 Distribution at 9 Inches Above Bottom of Active Fuel

ZION-2 EOC1 BENCHMARK GAMMA SCAN
FEBRUARY 1977

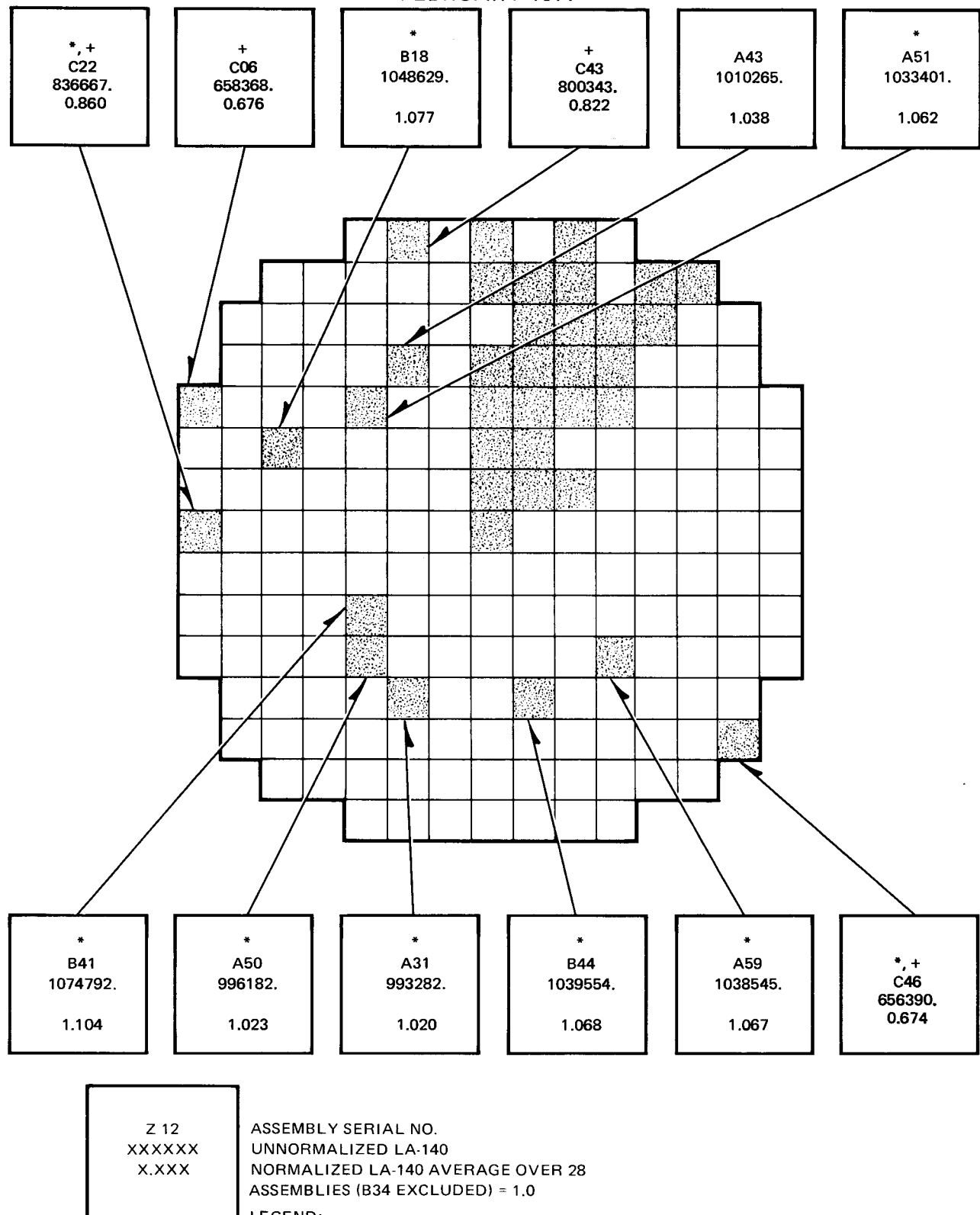
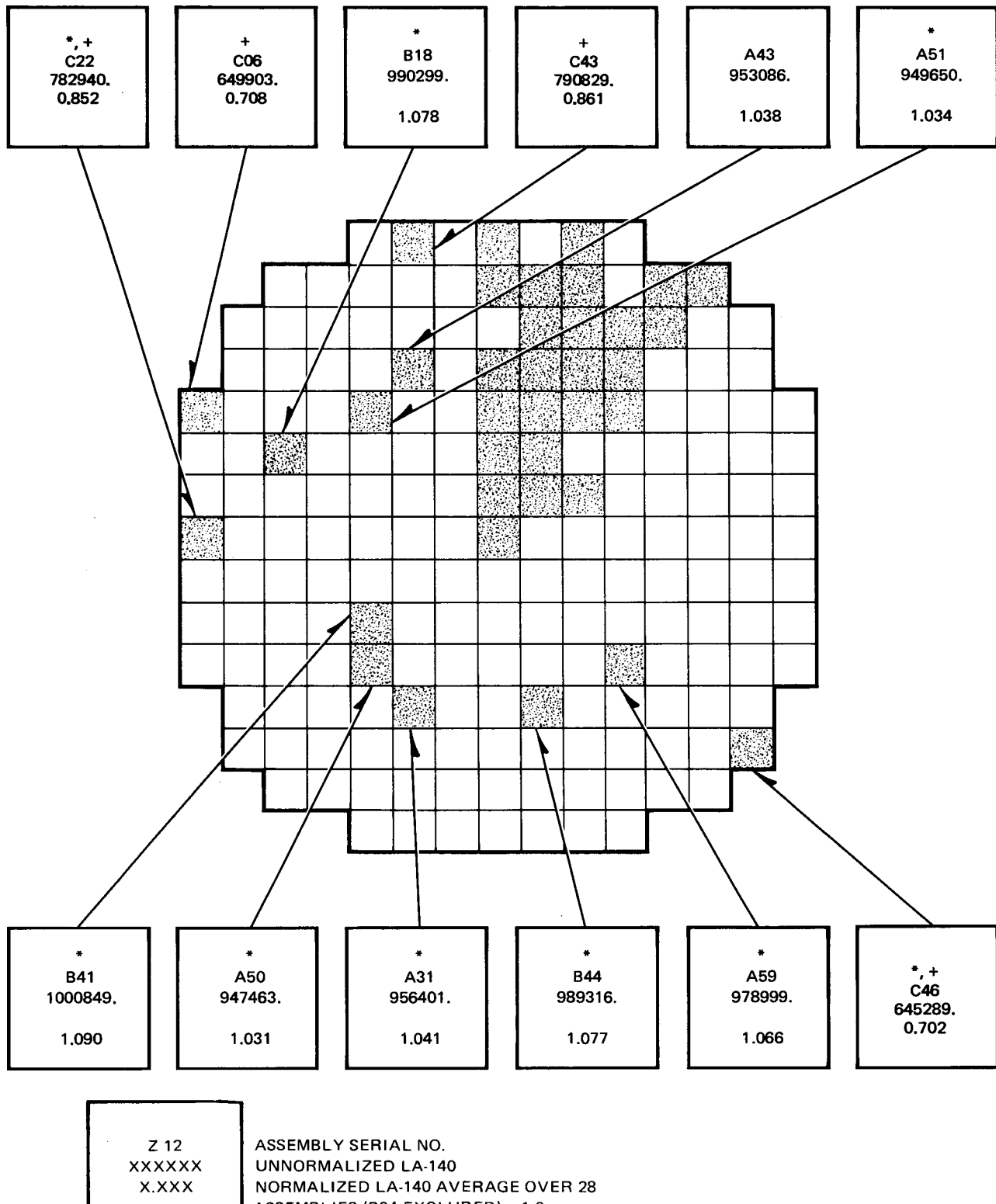


Figure B-2. Planar La-140 Distribution at 21 Inches Above Bottom of Active Fuel

ZION-2 EOC1 BENCHMARK GAMMA SCAN
FEBRUARY 1977



Z 12
XXXXXX
X.XXX

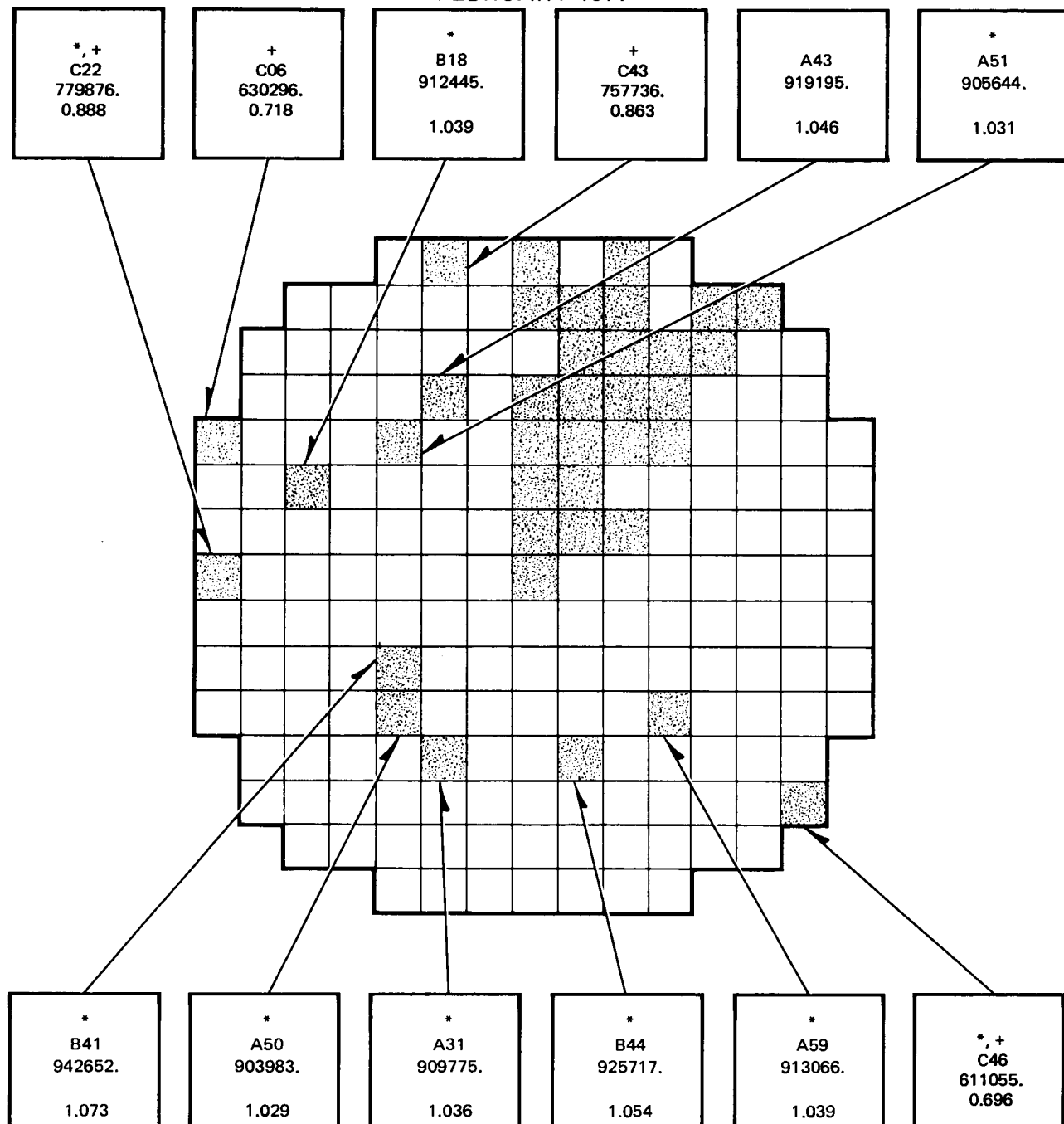
ASSEMBLY SERIAL NO.
UNNORMALIZED LA-140
NORMALIZED LA-140 AVERAGE OVER 28
ASSEMBLIES (B34 EXCLUDED) = 1.0

LEGEND:

- + EDGE ASSEMBLY. MEASURED LA-140 MULTIPLIED BY 1.03 BEFORE NORMALIZATION
- * FLUX MAPPING INSTRUMENTATION IN THIS ASSEMBLY LOCATION

Figure B-3. Planar La-140 Distribution at 33 Inches Above Bottom of Active Fuel

ZION-2 EOC1 BENCHMARK GAMMA SCAN
FEBRUARY 1977



Z 12
XXXXXX
X.XXX

ASSEMBLY SERIAL NO.
UNNORMALIZED LA-140
NORMALIZED LA-140 AVERAGE OVER 28
ASSEMBLIES (B34 EXCLUDED) = 1.0

LEGEND:

- + EDGE ASSEMBLY. MEASURED LA-140 MULTIPLIED BY 1.03 BEFORE NORMALIZATION
- * FLUX MAPPING INSTRUMENTATION IN THIS ASSEMBLY LOCATION

Figure B-4. Planar La-140 Distribution at 45 Inches Above Bottom of Active Fuel

ZION-2 EOC1 BENCHMARK GAMMA SCAN
FEBRUARY 1977

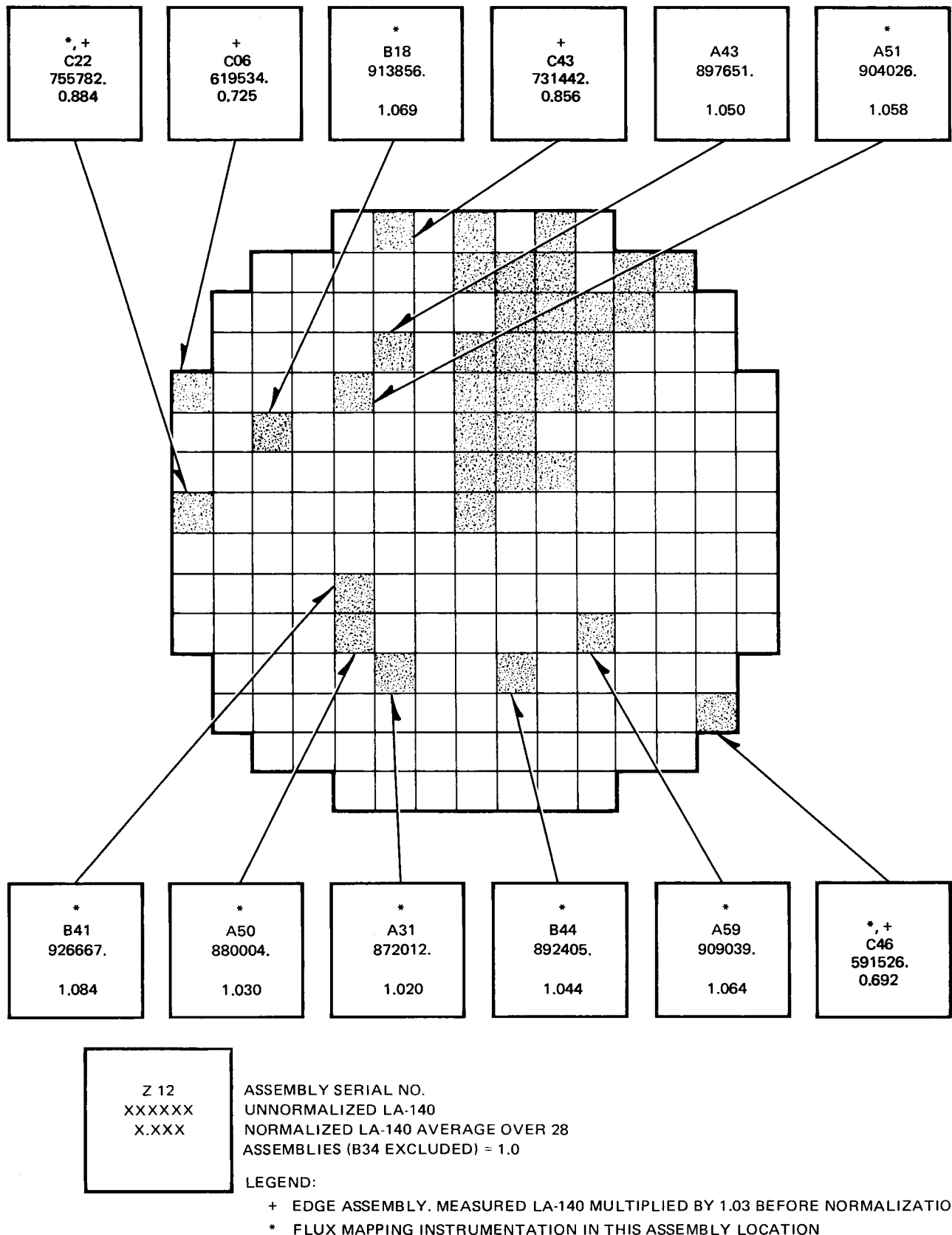
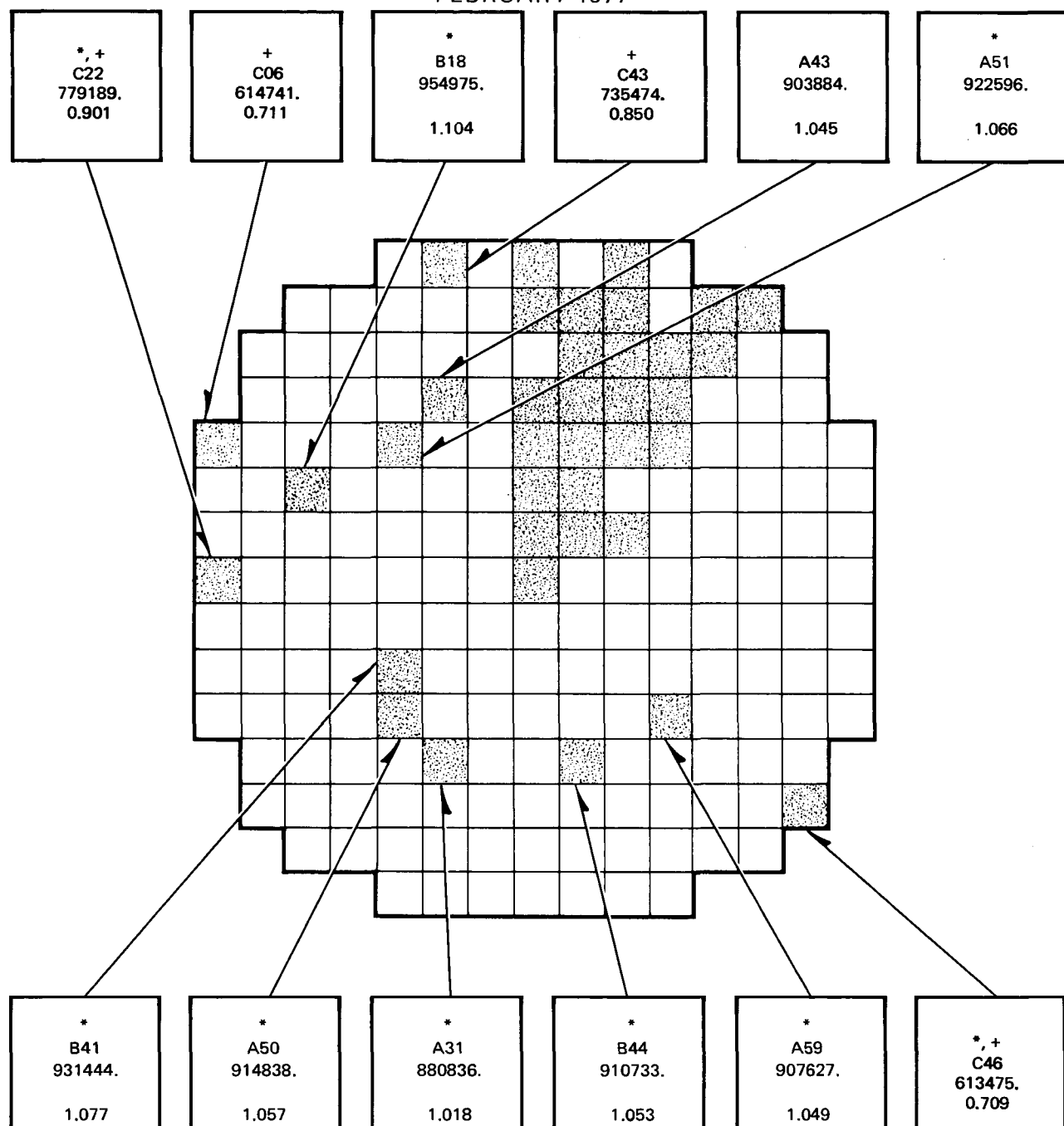


Figure B-5. Planar La-140 Distribution at 57 Inches Above Bottom of Active Fuel

ZION-2 EOC1 BENCHMARK GAMMA SCAN
FEBRUARY 1977



Z 12
XXXXXX
X.XXX

ASSEMBLY SERIAL NO.
UNNORMALIZED LA-140
NORMALIZED LA-140 AVERAGE OVER 28
ASSEMBLIES (B34 EXCLUDED) = 1.0

LEGEND:

- + EDGE ASSEMBLY. MEASURED LA-140 MULTIPLIED BY 1.03 BEFORE NORMALIZATION
- * FLUX MAPPING INSTRUMENTATION IN THIS ASSEMBLY LOCATION

Figure B-6. Planar La-140 Distribution at 69 Inches Above Bottom of Active Fuel

ZION-2 EOC1 BENCHMARK GAMMA SCAN
FEBRUARY 1977

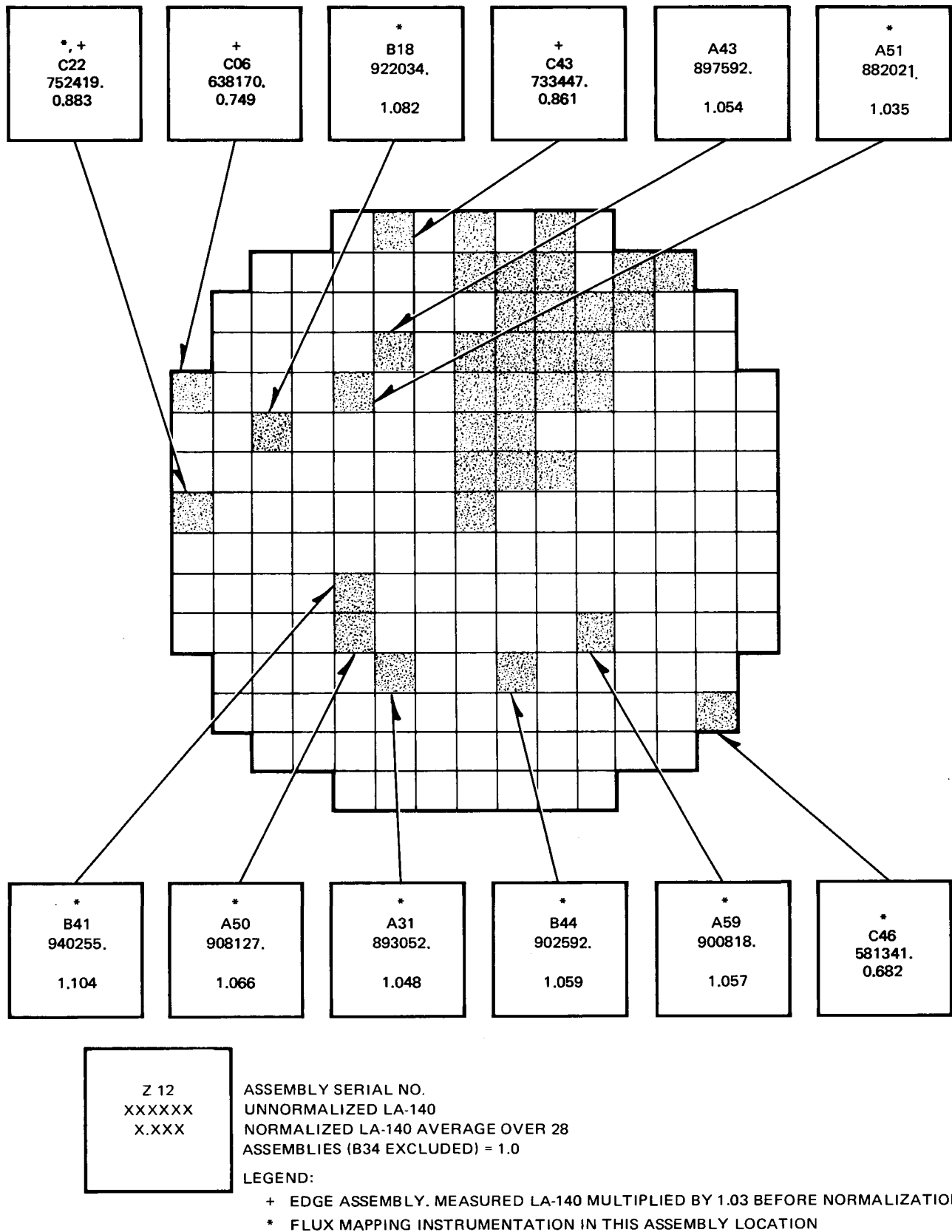


Figure B-7. Planar La-140 Distribution at 81 Inches Above Bottom of Active Fuel

ZION-2 EOC1 BENCHMARK GAMMA SCAN
FEBRUARY 1977

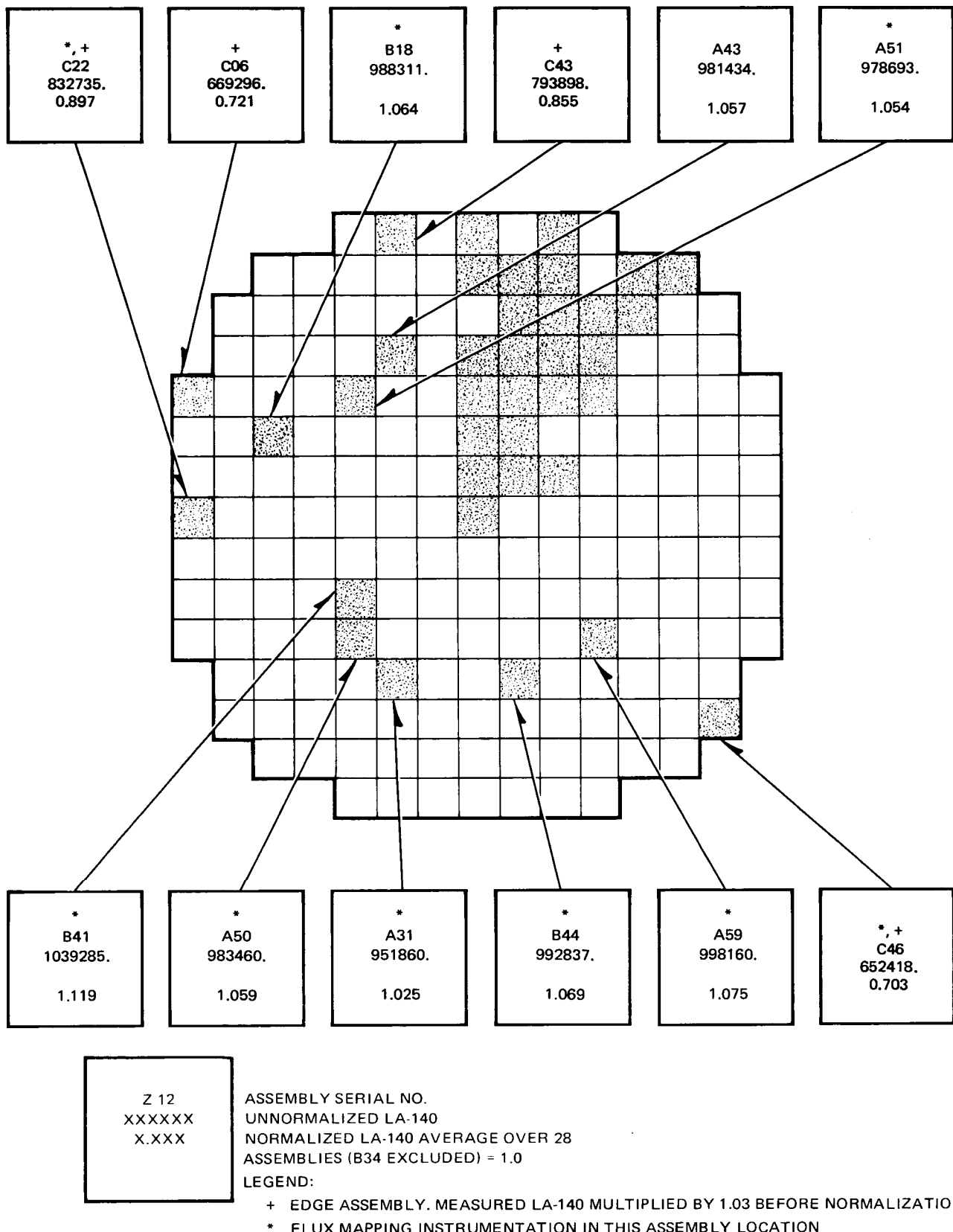


Figure B-8. Planar La-140 Distribution at 93 Inches Above Bottom of Active Fuel

ZION-2 EOC1 BENCHMARK GAMMA SCAN
FEBRUARY 1977

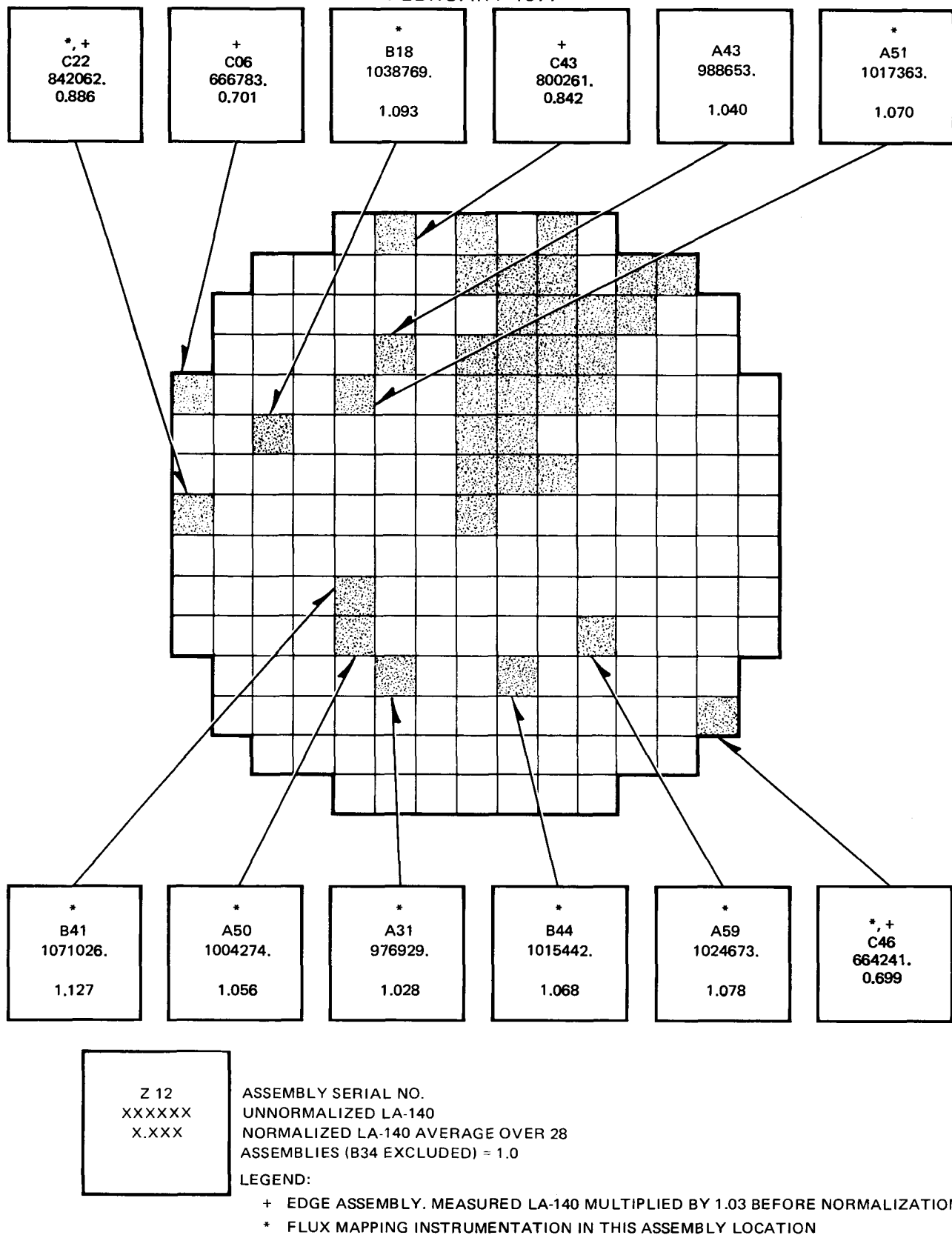


Figure B-9. Planar La-140 Distribution at 103 Inches Above Bottom of Active Fuel

ZION-2 EOC1 BENCHMARK GAMMA SCAN
FEBRUARY 1977

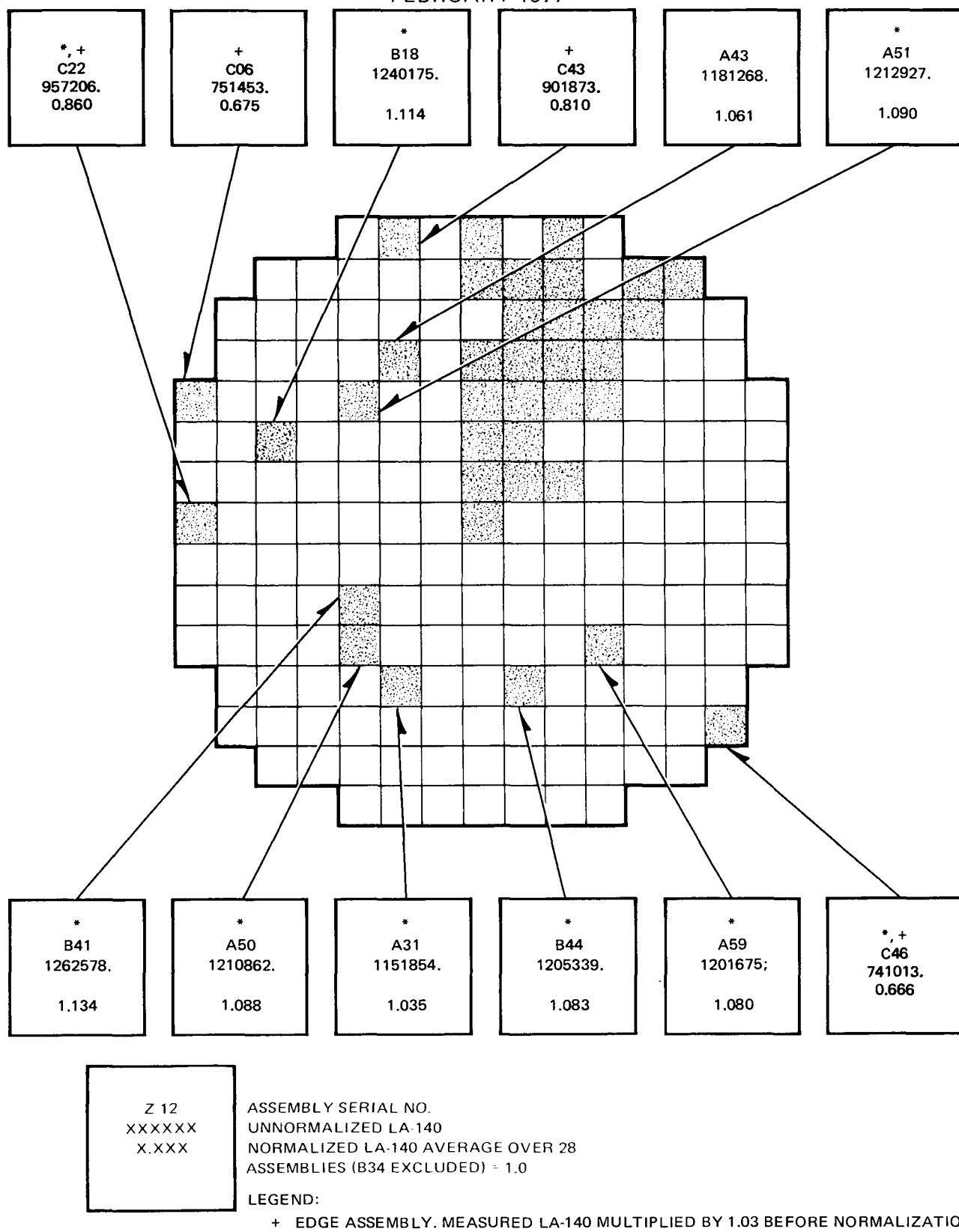


Figure B-10. Planar La-140 Distribution at 117 Inches Above Bottom of Active Fuel

ZION-2 EOC1 BENCHMARK GAMMA SCAN
FEBRUARY 1977

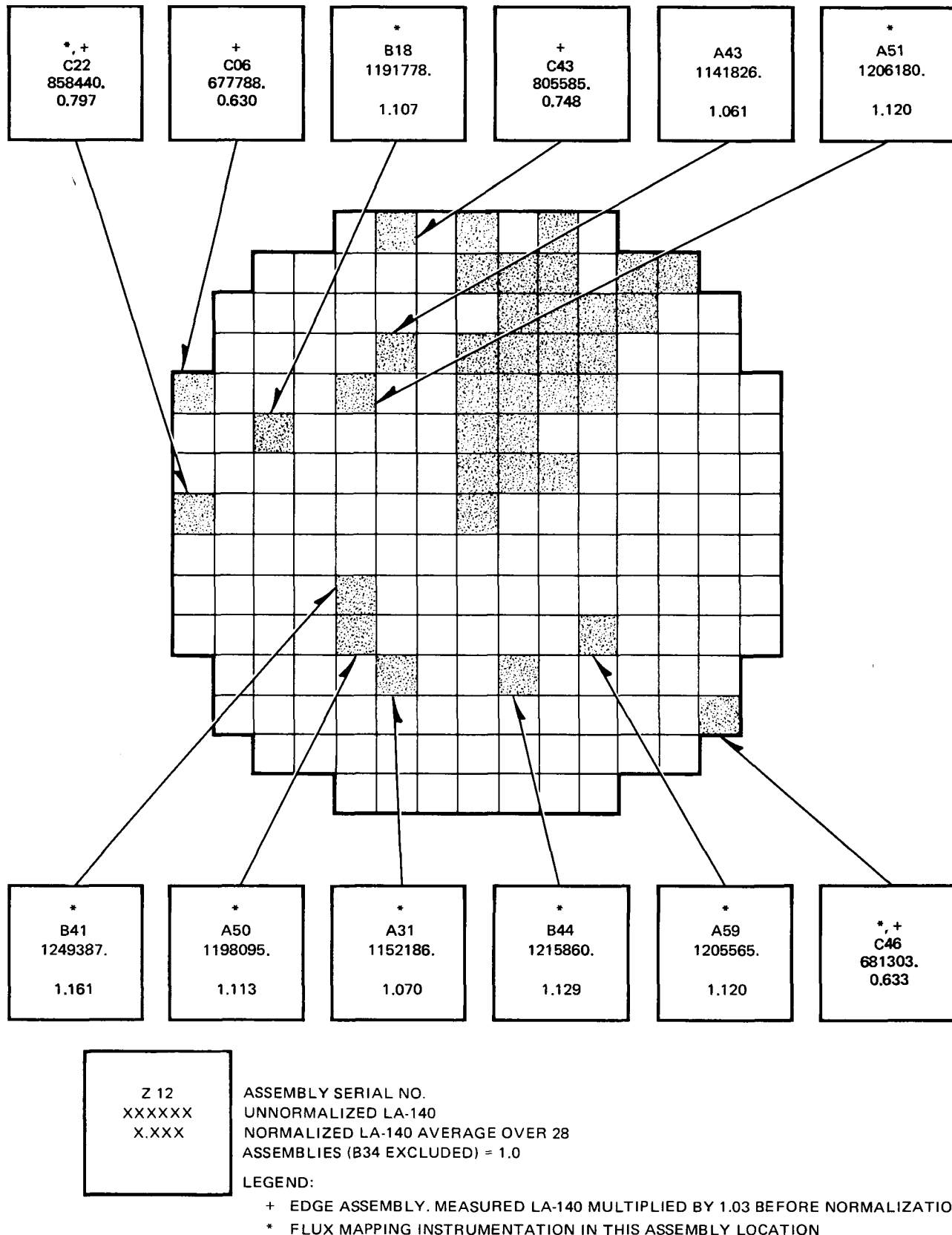


Figure B-11. Planar La-140 Distribution at 129 Inches Above Bottom of Active Fuel

ZION-2 EOC1 BENCHMARK GAMMA SCAN
FEBRUARY 1977

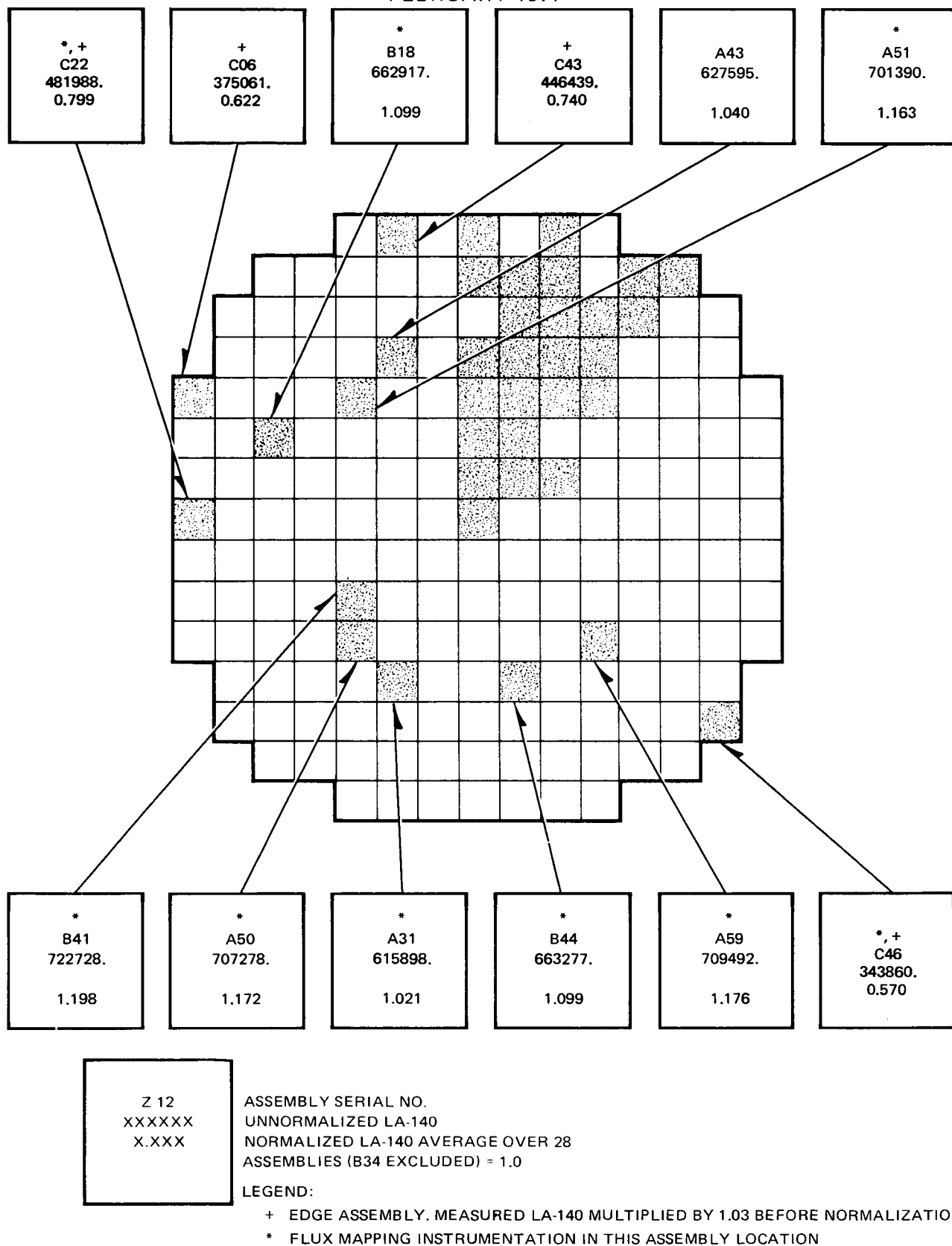


Figure B-12. Planar La-140 Distribution at 141 Inches Above Bottom of Active Fuel

APPENDIX C

**AXIAL PLOTS OF THE La-140 INTENSITY
FOR THE 37 ASSEMBLIES MEASURED**

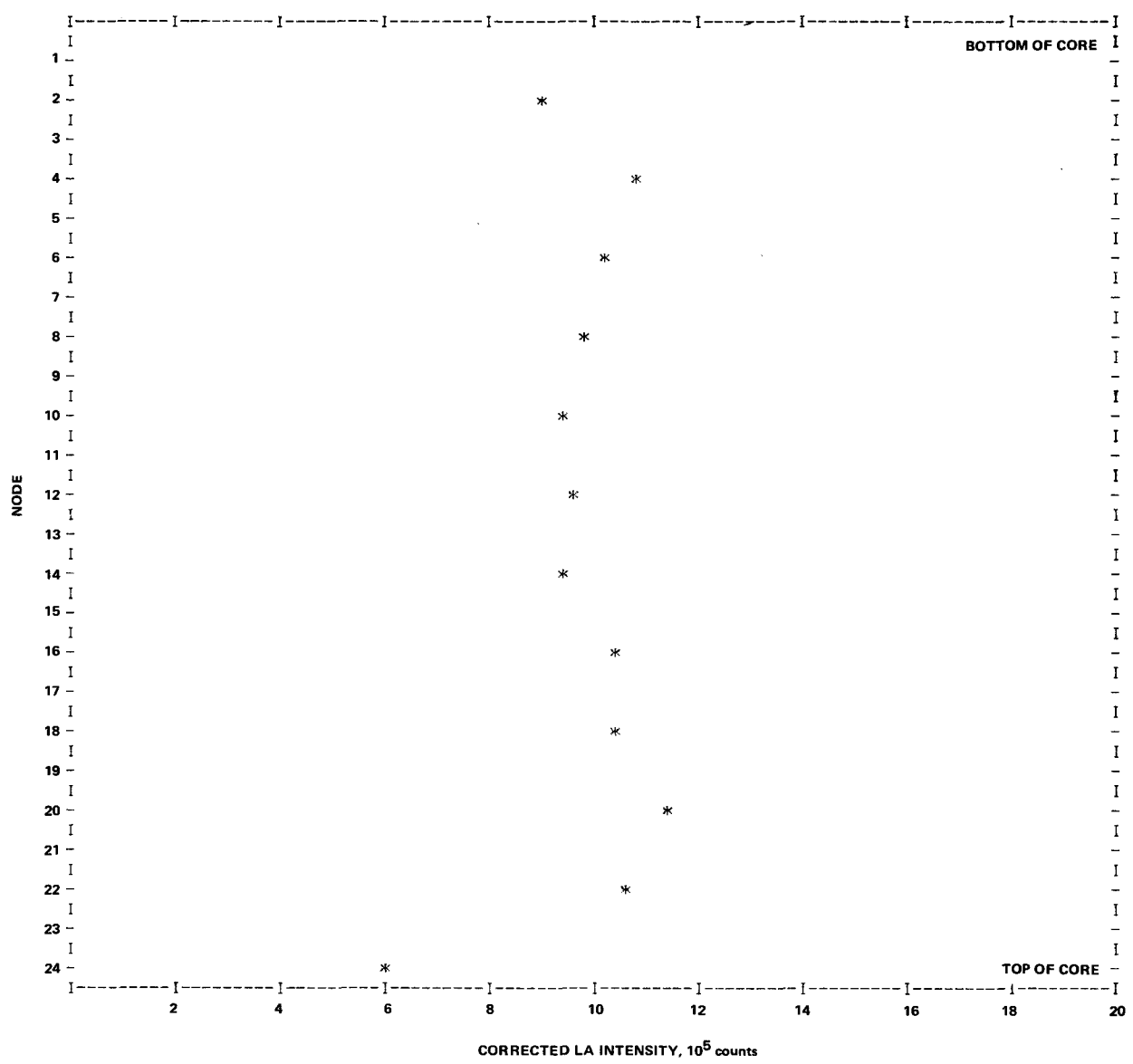


Figure C-1. Axial La-140 Intensity, Assembly C04

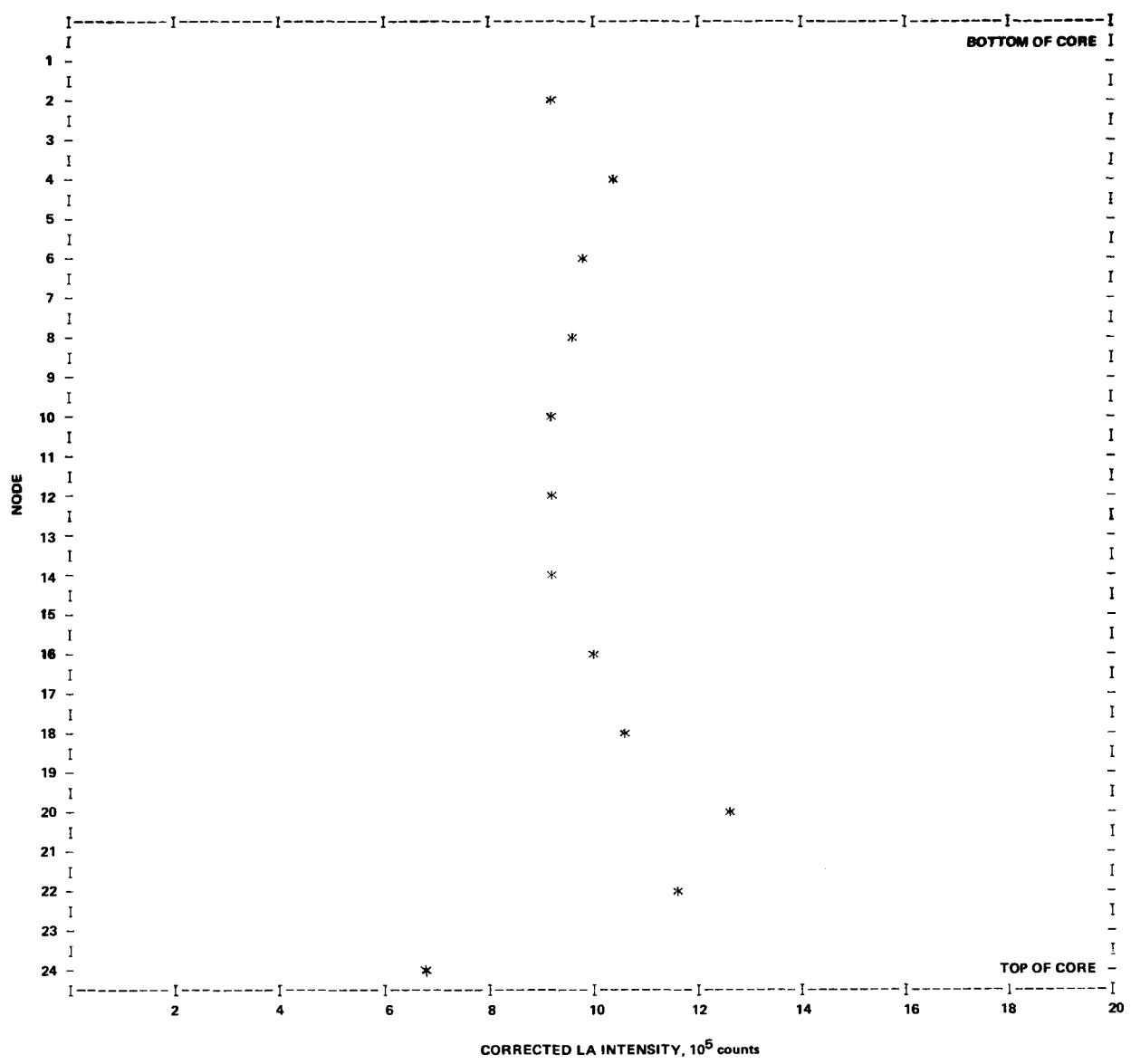


Figure C-2. Axial La-140 Intensity, Assembly B13

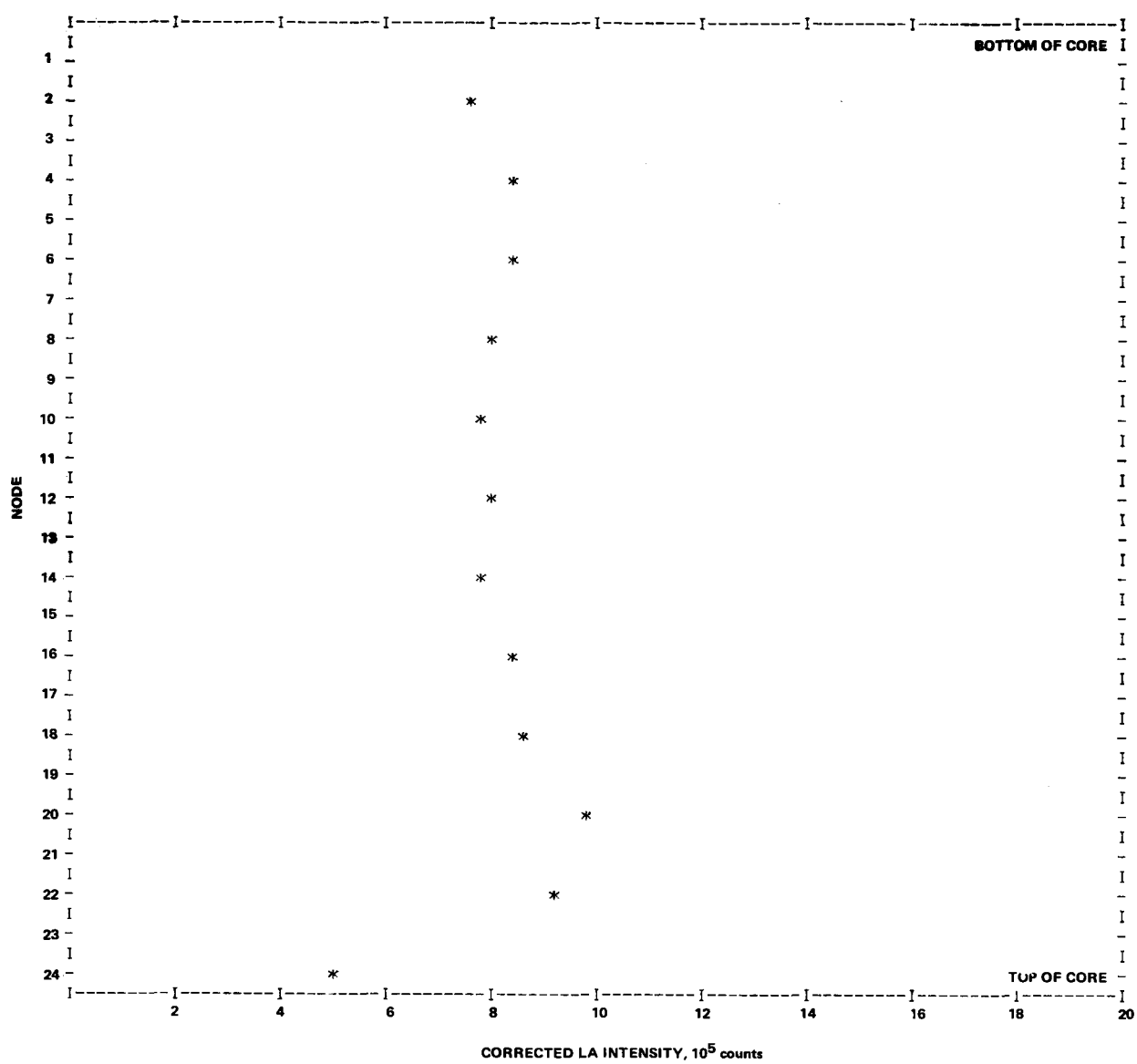


Figure C-3. Axial La-140 Intensity, Assembly C02

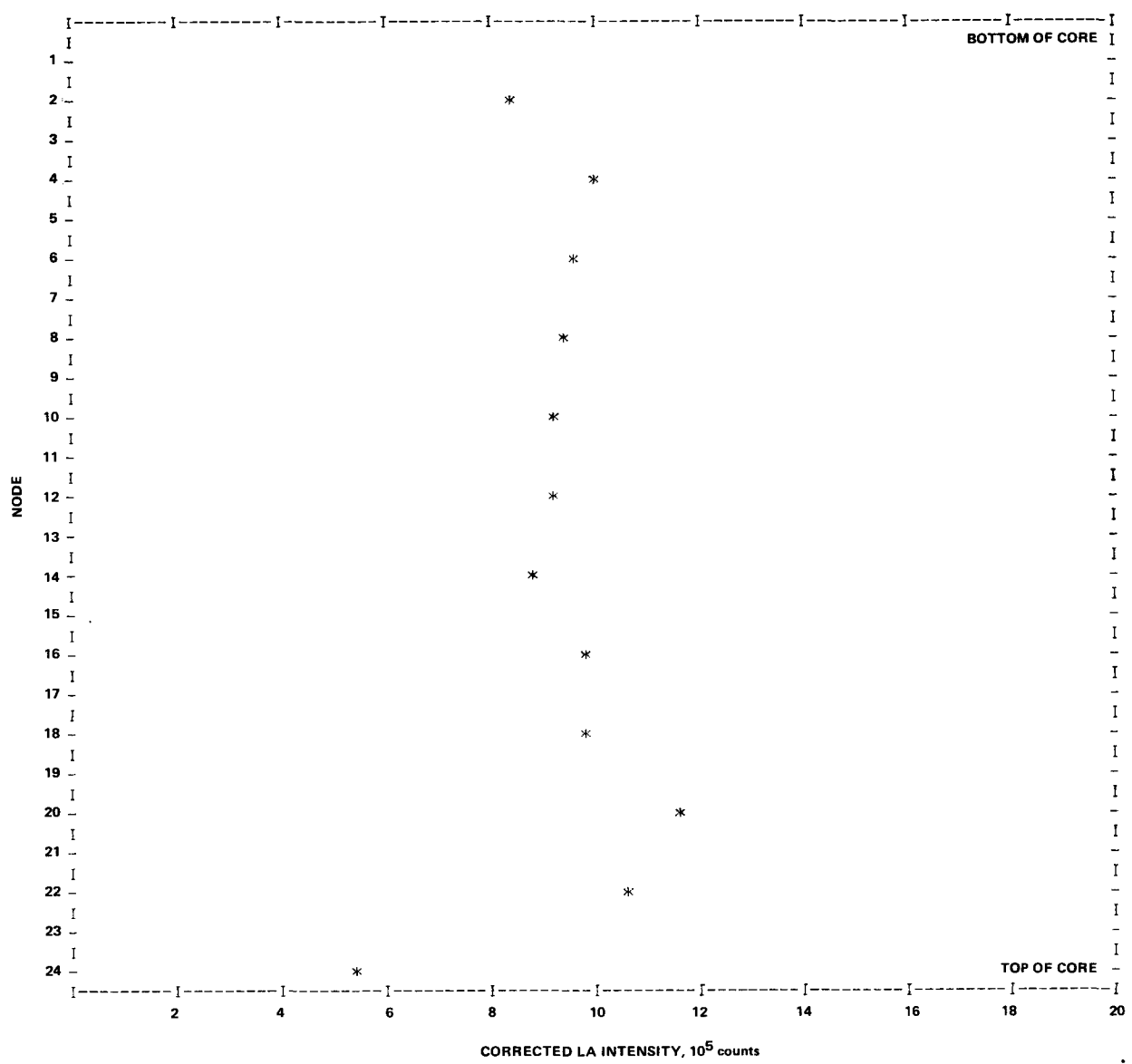


Figure C-4. Axial La-140 Intensity, Assembly B21

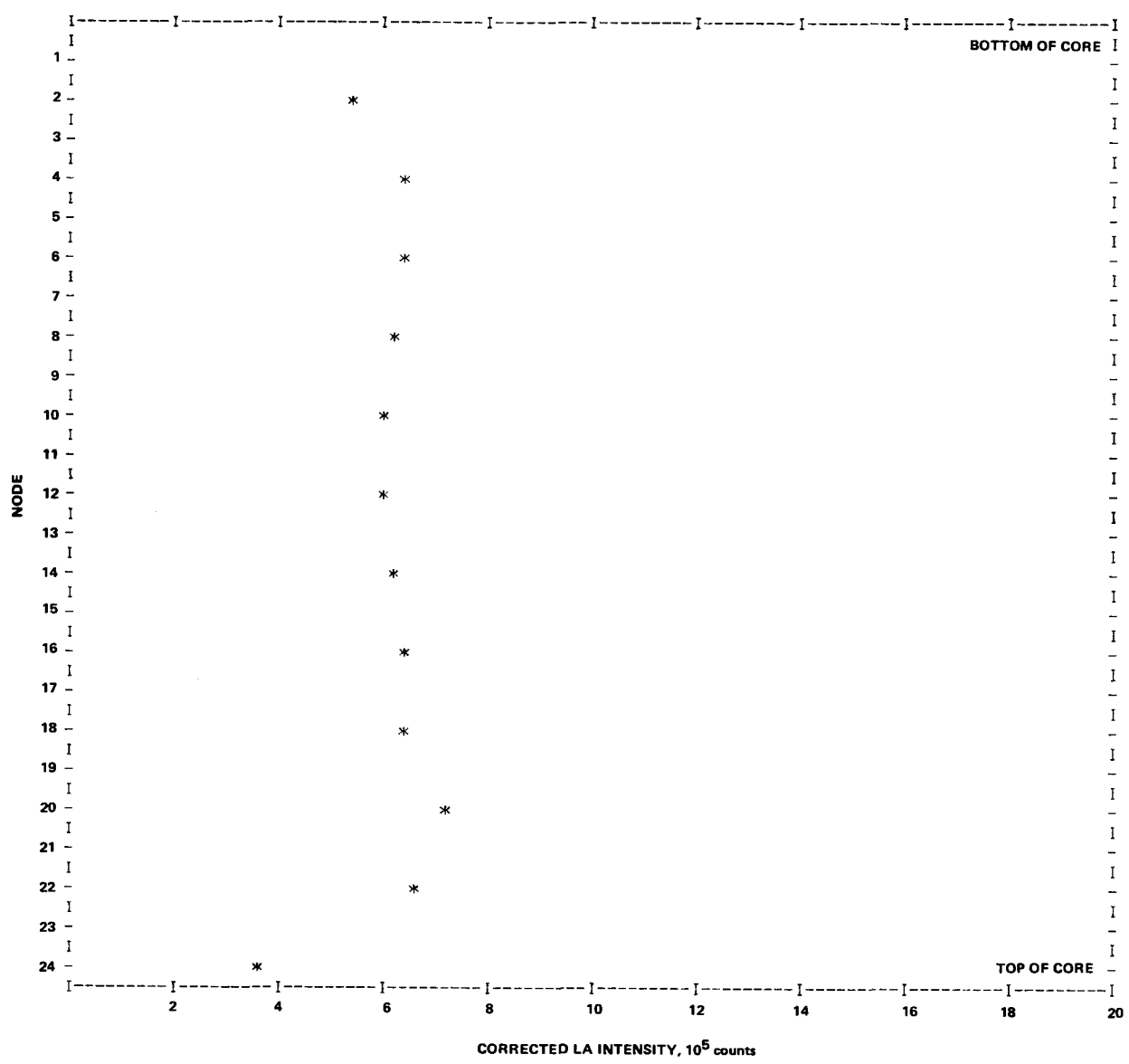


Figure C-5. Axial La-140 Intensity, Assembly C06

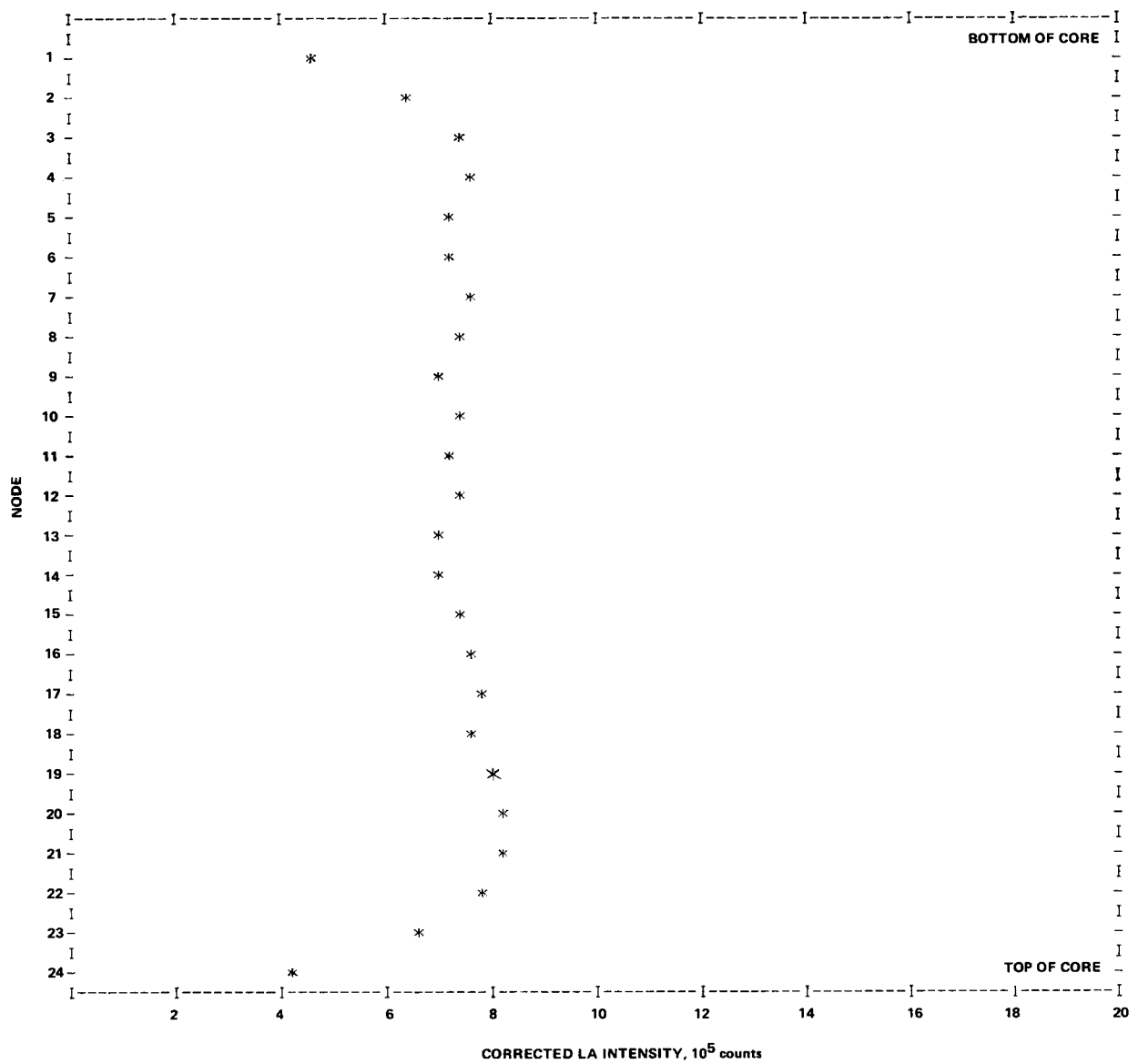


Figure C-6. Axial La-140 Intensity, Assembly C50

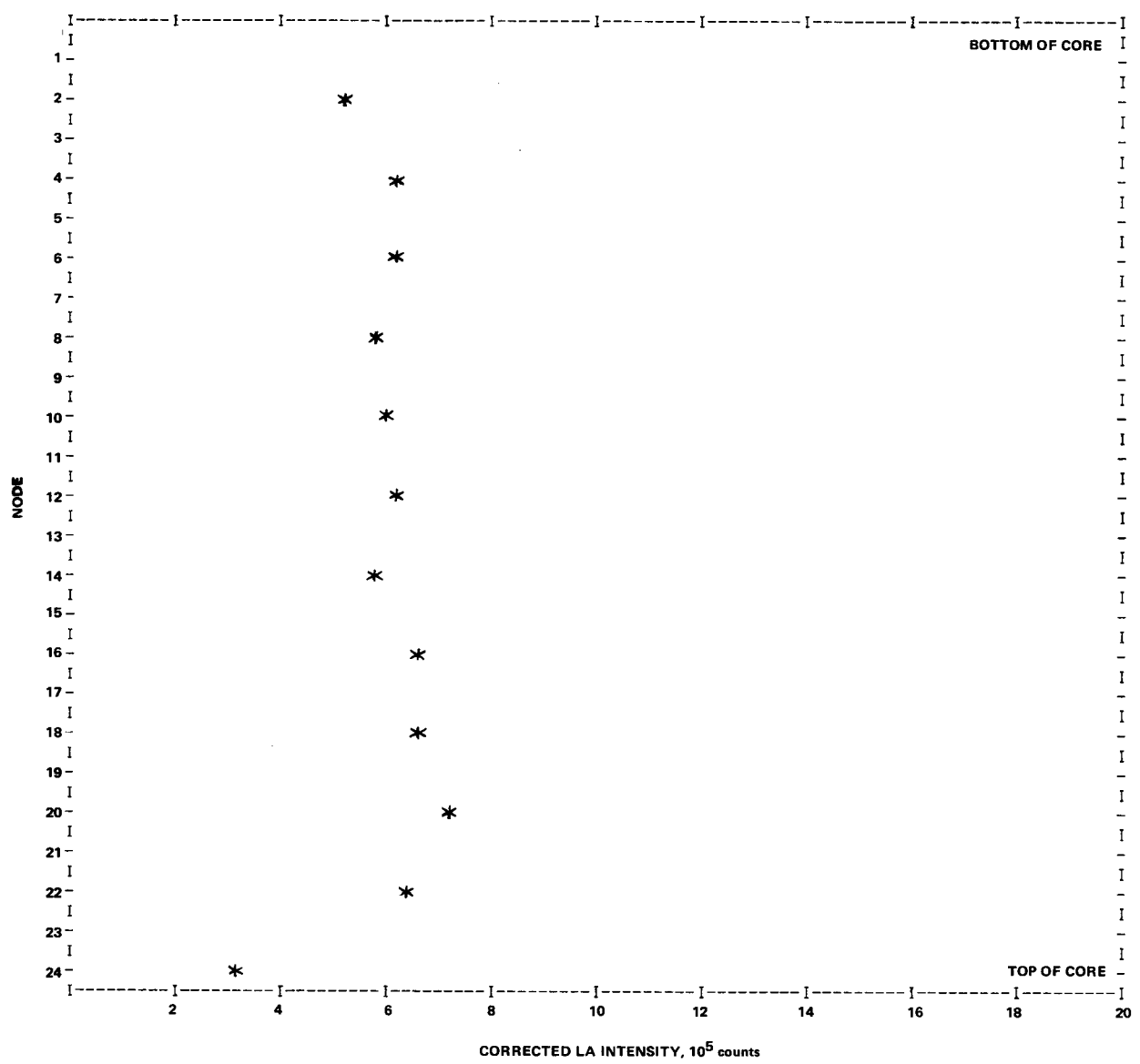


Figure C-7. Axial La-140 Intensity, Assembly C63

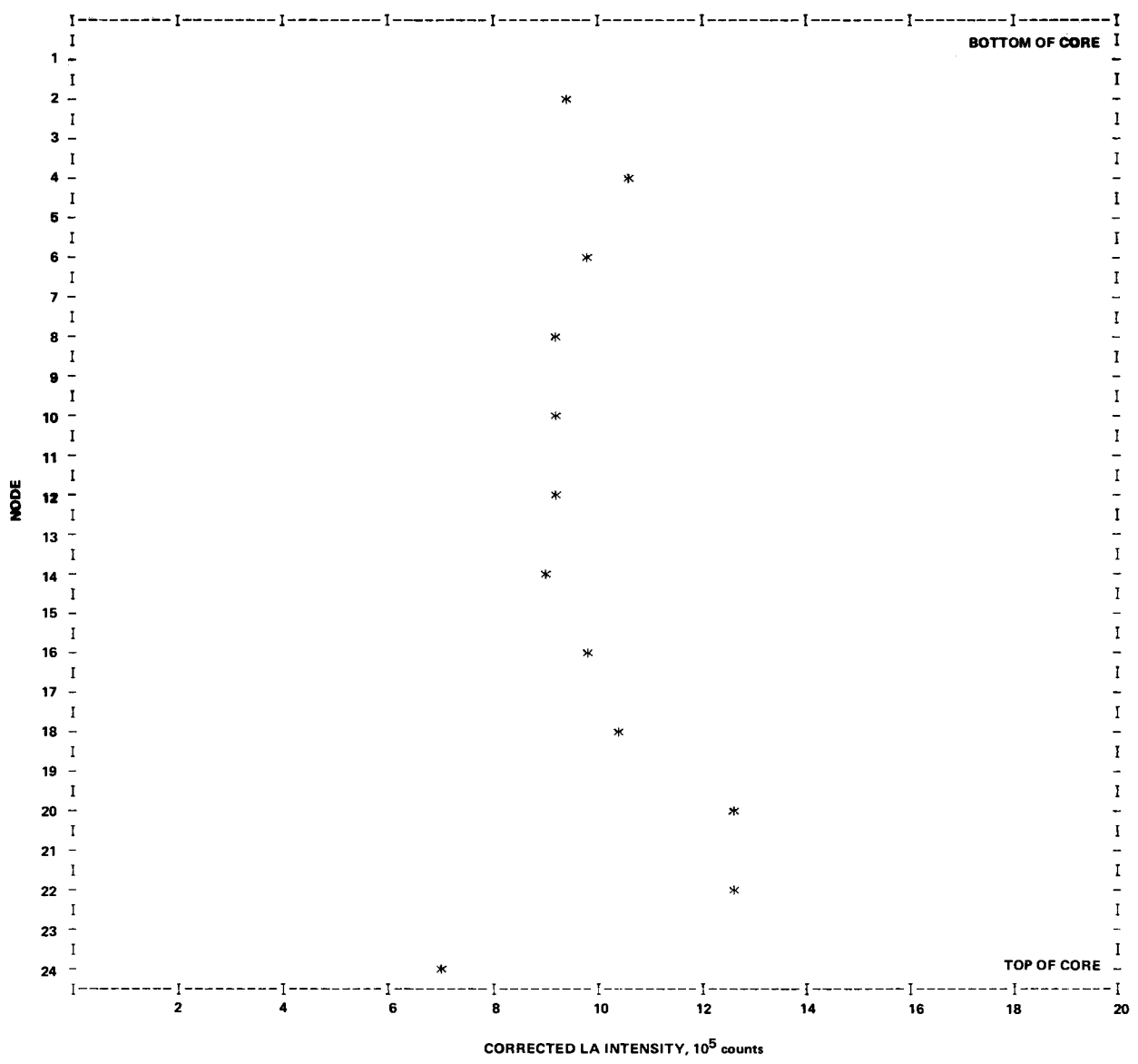


Figure C-8. Axial La-140 Intensity, Assembly B55

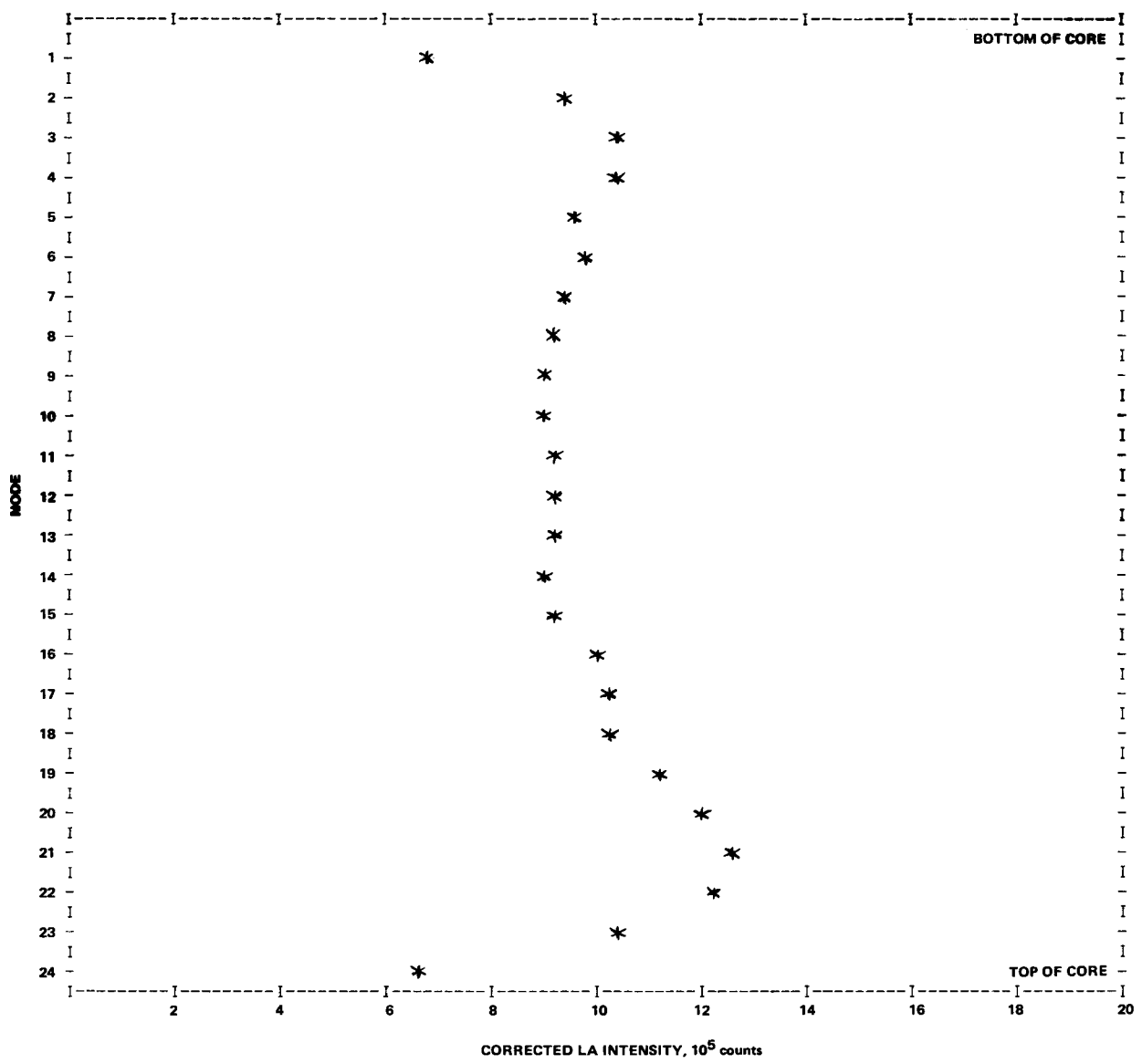


Figure C-9. Axial La-140 Intensity, Assembly B44

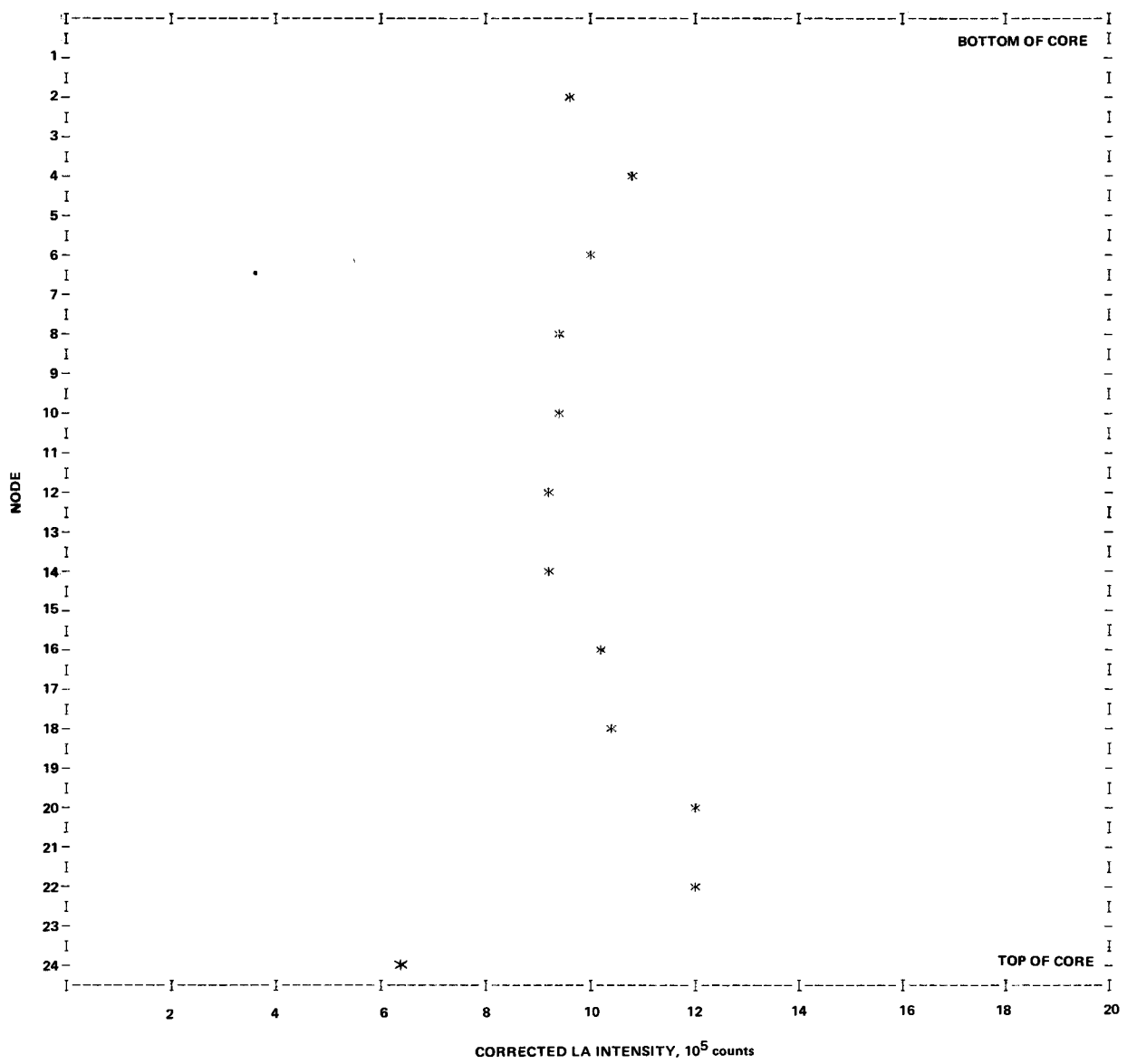


Figure C-10. Axial La-140 Intensity, Assembly B59

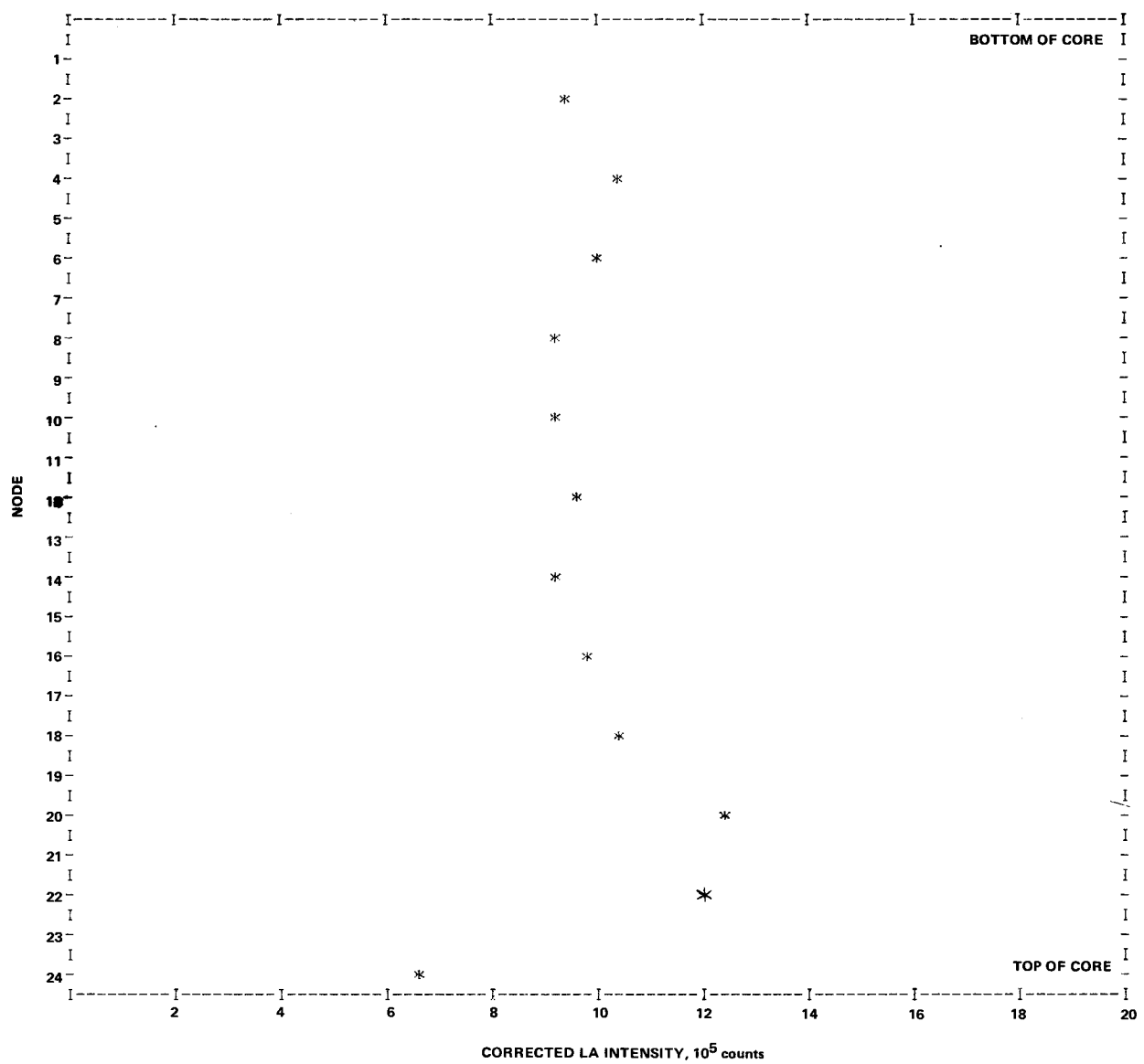


Figure C-11. Axial La-140 Intensity, Assembly B18

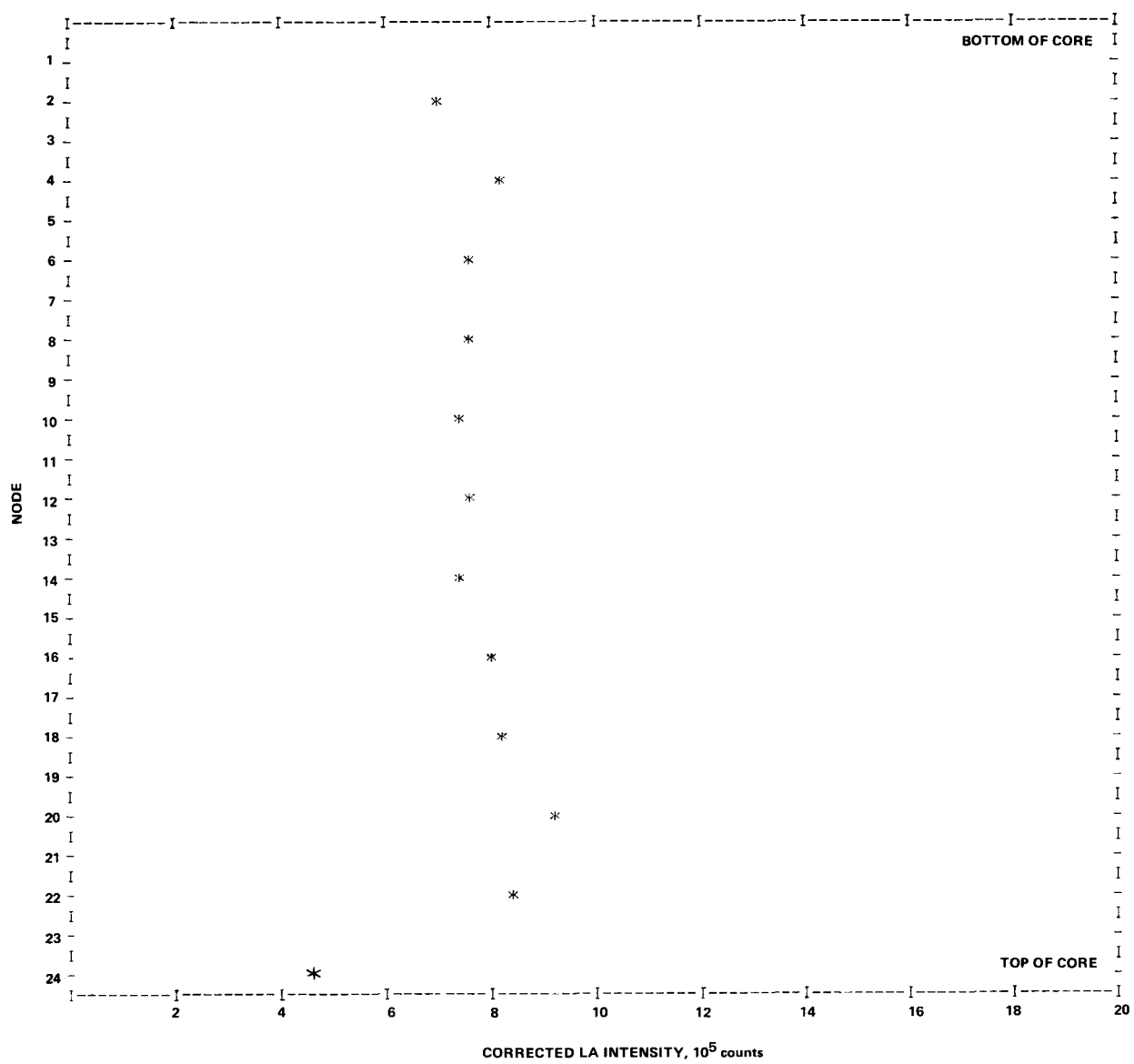


Figure C-12. Axial La-140 Intensity, Assembly C22

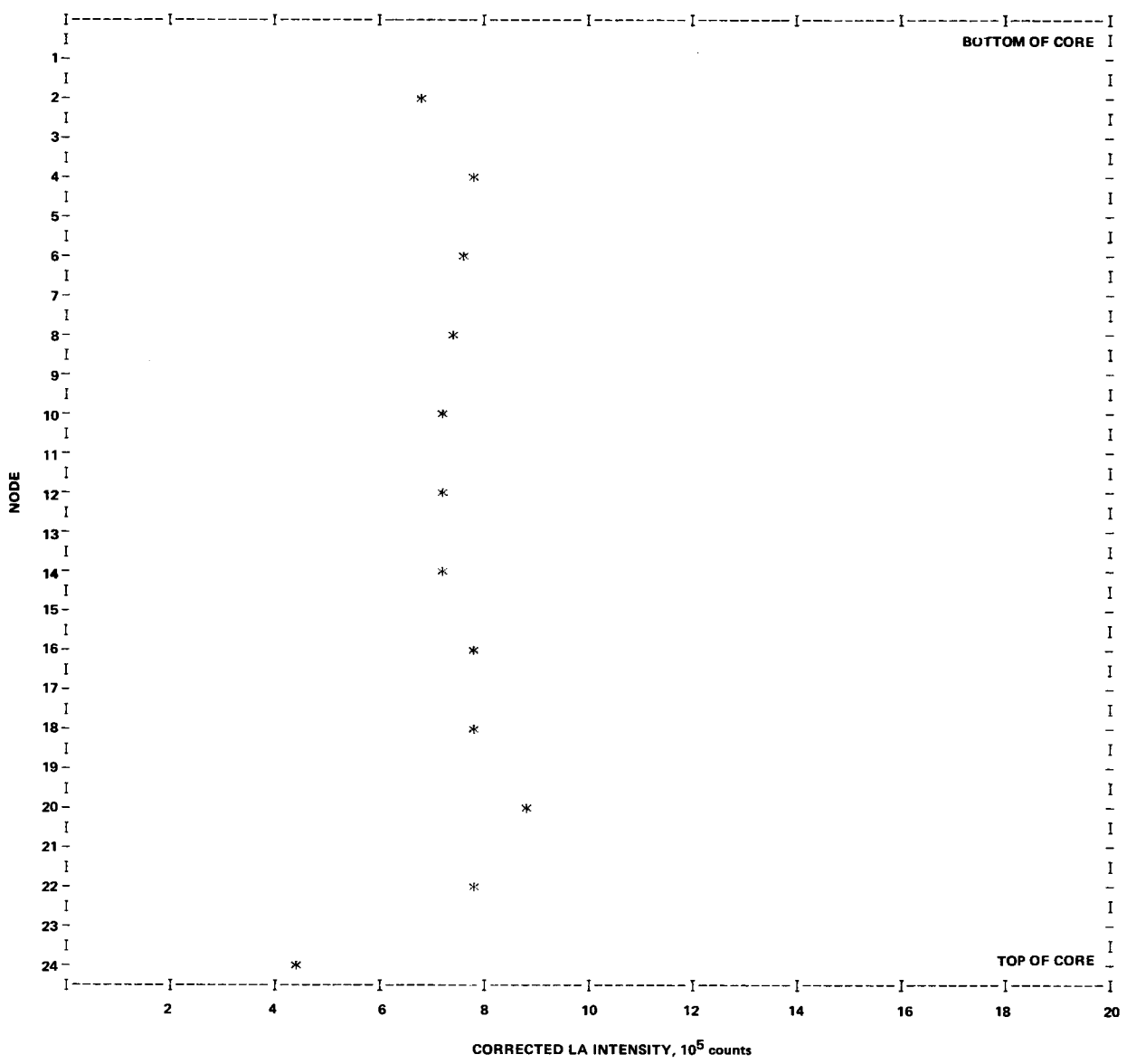


Figure C-13. Axial La-140 Intensity, Assembly C43

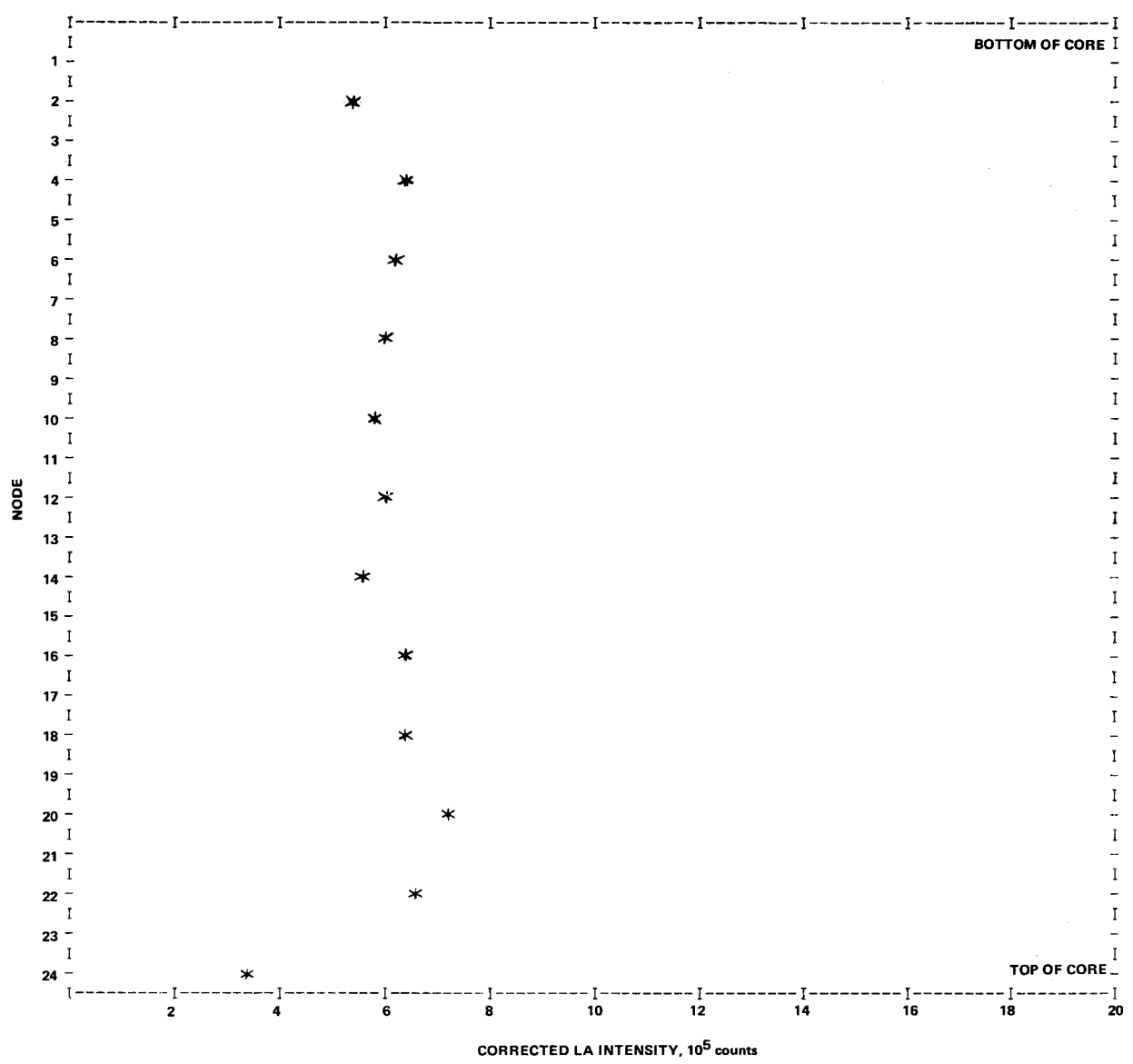


Figure C-14. Axial La-140 Intensity, Assembly C46

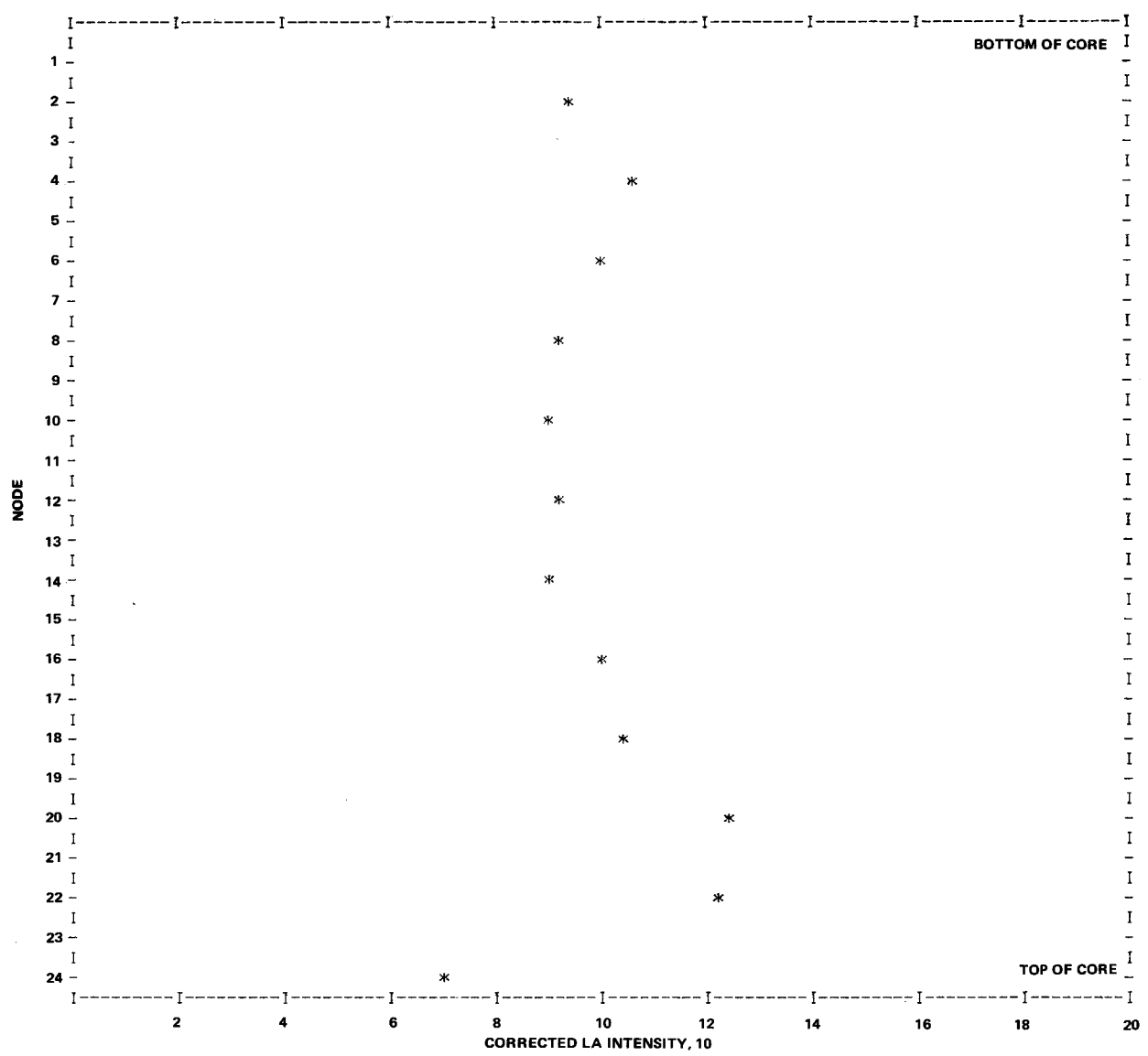


Figure C-15. Axial La-140 Intensity, Assembly B34

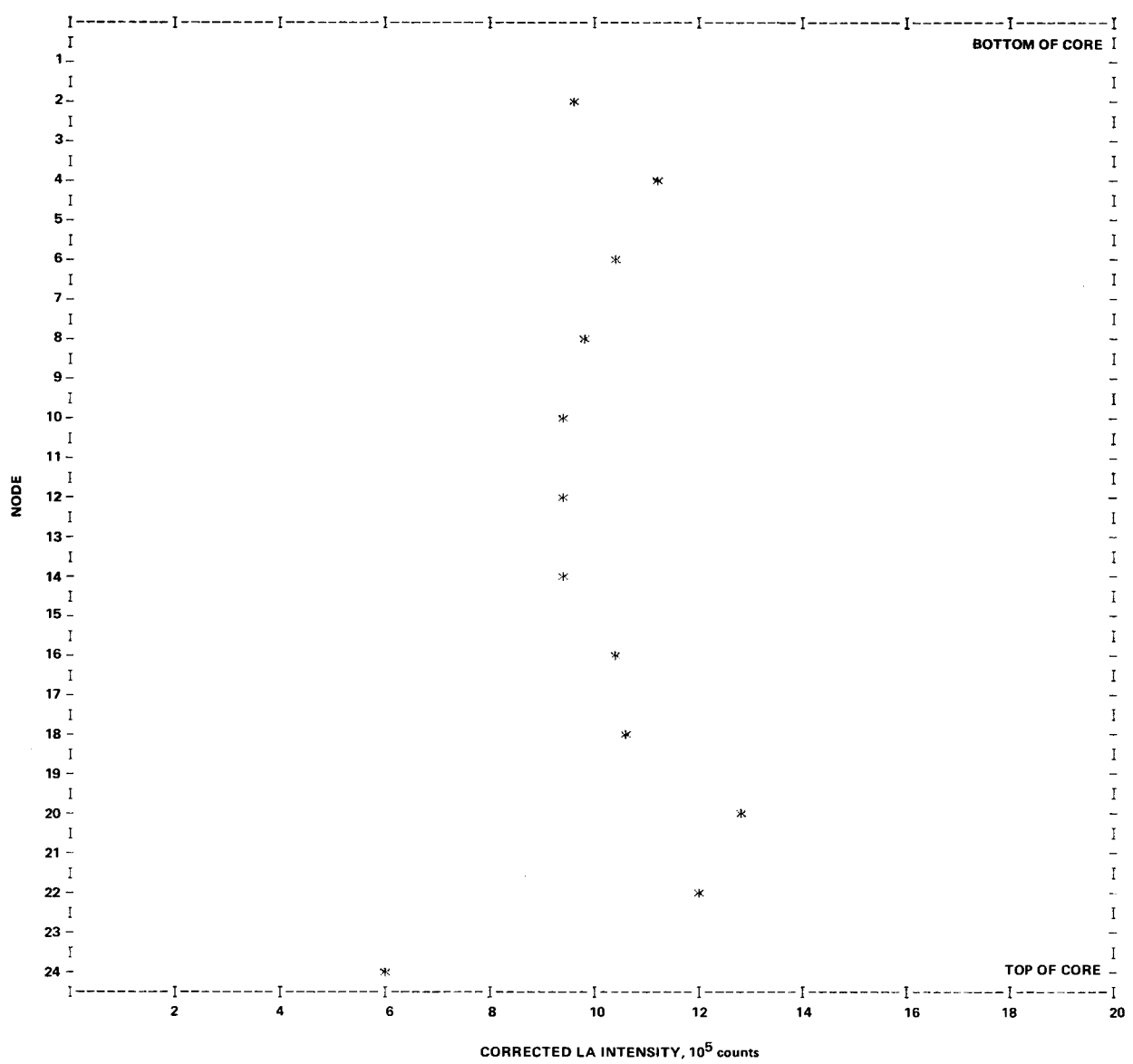


Figure C-16. Axial La-140 Intensity, Assembly B15

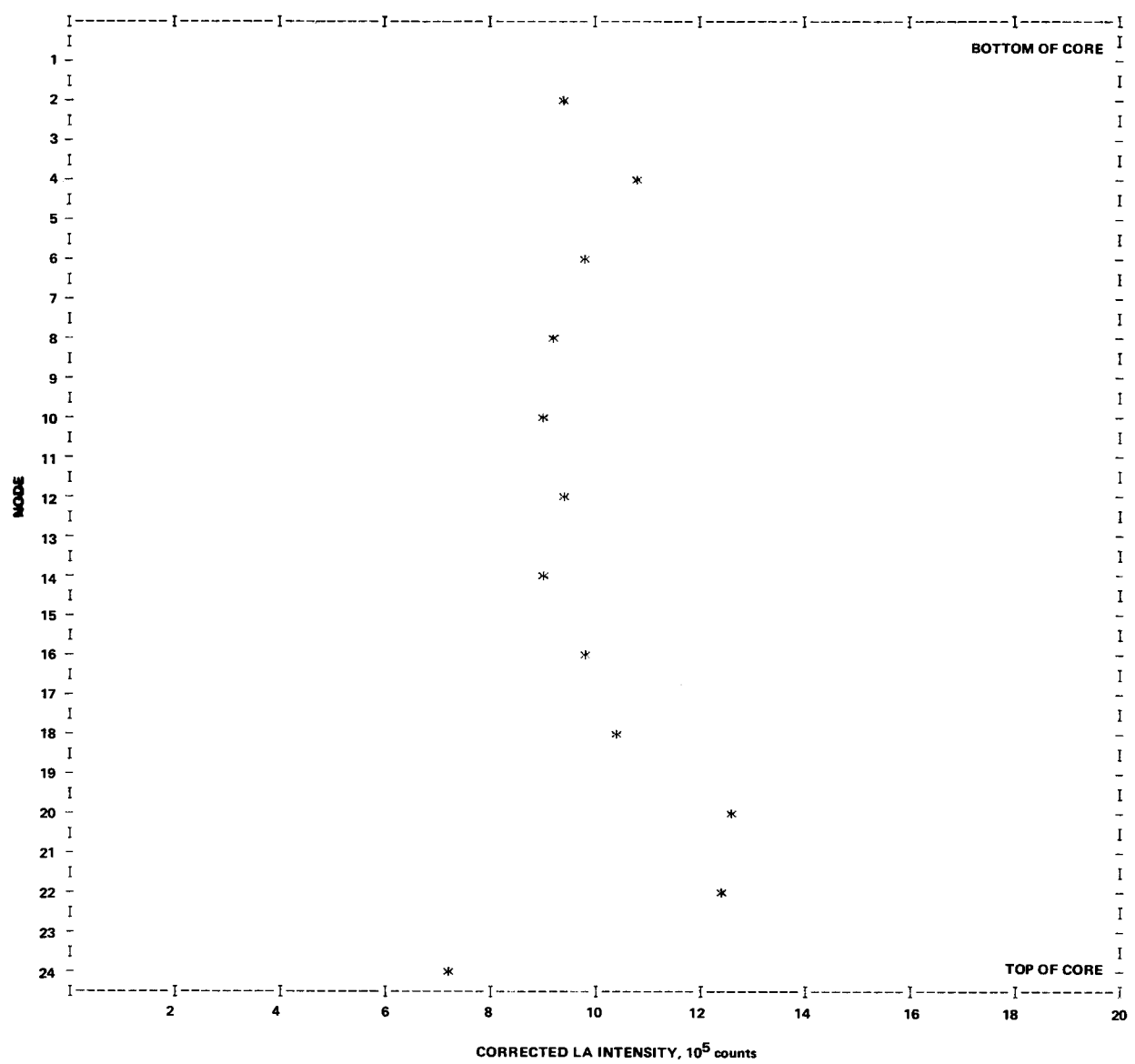


Figure C-17. Axial La-140 Intensity, Assembly B48

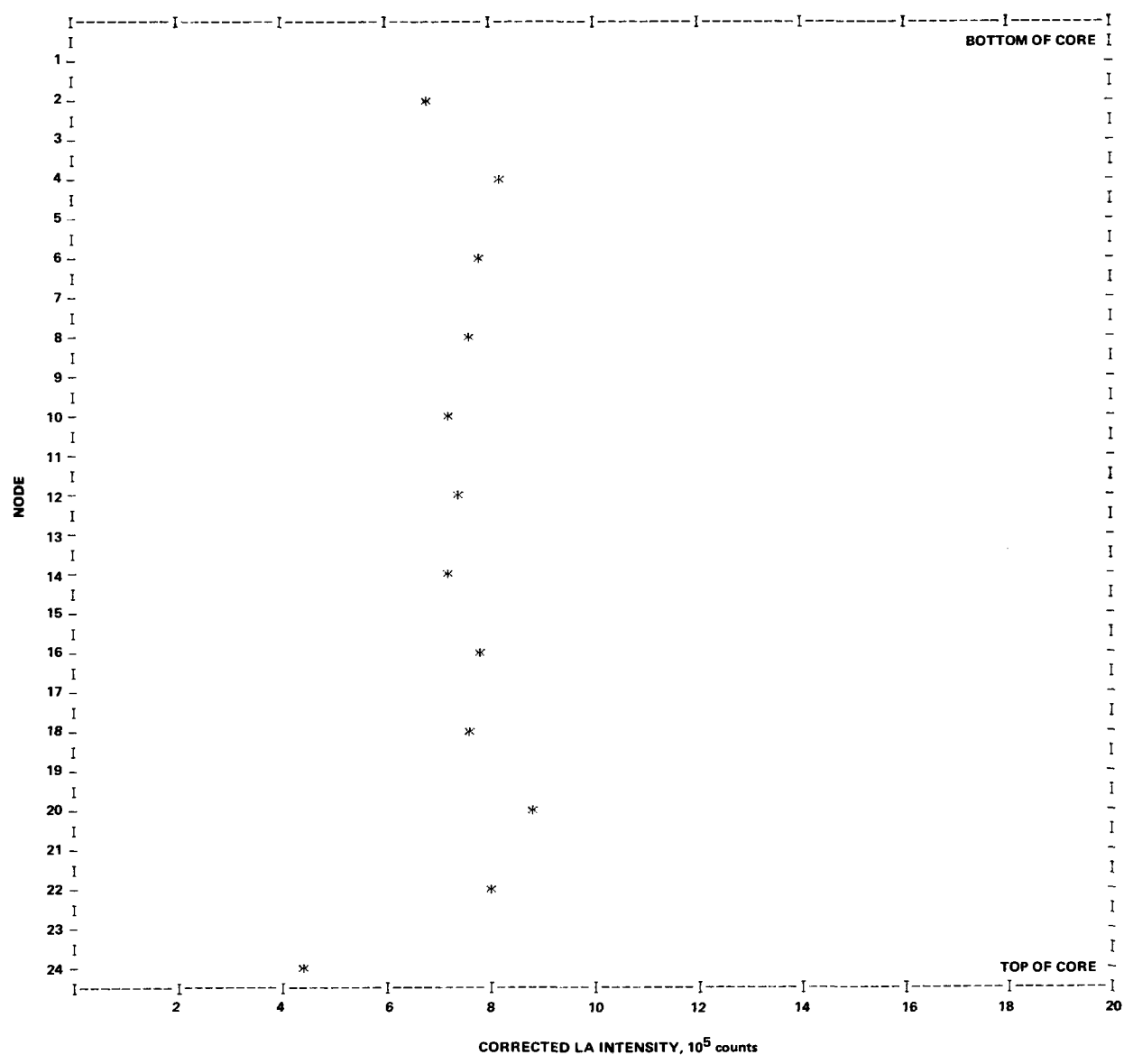


Figure C-18. Axial La-140 Intensity, Assembly C12

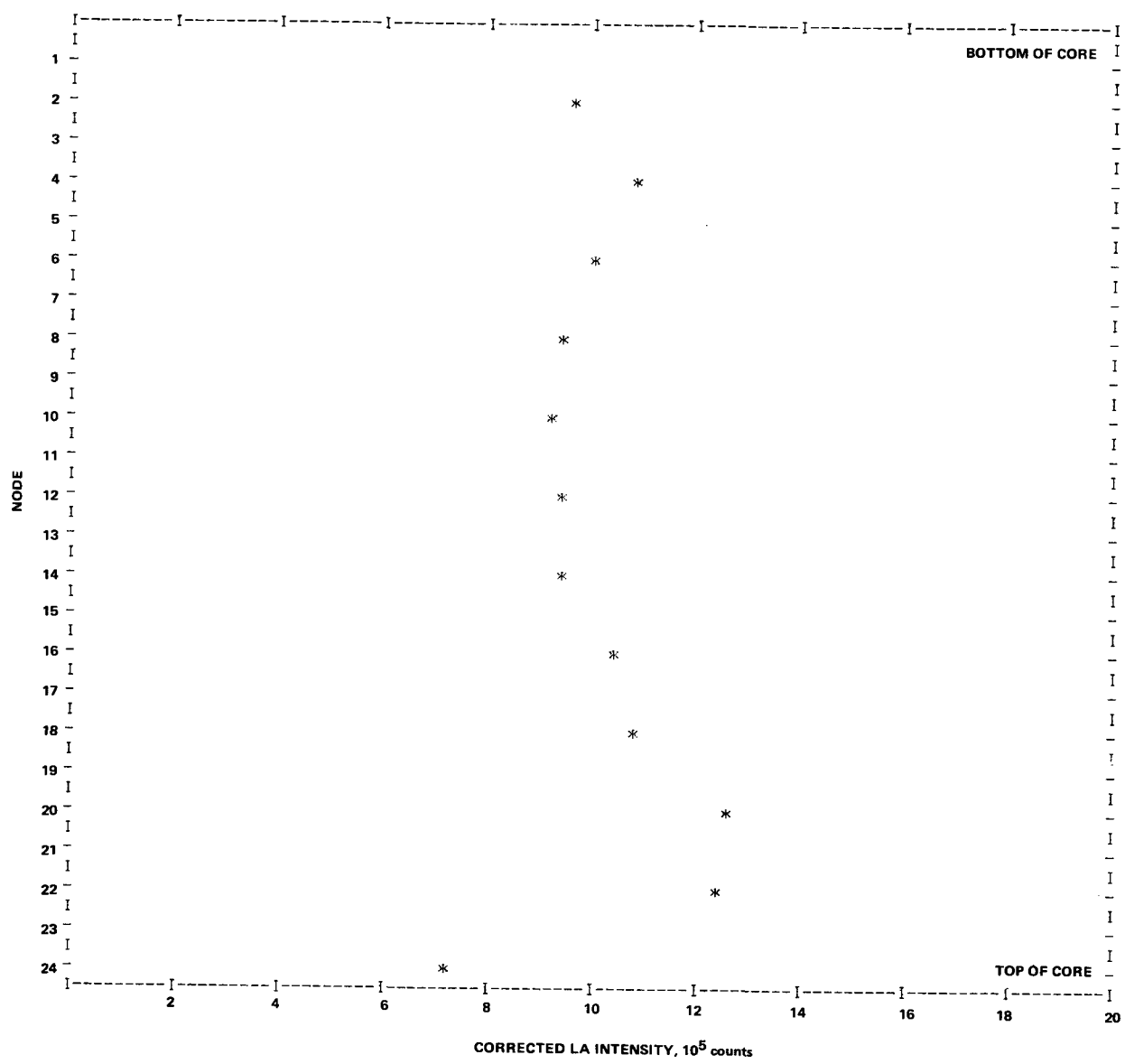


Figure C-19. Axial La-140 Intensity, Assembly B41

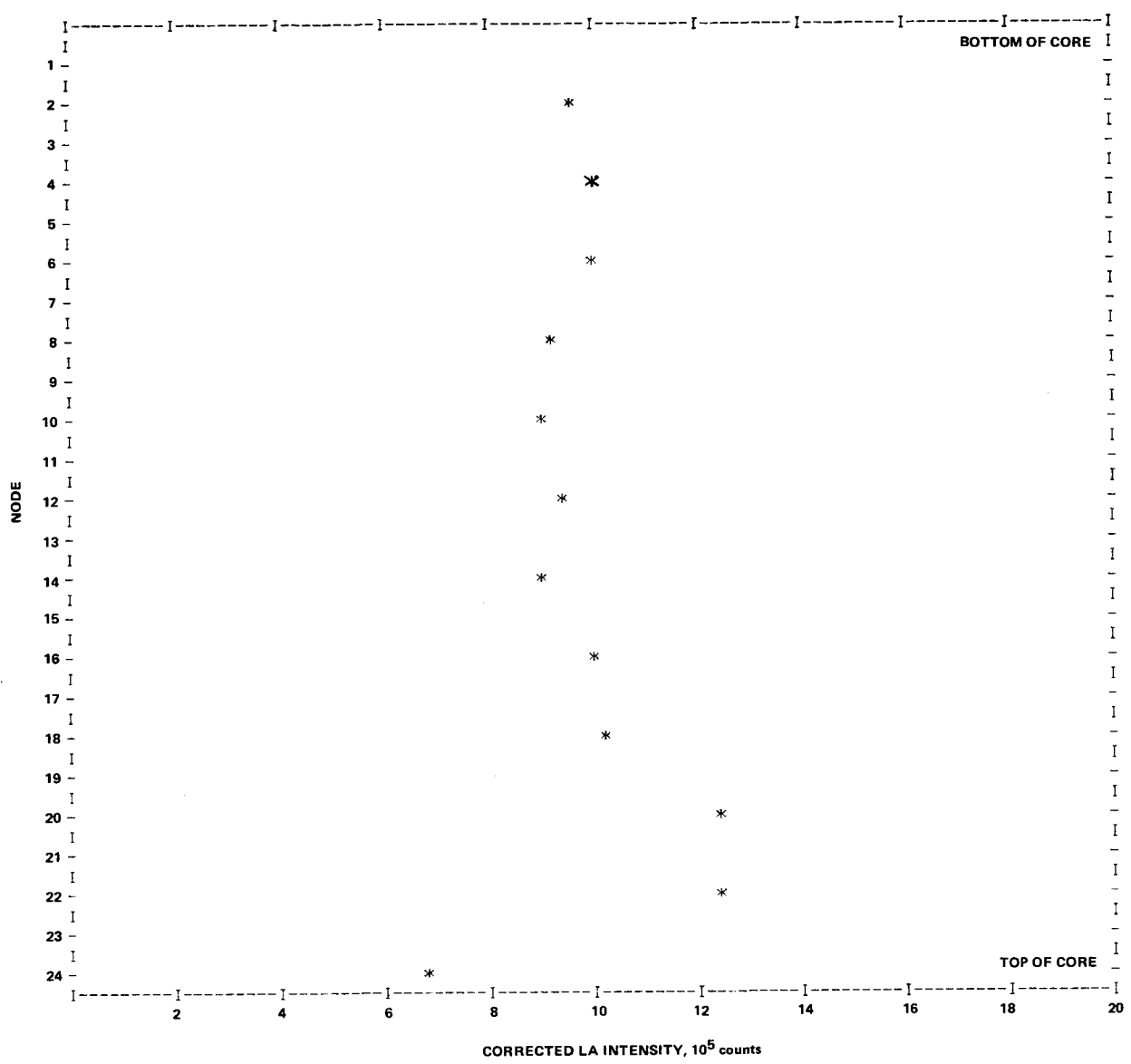


Figure C-20. Axial La-140 Intensity, Assembly B45

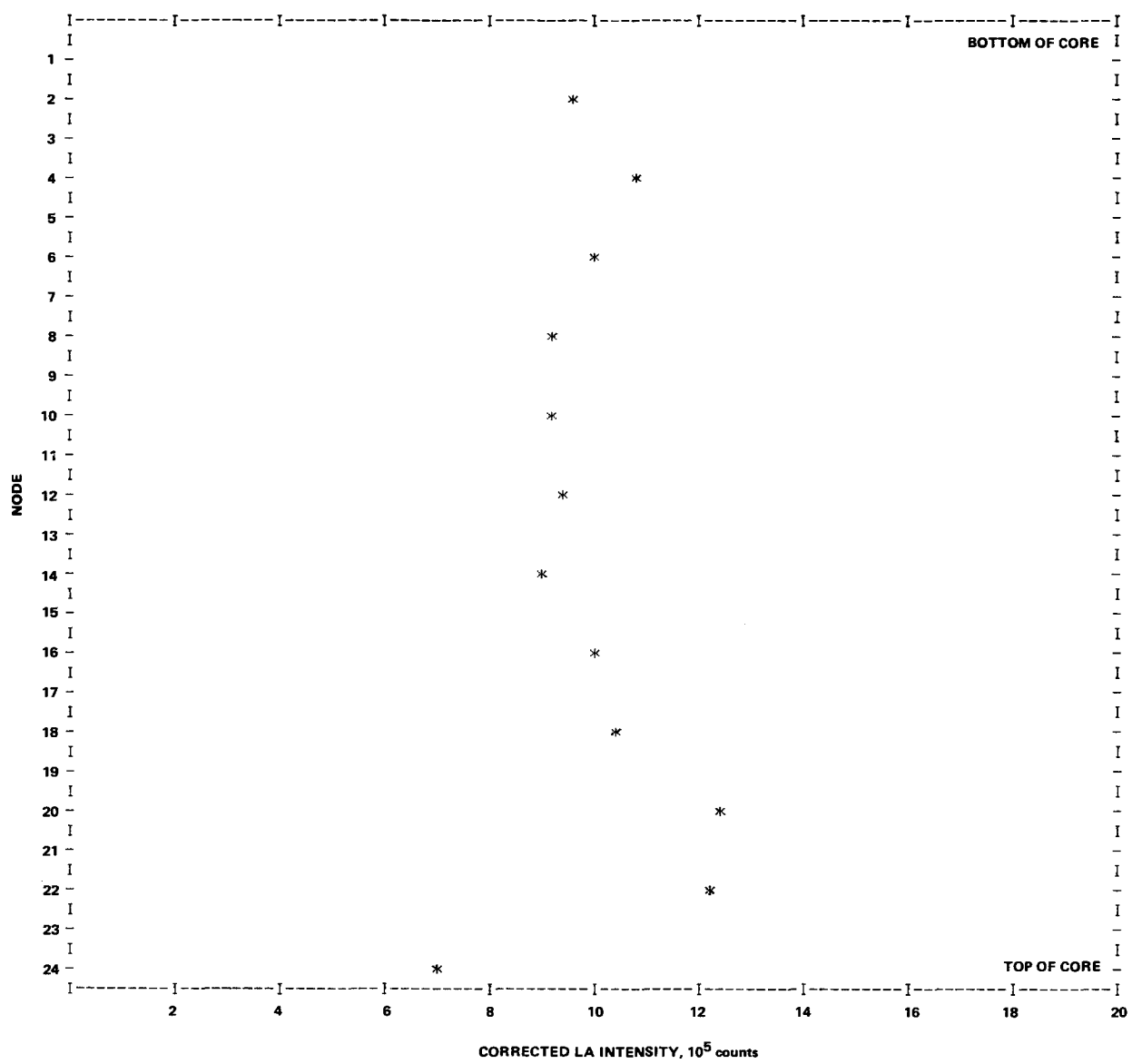


Figure C-21. Axial La-140 Intensity, Assembly B03

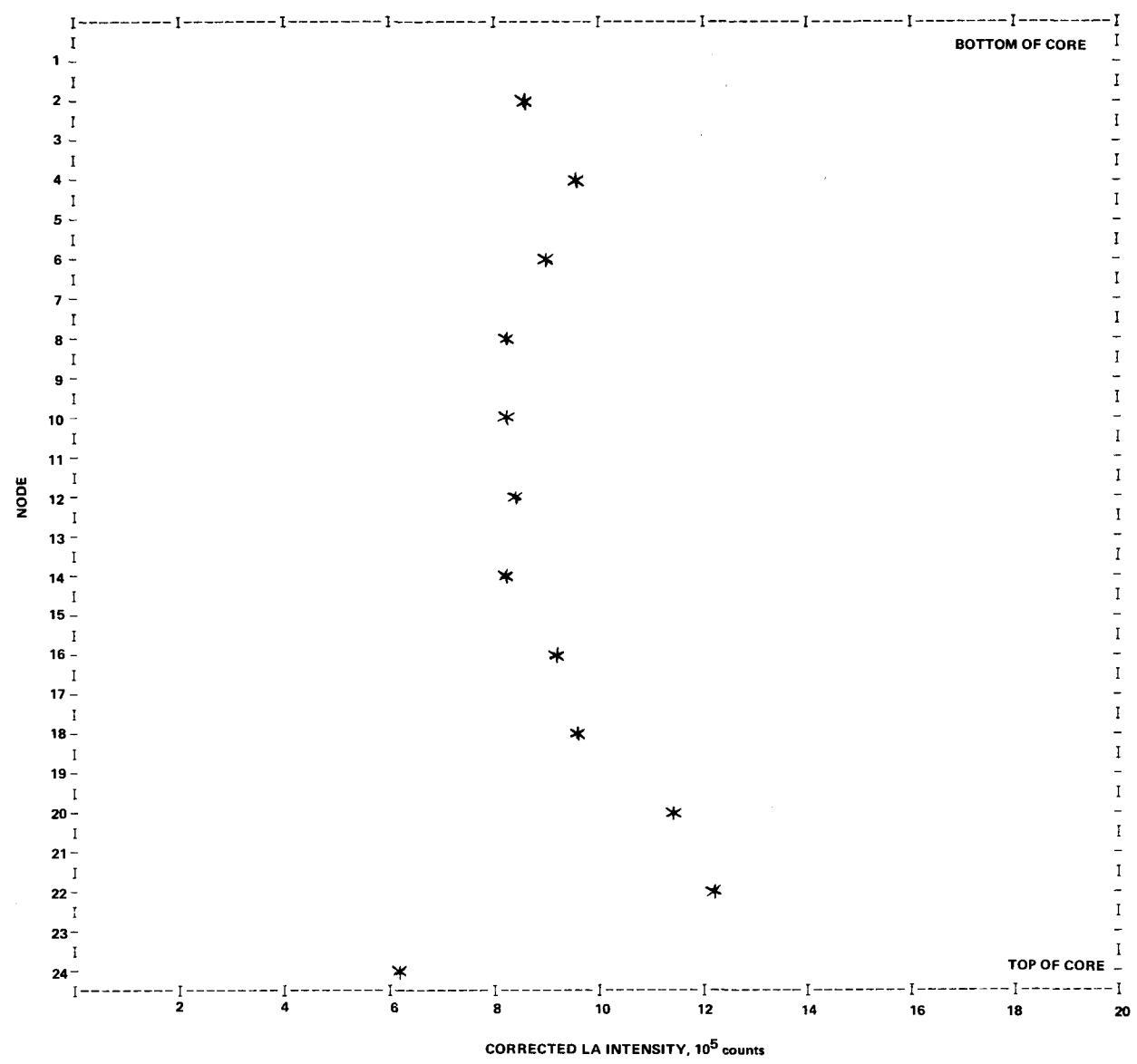


Figure C-22. Axial La-140 Intensity, Assembly A29 (With Control Rod Cluster)

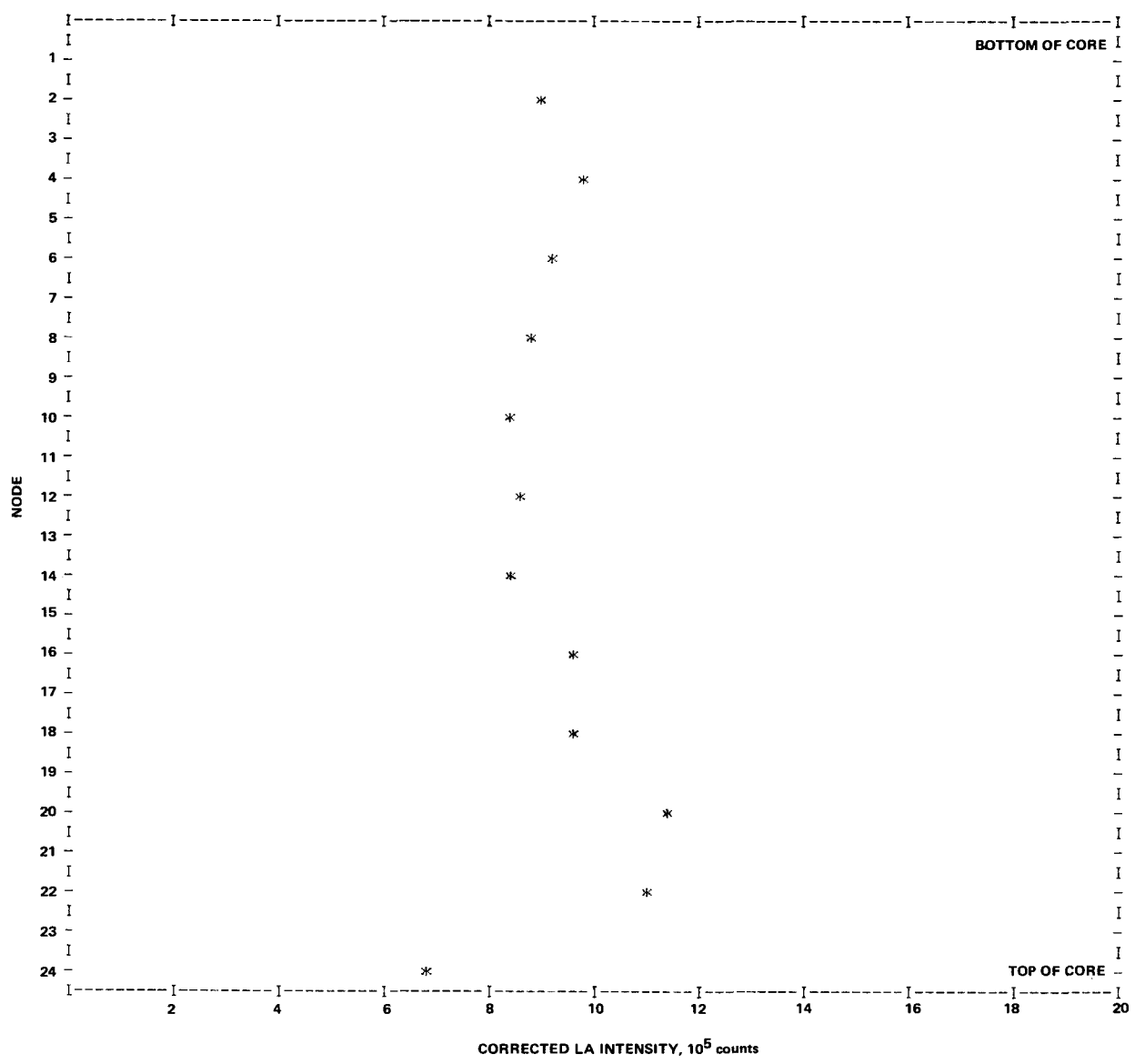


Figure C-23. Axial La-140 Intensity, Assembly A42

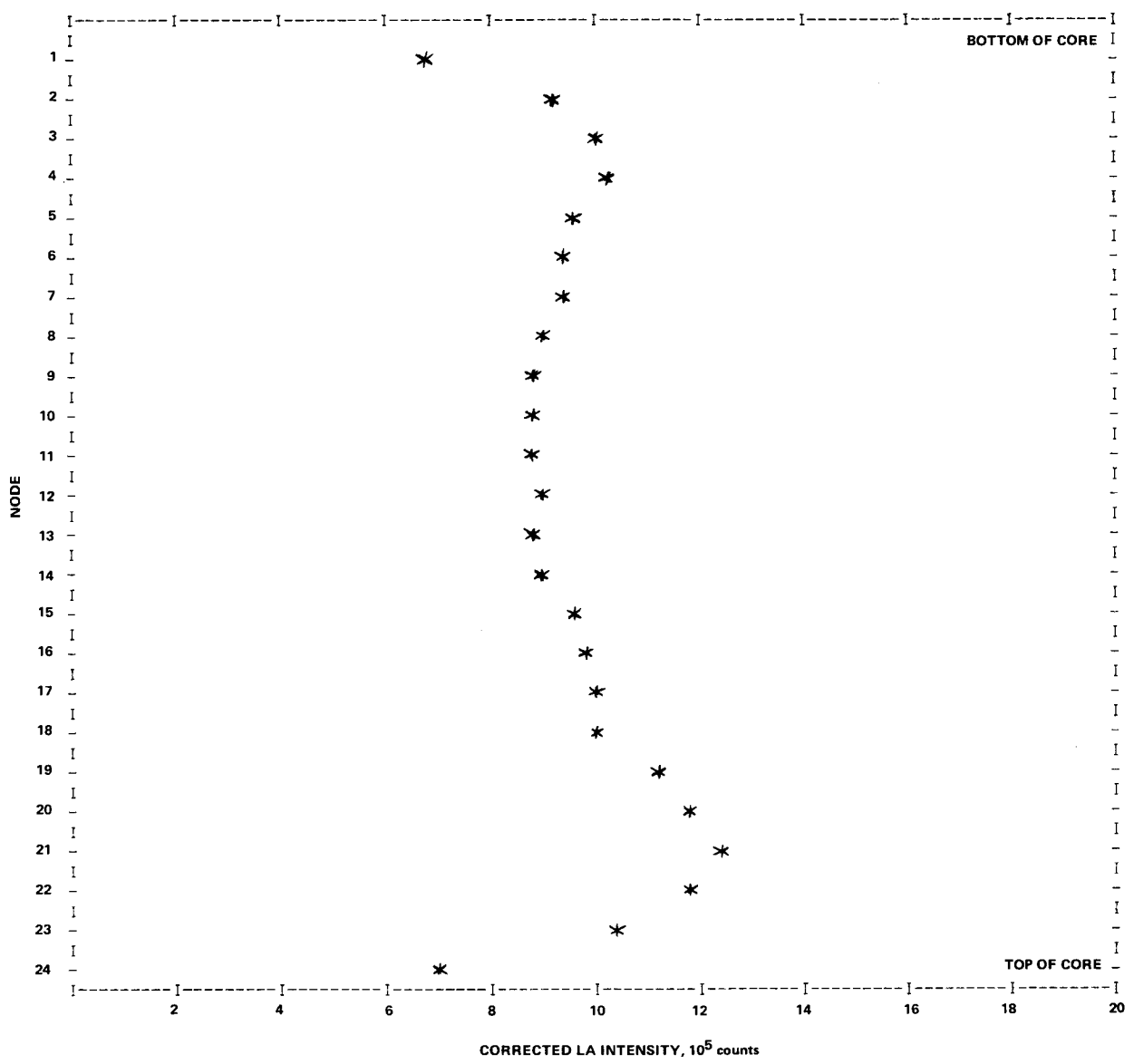


Figure C-24. Axial La-140 Intensity, Assembly A14

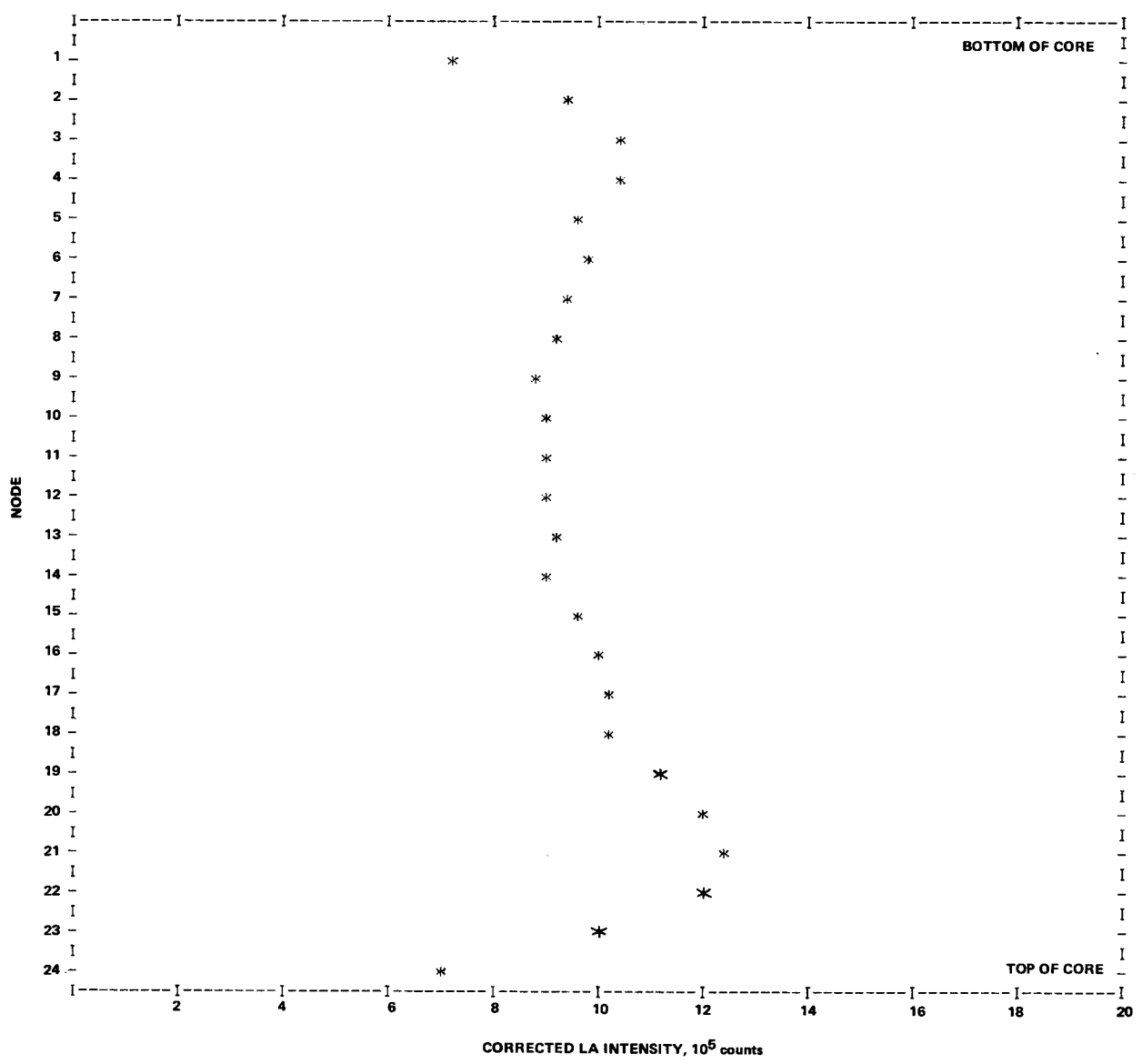


Figure C-25. Axial La-140 Intensity, Assembly A59

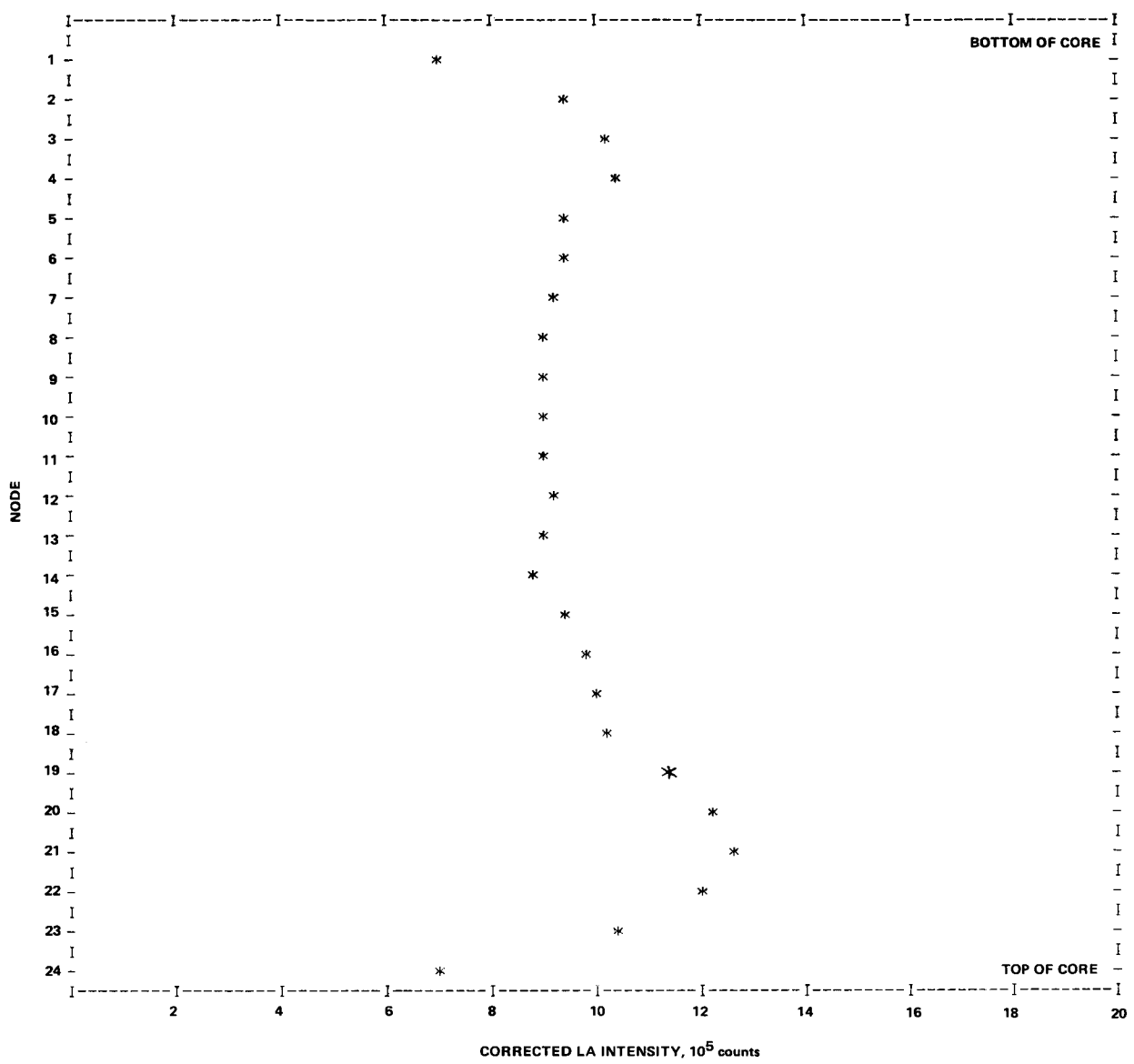


Figure C-26. Axial La-140 Intensity, Assembly A51

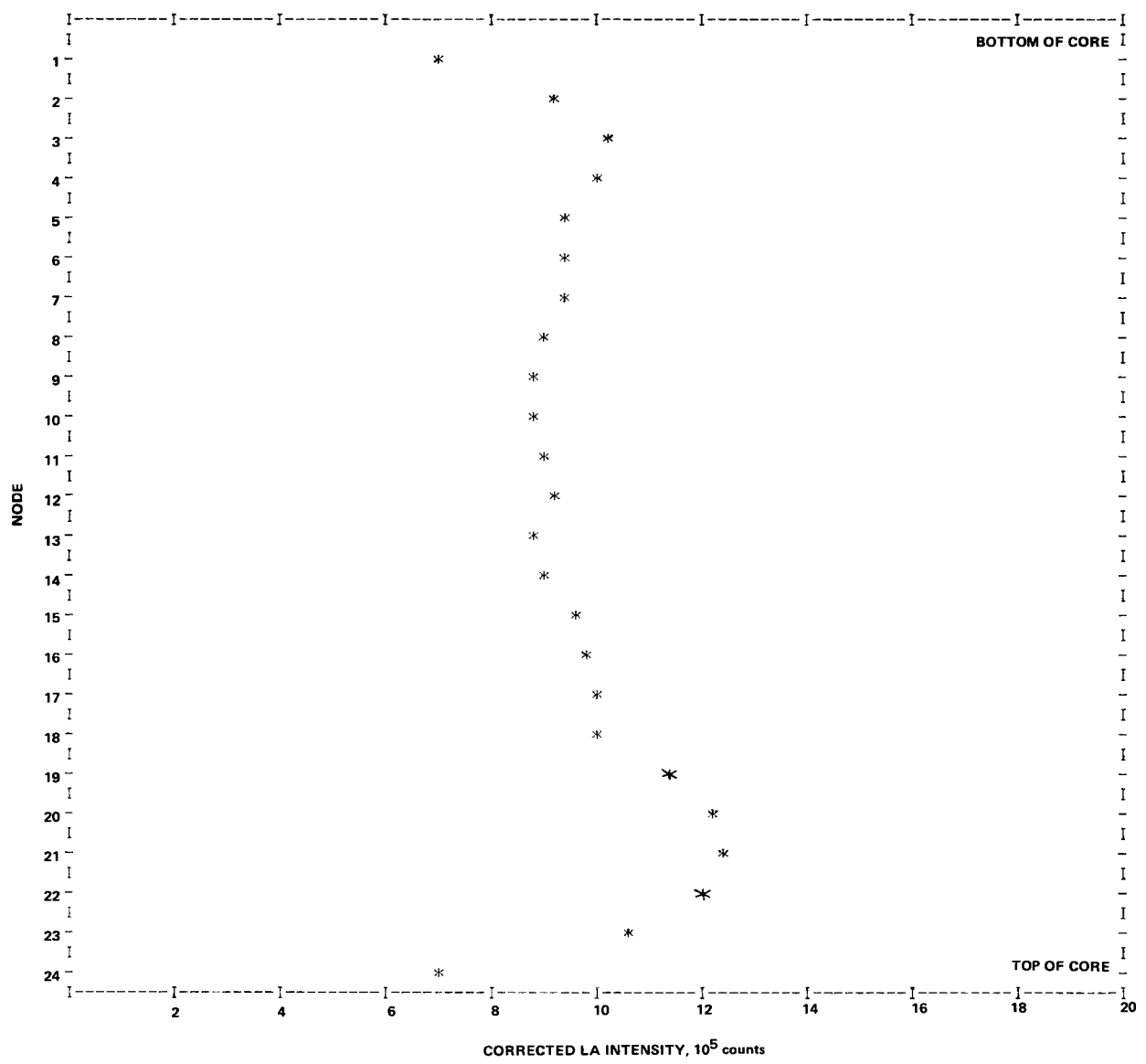


Figure C-27 Axial La-140 Intensity, Assembly A50

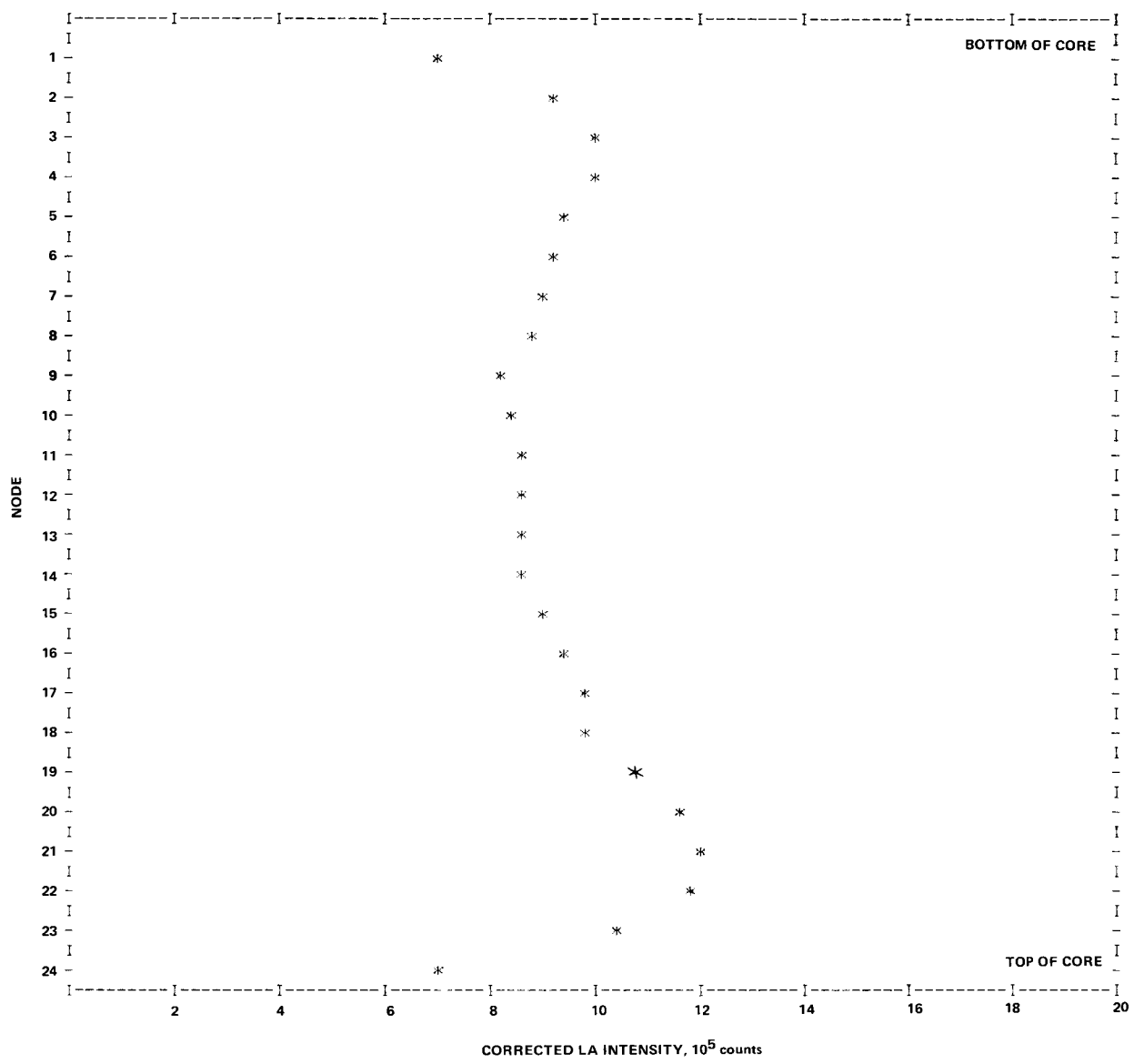


Figure C-28. Axial La-140 Intensity, Assembly A26

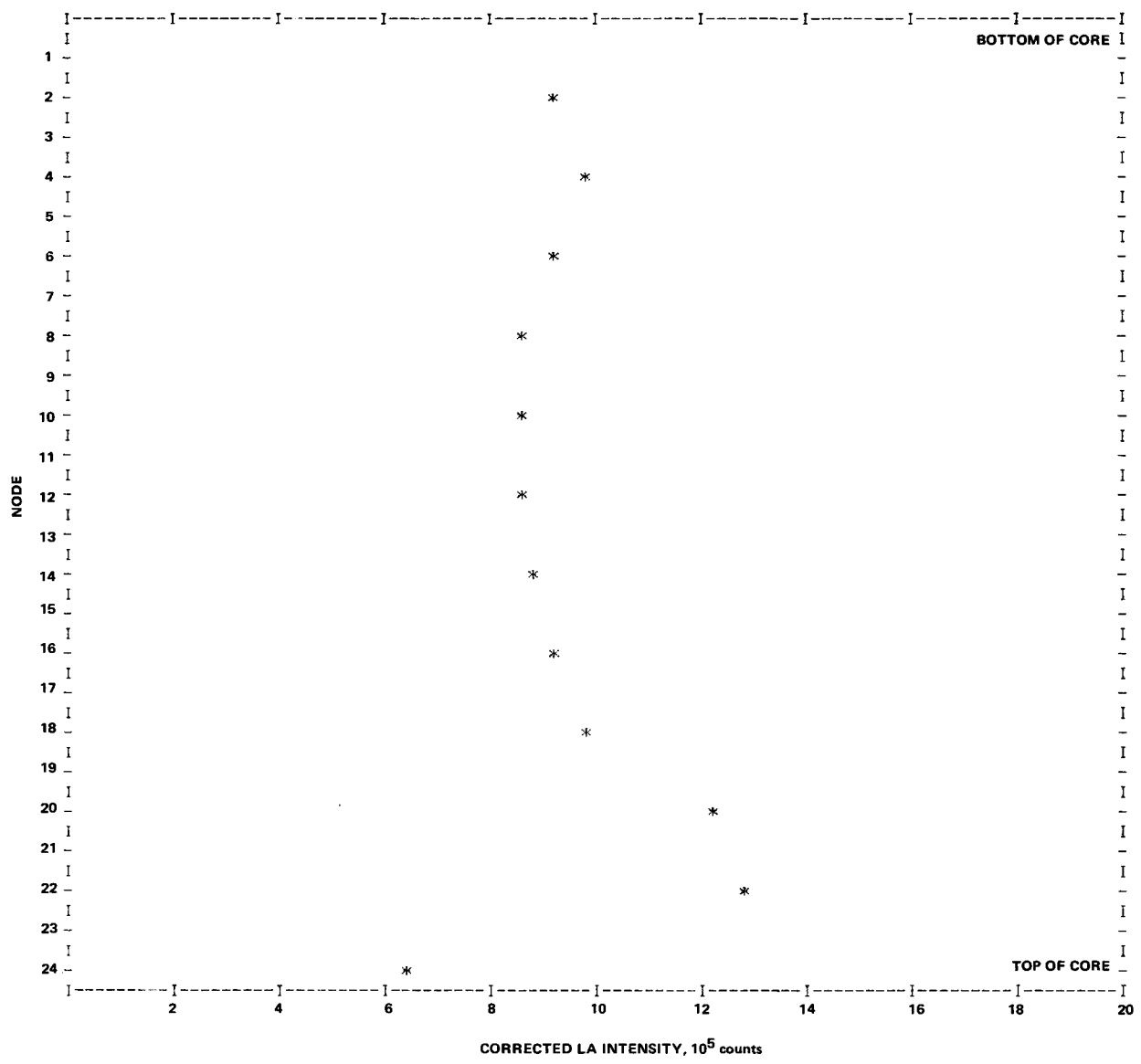


Figure C-29. Axial La-140 Intensity, Assembly A29 (Without Control Rod Cluster)

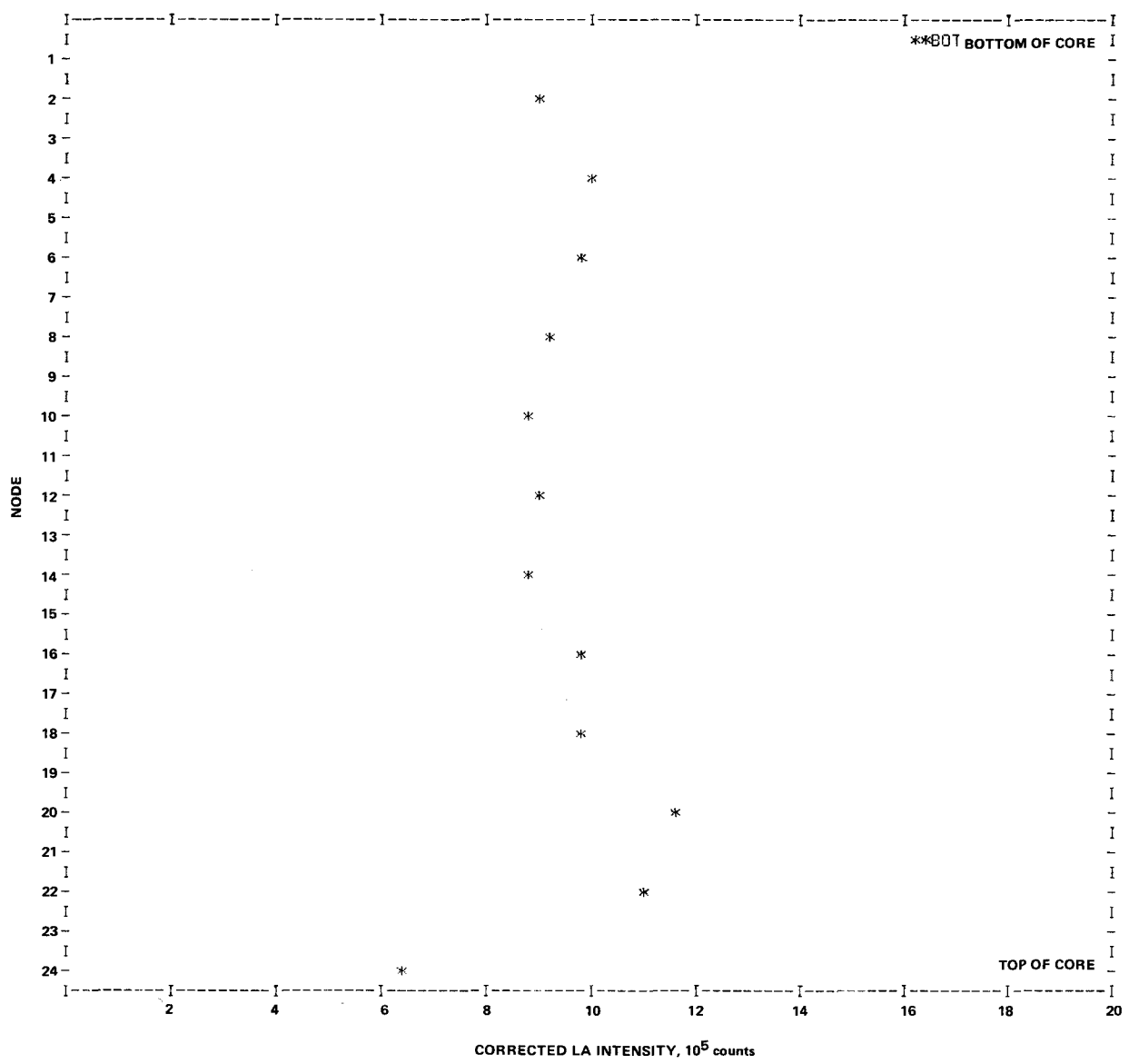


Figure C-30. Axial La-140 Intensity, Assembly A33

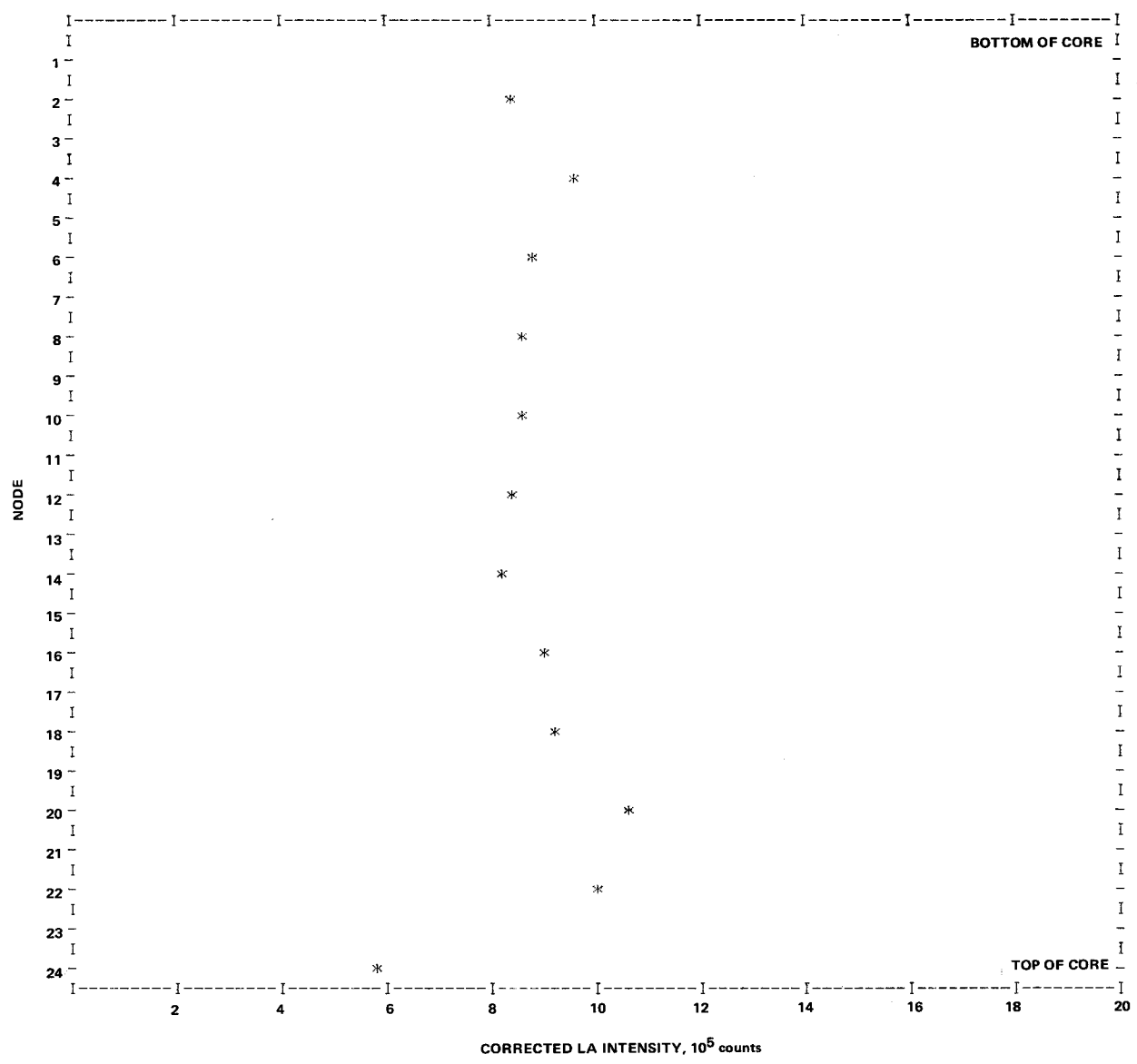


Figure C-31. Axial La-140 Intensity, Assembly A16

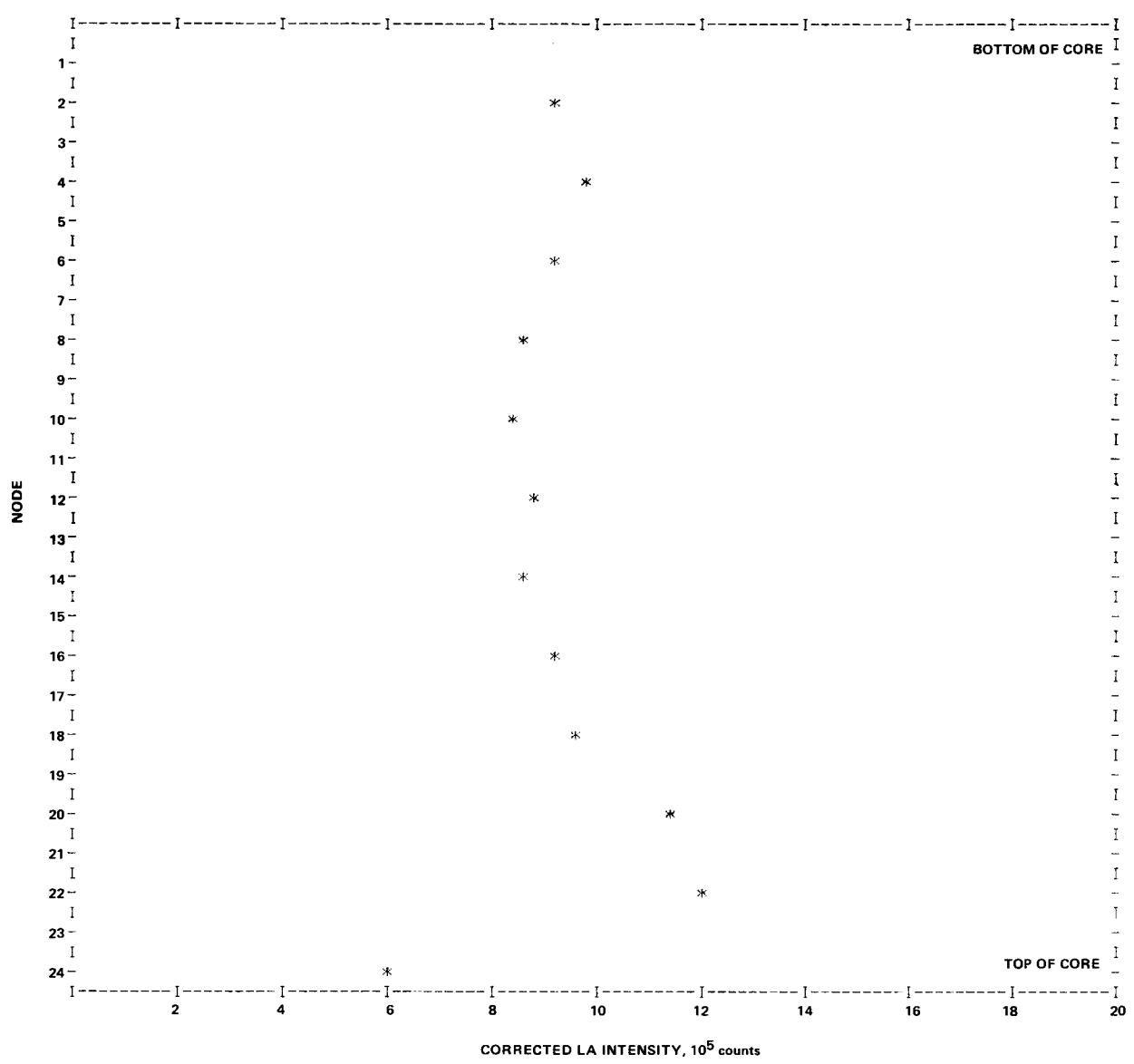


Figure C-32. Axial La-140 Intensity, Assembly A52

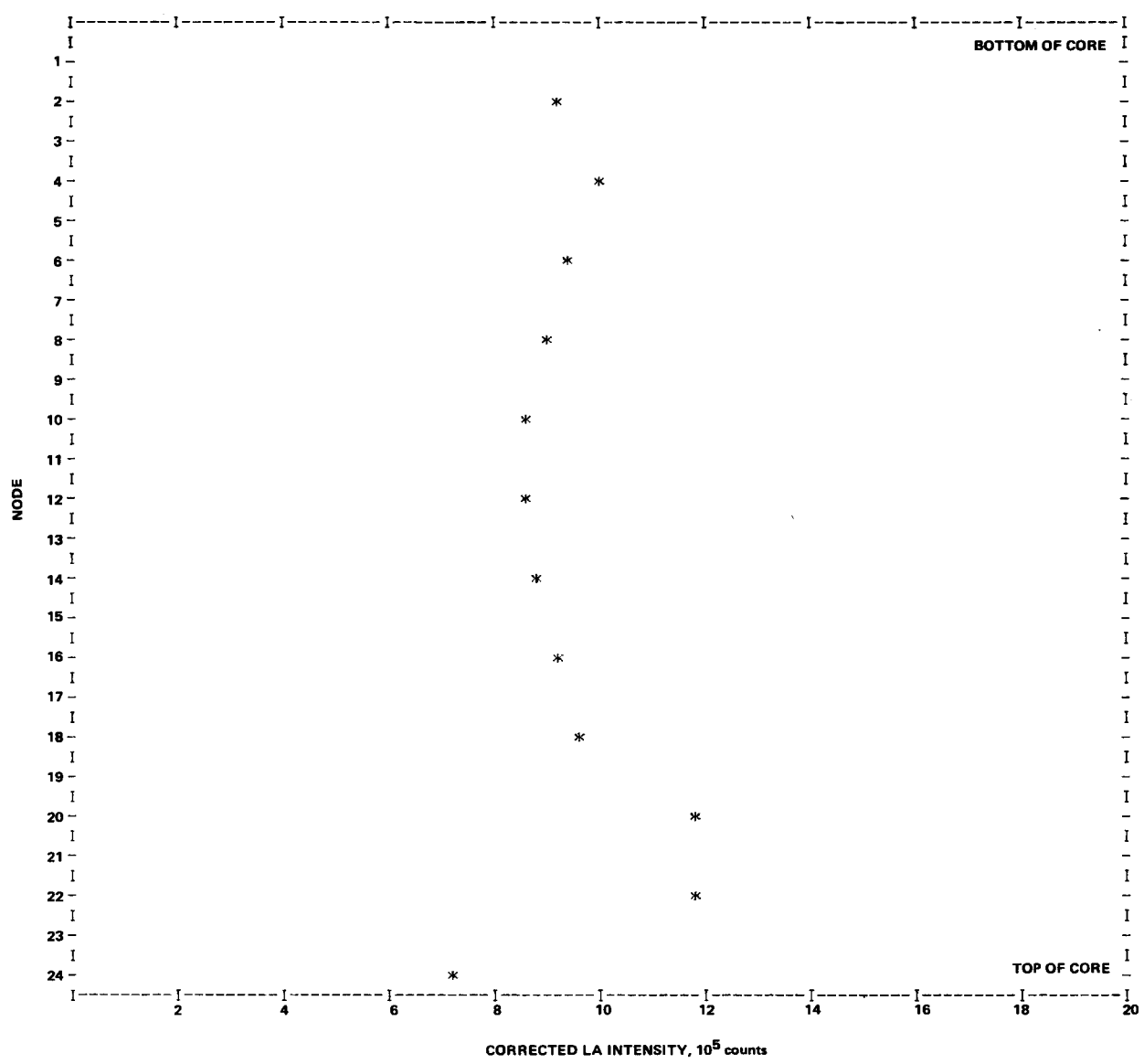


Figure C-33. Axial La-140 Intensity, Assembly A03

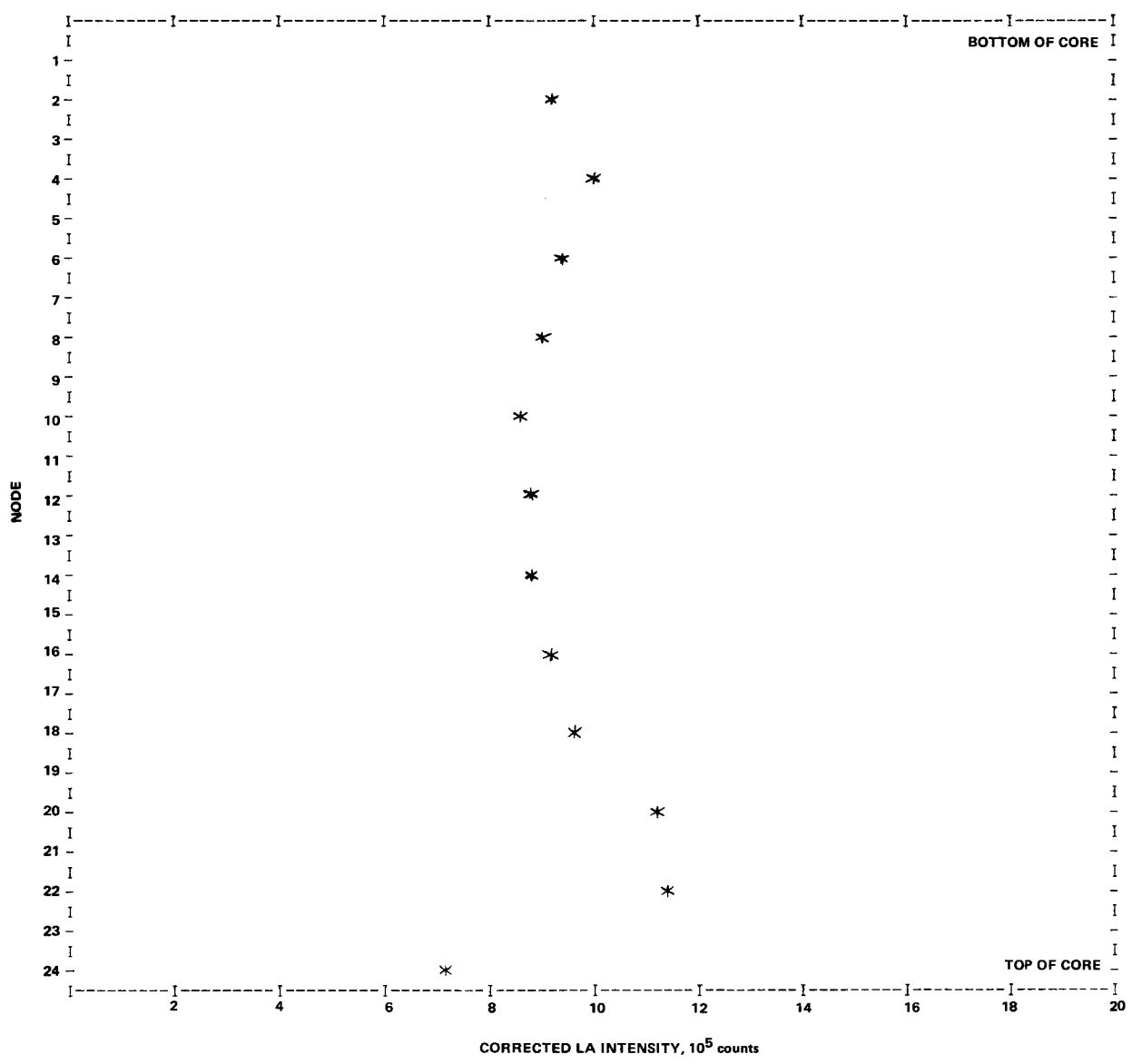


Figure C-34. Axial La-140 Intensity, Assembly A23

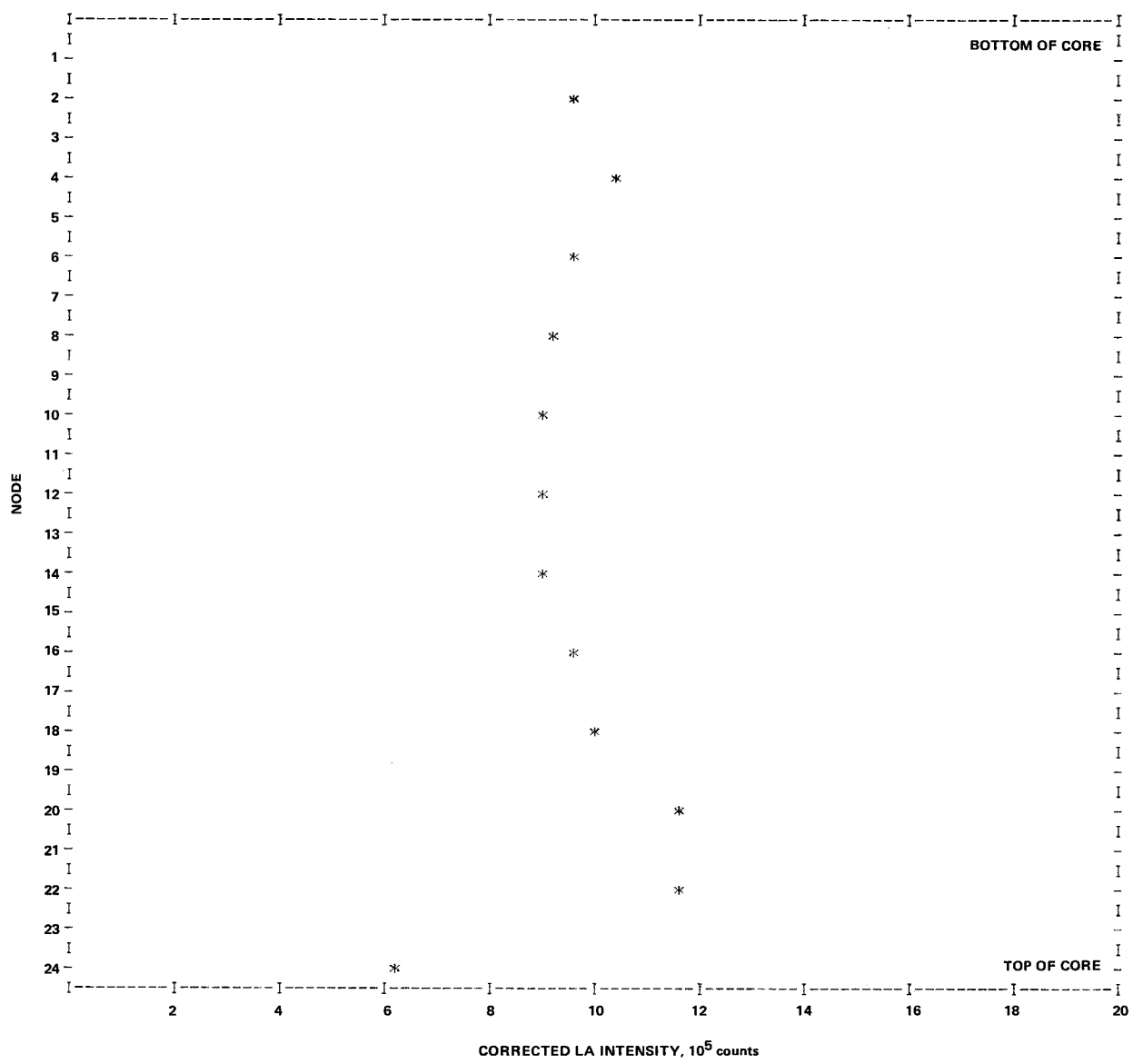


Figure C-35. Axial La-140 Intensity, Assembly A01

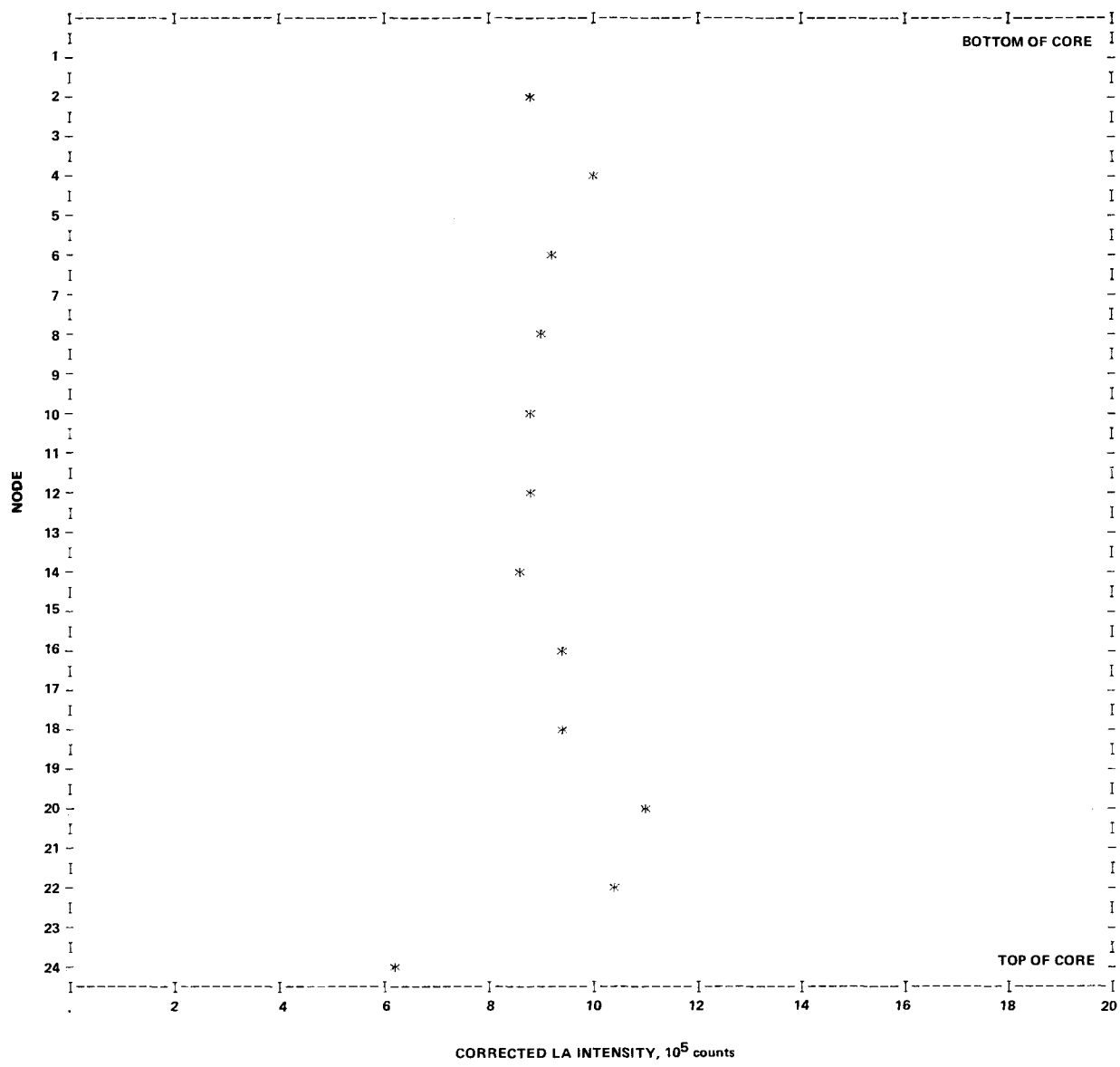


Figure C-36. Axial La-140 Intensity, Assembly A22

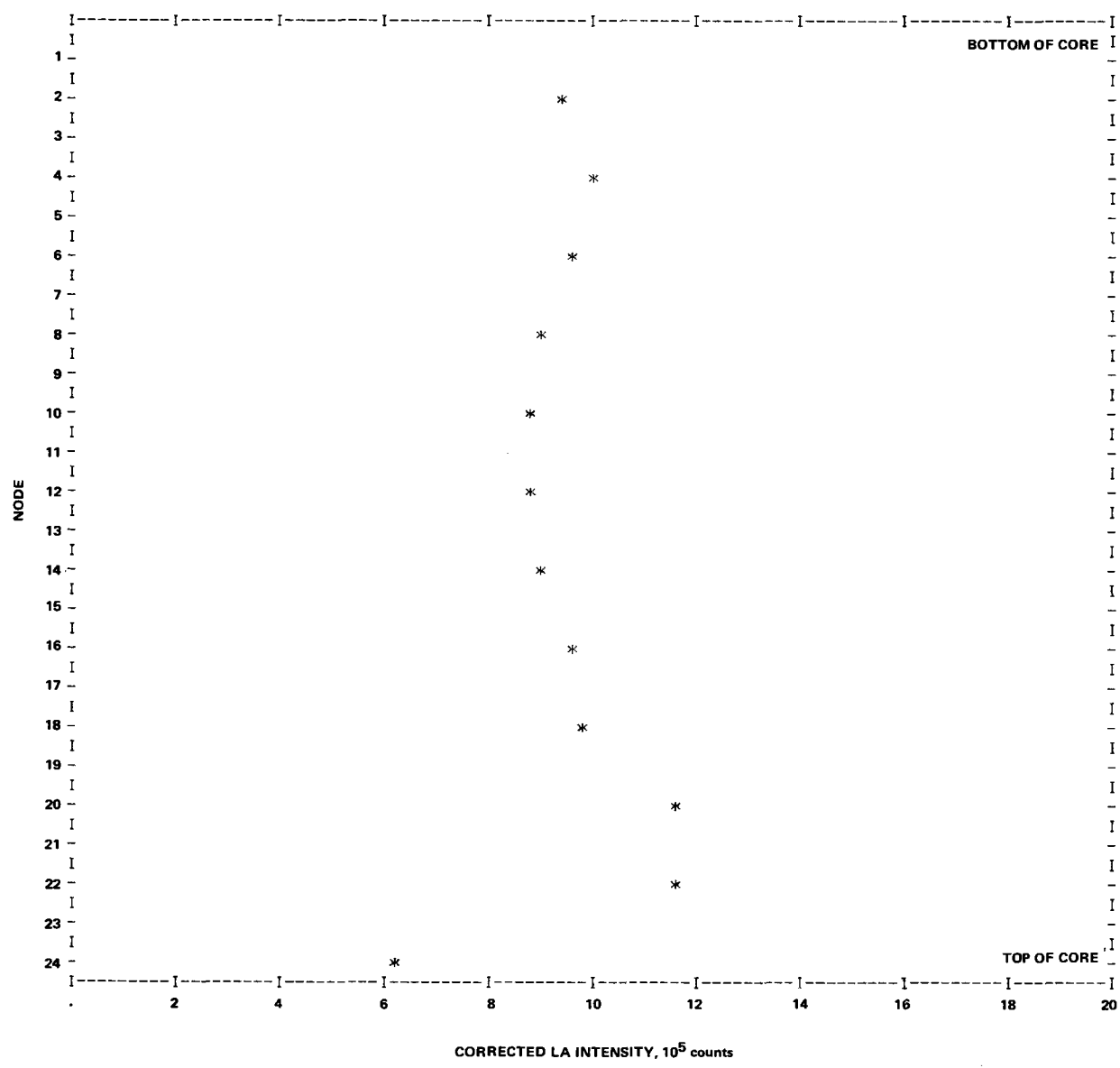


Figure C-37. Axial La-140 Intensity, Assembly A31

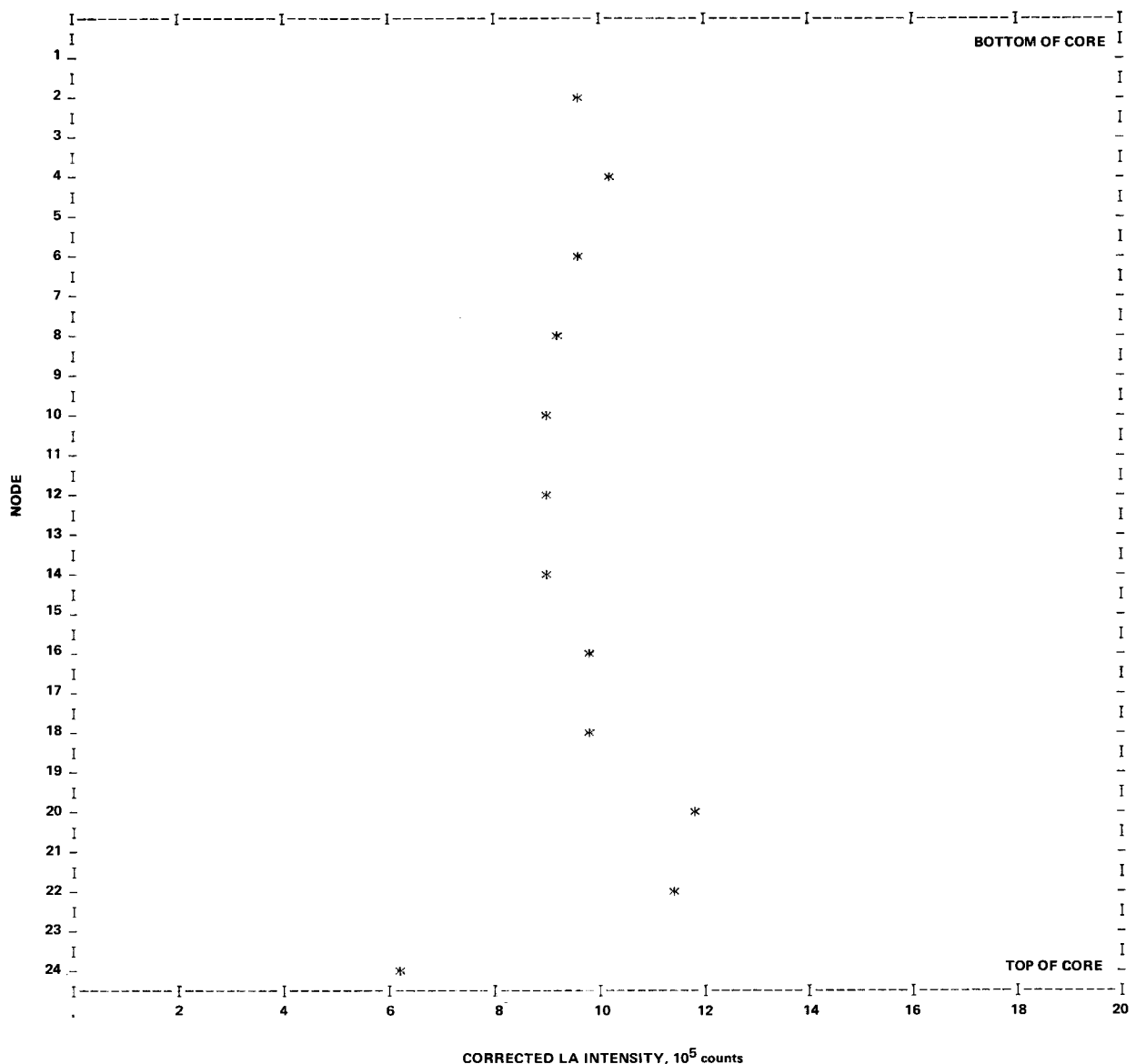


Figure C-38. Axial La-140 Intensity, Assembly A43

APPENDIX D
DATA LISTINGS OF THE La-140 INTENSITIES
FOR THE 37 ASSEMBLIES MEASURED

NODAL INTENSITIES

Node	C04	B13	C02	B21	C06	C50	C63	B55	Inches
1	0.	0.	0.	0.	0.	469700.	0.	0.	4
2	892600.	917800.	760500.	838500.	538900.	644600.	511000.	937200.	9
3	0.	0.	0.	0.	0.	743900.	0.	0.	15
4	1072000.	1047000.	844100.	993400.	639200.	751800.	625400.	1054000.	21
5	0.	0.	0.	0.	0.	711400.	0.	0.	29
6	1022000.	987300.	837200.	968300.	631000.	716600.	612100.	990000.	33
7	0.	0.	0.	0.	0.	759000.	0.	0.	39
8	978000.	952300.	795600.	930300.	611900.	744300.	584700.	914000.	45
9	0.	0.	0.	0.	0.	700000.	0.	0.	50
10	946400.	926600.	777100.	915400.	601500.	735200.	598700.	919500.	57
11	0.	0.	0.	0.	0.	712400.	0.	0.	63
12	726600.	919600.	794500.	913200.	596800.	730400.	621700.	912000.	69
13	0.	0.	0.	0.	0.	707800.	0.	0.	75
14	697100.	922500.	775200.	887100.	619600.	702700.	587700.	897400.	81
15	0.	0.	0.	0.	0.	747600.	0.	0.	87
16	765400.	1004000.	842400.	980600.	649800.	751000.	642300.	972000.	93
17	0.	0.	0.	0.	0.	770200.	0.	0.	99
18	775900.	1055000.	866200.	983400.	647400.	756700.	643100.	1040000.	103
19	0.	0.	0.	0.	0.	805600.	0.	0.	111
20	852200.	1256000.	978400.	1158000.	729600.	827200.	712500.	1260000.	117
21	0.	0.	0.	0.	0.	825900.	0.	0.	123
22	792300.	1168000.	917800.	1056000.	658000.	770300.	638600.	1267000.	129
23	0.	0.	0.	0.	0.	654200.	0.	0.	135
24	435800.	682600.	509800.	530500.	364100.	424800.	329500.	699800.	141
Integral	839816.	993172.	814388.	937206.	611512.	718069.	596544.	995497.	

ASSEMBLY NORMALIZED NODAL INTENSITIES

Node	C04	B13	C02	B21	C06	C50	C63	B55	Inches
1	0.	0.	0.	0.	0.	0.6568	0.	0.	4
2	1.0760	0.9303	0.9409	0.9021	0.8873	0.9013	0.8627	0.9481	9
3	0.	0.	0.	0.	0.	1.0400	0.	0.	15
4	1.2920	1.0620	1.0440	1.0690	1.0520	1.0510	1.0560	1.0660	21
5	0.	0.	0.	0.	0.	0.9948	0.	0.	29
6	1.2320	1.0010	1.0360	1.0420	1.0390	1.0020	1.0340	1.0010	33
7	0.	0.	0.	0.	0.	1.0610	0.	0.	39
8	1.1790	0.9653	0.9844	1.0010	1.0080	1.0410	0.9873	0.9245	45
9	0.	0.	0.	0.	0.	0.9788	0.	0.	50
10	1.1410	0.9392	0.9614	0.9848	0.9904	1.0280	1.0110	0.9301	57
11	0.	0.	0.	0.	0.	0.9962	0.	0.	63
12	0.8757	0.9321	0.9831	0.9824	0.9827	1.0210	1.0500	0.9226	69
13	0.	0.	0.	0.	0.	0.9897	0.	0.	75
14	0.8402	0.9351	0.9591	0.9543	1.0200	0.9826	0.9922	0.9078	81
15	0.	0.	0.	0.	0.	1.0450	0.	0.	87
16	0.9225	1.0180	1.0420	1.0550	1.0700	1.0500	1.0840	0.9832	93
17	0.	0.	0.	0.	0.	1.0770	0.	0.	99
18	0.9352	1.0690	1.0720	1.0580	1.0660	1.0580	1.0860	1.0520	103
19	0.	0.	0.	0.	0.	1.1270	0.	0.	111
20	1.0270	1.2730	1.2110	1.2460	1.2010	1.1570	1.2030	1.2750	117
21	0.	0.	0.	0.	0.	1.1550	0.	0.	123
22	0.9549	1.1840	1.1360	1.1360	1.0840	1.0770	1.0780	1.2820	129
23	0.	0.	0.	0.	0.	0.9148	0.	0.	135
24	0.5252	0.6919	0.6308	0.5707	0.5996	0.5941	0.5563	0.7079	141

NODAL INTENSITIES

Node	B44	B59	B18	C22	C43	B34	C46	B15	Inches
1	677000.	0.	0.	0.	0.	0.	0.	0.	4
2	946100.	968400.	949700.	704100.	684400.	949500.	542500.	955100.	9
3	1030000.	0.	0.	0.	0.	0.	0.	0.	15
4	1040000.	1077000.	1049000.	812300.	777000.	1056000.	637300.	1121000.	21
5	964300.	0.	0.	0.	0.	0.	0.	0.	29
6	989300.	998200.	990300.	760100.	767800.	994900.	626500.	1032000.	33
7	944700.	0.	0.	0.	0.	0.	0.	0.	39
8	925700.	933800.	912400.	757200.	735700.	917400.	594600.	974000.	45
9	898000.	0.	0.	0.	0.	0.	0.	0.	50
10	892400.	946900.	913900.	733800.	710100.	906100.	574300.	933600.	57
11	922900.	0.	0.	0.	0.	0.	0.	0.	63
12	910700.	926300.	955000.	756500.	714100.	918500.	595600.	946600.	69
13	914300.	0.	0.	0.	0.	0.	0.	0.	75
14	902600.	922600.	922000.	730500.	712100.	907300.	564400.	935800.	81
15	918100.	0.	0.	0.	0.	0.	0.	0.	87
16	992800.	1017000.	988300.	808500.	770800.	997900.	633400.	1037000.	93
17	1012000.	0.	0.	0.	0.	0.	0.	0.	99
18	1015000.	1039000.	1039000.	817500.	777000.	1035000.	644900.	1051000.	103
19	1125000.	0.	0.	0.	0.	0.	0.	0.	111
20	1205000.	1193000.	1240000.	929300.	875600.	1231000.	719400.	1281000.	117
21	1255000.	0.	0.	0.	0.	0.	0.	0.	123
22	1216000.	1195000.	1192000.	833400.	782100.	1211000.	661500.	1201000.	129
23	1030000.	0.	0.	0.	0.	0.	0.	0.	135
24	663300.	644100.	662900.	468000.	433400.	695800.	333800.	605200.	141
Integral	982298.	996399.	992217.	765024.	734296.	991876.	598966.	1015034.	

ASSEMBLY NORMALIZED NODAL INTENSITIES

Node	B44	B59	B18	C22	C43	B34	C46	B15	Inches
1	0.6946	0.	0.	0.	0.	0.	0.	0.	4
2	0.9707	0.9798	0.9647	0.9273	0.9397	0.9640	0.9133	0.9493	9
3	1.0570	0.	0.	0.	0.	0.	0.	0.	15
4	1.0670	1.0890	1.0650	1.0698	1.0670	1.0720	1.0730	1.1140	21
5	0.9894	0.	0.	0.	0.	0.	0.	0.	29
6	1.0150	1.0100	1.0060	1.0011	1.0540	1.0100	1.0550	1.0260	33
7	0.9693	0.	0.	0.	0.	0.	0.	0.	39
8	0.9498	0.9447	0.9268	0.9973	1.0100	0.9314	1.0010	0.9681	45
9	0.9214	0.	0.	0.	0.	0.	0.	0.	50
10	0.9157	0.9580	0.9283	0.9665	0.9750	0.9199	0.9668	0.9280	57
11	0.9469	0.	0.	0.	0.	0.	0.	0.	63
12	0.9345	0.9371	0.9700	0.9964	0.9804	0.9325	1.0030	0.9409	69
13	0.9382	0.	0.	0.	0.	0.	0.	0.	75
14	0.9261	0.9334	0.9366	0.9621	0.9777	0.9212	0.9501	0.9302	81
15	0.9420	0.	0.	0.	0.	0.	0.	0.	87
16	1.0190	1.0280	1.0040	1.0648	1.0580	1.0130	1.0660	1.0310	93
17	1.0380	0.	0.	0.	0.	0.	0.	0.	99
18	1.0420	1.0520	1.0550	1.0767	1.0670	1.0510	1.0860	1.0440	103
19	1.1540	0.	0.	0.	0.	0.	0.	0.	111
20	1.2370	1.2070	1.2600	1.2239	1.2020	1.2490	1.2110	1.2740	117
21	1.2870	0.	0.	0.	0.	0.	0.	0.	123
22	1.2480	1.2090	1.2110	1.0976	1.0740	1.2290	1.1140	1.1940	129
23	1.0570	0.	0.	0.	0.	0.	0.	0.	135
24	0.6806	0.6516	0.6734	0.6164	0.5951	0.7064	0.5620	0.6016	141

NODAL INTENSITIES

Node	B48	C12	B41	B45	B03	A29 ^a	A42	A14	Inches
1	0.	0.	0.	0.	0.	0.	0.	685900.	4
2	946000.	688600.	966100.	969200.	957700.	852200.	891400.	922000.	9
3	0.	0.	0.	0.	0.	0.	0.	1006000.	15
4	1076000.	811300.	1075000.	1058000.	1086000.	955600.	970600.	1021000.	21
5	0.	0.	0.	0.	0.	0.	0.	955900.	29
6	983200.	778200.	1001000.	1002000.	1003000.	890200.	929400.	944400.	33
7	0.	0.	0.	0.	0.	0.	0.	933000.	39
8	928900.	751200.	942700.	929100.	928600.	819300.	880200.	907100.	45
9	0.	0.	0.	0.	0.	0.	0.	888500.	50
10	896800.	716200.	926700.	892500.	919700.	813800.	842800.	875300.	57
11	0.	0.	0.	0.	0.	0.	0.	872100.	63
12	930700.	733400.	931400.	940300.	933600.	835800.	855400.	892300.	69
13	0.	0.	0.	0.	0.	0.	0.	883600.	75
14	898000.	718200.	940300.	904000.	909800.	820500.	849100.	893700.	81
15	0.	0.	0.	0.	0.	0.	0.	952600.	87
16	982000.	783600.	1039000.	1002000.	999500.	924000.	953700.	970800.	93
17	0.	0.	0.	0.	0.	0.	0.	989600.	99
18	1035000.	767100.	1071000.	1012000.	1047000.	963100.	969600.	1004000.	103
19	0.	0.	0.	0.	0.	0.	0.	1110000.	111
20	1255000.	879600.	1263000.	1233000.	1246000.	1148000.	1132000.	1174000.	117
21	0.	0.	0.	0.	0.	0.	0.	1236000.	123
22	1232000.	790800.	1249000.	1230000.	1227000.	1223000.	1100000.	1182000.	129
23	0.	0.	0.	0.	0.	0.	0.	1041000.	135
24	714800.	433300.	722700.	688000.	705800.	626800.	674900.	691000.	141
Integral	996637.	743601.	1017266.	995861.	1003905.	912272.	926518.	962679.	

^a With control rod cluster

ASSEMBLY NORMALIZED NODAL INTENSITIES

Node	B48	C12	B41	B45	B03	A29 ^a	A42	A14	Inches
1	0.	0.	0.	0.	0.	0.	0.	0.7147	4
2	0.9556	0.9335	0.9559	0.9806	0.9606	0.9406	0.9681	0.9608	9
3	0.	0.	0.	0.	0.	0.	0.	1.0483	15
4	1.0870	1.0999	1.0630	1.0710	1.0890	1.0550	1.0540	1.0639	21
5	0.	0.	0.	0.	0.	0.	0.	0.9961	29
6	0.9932	1.0550	0.9903	1.0140	1.0060	0.9825	1.0090	0.9841	33
7	0.	0.	0.	0.	0.	0.	0.	0.9722	39
8	0.9383	1.0184	0.9327	0.9400	0.9314	0.9043	0.9559	0.9452	45
9	0.	0.	0.	0.	0.	0.	0.	0.9259	50
10	0.9059	0.9710	0.9169	0.9030	0.9225	0.8982	0.9154	0.9121	57
11	0.	0.	0.	0.	0.	0.	0.	0.9088	63
12	0.9402	0.9943	0.9216	0.9513	0.9364	0.9225	0.9290	0.9298	69
13	0.	0.	0.	0.	0.	0.	0.	0.9207	75
14	0.9072	0.9737	0.9304	0.9146	0.9126	0.9056	0.9221	0.9312	81
15	0.	0.	0.	0.	0.	0.	0.	0.9926	87
16	0.9920	1.0623	1.0280	1.0140	1.0030	1.0200	1.0360	1.0116	93
17	0.	0.	0.	0.	0.	0.	0.	1.0312	99
18	1.0460	1.0400	1.0600	1.0240	1.0500	1.0630	1.0530	1.0462	103
19	0.	0.	0.	0.	0.	0.	0.	1.1567	111
20	1.2680	1.1925	1.2490	1.2470	1.2500	1.2670	1.2290	1.2234	117
21	0.	0.	0.	0.	0.	0.	0.	1.2880	123
22	1.2440	1.0721	1.2360	1.2450	1.2310	1.3500	1.1950	1.2317	129
23	0.	0.	0.	0.	0.	0.	0.	1.0848	135
24	0.7221	0.5874	0.7151	0.6960	0.7079	0.6918	0.7330	0.7200	141

^a With control rod cluster

NODAL INTENSITIES

Node	A59	A51	A50	A26	A29	A33	A16	A52	Inches
1	711600.	709400.	701400.	696900.	0.	0.	0.	0.	4
2	936500.	933600.	924400.	917200.	918000.	895400.	833800.	911600.	9
3	1033000.	1018000.	1029000.	1005000.	0.	0.	0.	0.	15
4	1039000.	1033000.	996200.	995800.	986600.	1009000.	952100.	972000.	21
5	965700.	949300.	939000.	931900.	0.	0.	0.	0.	29
6	979000.	949700.	947500.	910700.	920500.	972800.	889200.	913300.	33
7	949100.	925200.	930800.	893200.	0.	0.	0.	0.	39
8	913100.	905600.	904000.	872700.	869200.	910800.	861600.	864300.	45
9	887100.	899300.	887900.	829500.	0.	0.	0.	0.	50
10	909000.	904000.	880000.	847100.	859400.	873700.	858300.	836300.	57
11	903000.	894000.	899300.	864800.	0.	0.	0.	0.	63
12	907600.	922600.	914800.	864400.	860000.	893600.	849600.	876300.	69
13	922400.	896900.	890000.	857500.	0.	0.	0.	0.	75
14	900800.	882000.	908100.	866900.	871200.	871800.	826900.	855900.	81
15	963900.	938700.	957200.	899900.	0.	0.	0.	0.	87
16	998200.	978700.	983500.	935500.	926100.	975100.	895100.	923100.	93
17	1011000.	990800.	1005000.	971600.	0.	0.	0.	0.	99
18	1025000.	1017000.	1004000.	978900.	980400.	973000.	928700.	955100.	103
19	1114000.	1137000.	1142000.	1081000.	0.	0.	0.	0.	111
20	1202000.	1213000.	1211000.	1162000.	1223000.	1157000.	1058000.	1142000.	117
21	1246000.	1266000.	1250000.	1208000.	0.	0.	0.	0.	123
22	1206000.	1206000.	1198000.	1173000.	1277000.	1094000.	998700.	1201000.	129
23	1041000.	1042000.	1059000.	1043000.	0.	0.	0.	0.	135
24	709500.	701400.	707300.	709500.	647200.	635700.	588300.	592900.	141
Integral	983155.	977093.	971015.	942033.	952650.	945124.	884636.	928501.	

ASSEMBLY NORMALIZED NODAL INTENSITIES

Node	A59	A51	A50	A26	A29	A33	A16	A52	Inches
1	0.7276	0.7303	0.7234	0.7428	0.	0.	0.	0.	4
2	0.9575	0.9611	0.9534	0.9777	0.9715	0.9541	0.9492	0.9905	9
3	1.0562	1.0480	1.0613	1.0710	0.	0.	0.	0.	15
4	1.0623	1.0640	1.0275	1.0620	1.0440	1.0750	1.0840	1.0560	21
5	0.9874	0.9772	0.9685	0.9934	0.	0.	0.	0.	29
6	1.0010	0.9776	0.9972	0.9707	0.9741	1.0370	1.0120	0.9924	33
7	0.9704	0.9524	0.9600	0.9521	0.	0.	0.	0.	39
8	0.9336	0.9323	0.9324	0.9302	0.9199	0.9705	0.9809	0.9391	45
9	0.9070	0.9257	0.9158	0.8843	0.	0.	0.	0.	50
10	0.9294	0.9306	0.9076	0.9029	0.9094	0.9310	0.9772	0.9087	57
11	0.9233	0.9203	0.9275	0.9219	0.	0.	0.	0.	63
12	0.9280	0.9497	0.9435	0.9214	0.9101	0.9522	0.9672	0.9522	69
13	0.9431	0.9232	0.9179	0.9140	0.	0.	0.	0.	75
14	0.9210	0.9080	0.9366	0.9241	0.9220	0.9289	0.9414	0.9300	81
15	0.9855	0.9663	0.9873	0.9593	0.	0.	0.	0.	87
16	1.0206	1.0070	1.0144	0.9972	0.9800	1.0390	1.0190	1.0030	93
17	1.0337	1.0200	1.0366	1.0360	0.	0.	0.	0.	99
18	1.0480	1.0470	1.0355	1.0430	1.0380	1.0370	1.0570	1.0380	103
19	1.1390	1.1700	1.1779	1.1520	0.	0.	0.	0.	111
20	1.2290	1.2490	1.2490	1.2390	1.2950	1.2330	1.2050	1.2410	117
21	1.2739	1.3040	1.2892	1.2870	0.	0.	0.	0.	123
22	1.2331	1.2420	1.2356	1.2500	1.3520	1.1660	1.1370	1.3050	129
23	1.0643	1.0730	1.0922	1.1120	0.	0.	0.	0.	135
24	0.7254	0.7220	0.7295	0.7563	0.6849	0.6774	0.6698	0.6442	141

NODAL INTENSITIES

Node	A03	A23	A01	A22	A31	A43	Inches
1	0.	0.	0.	0.	0.	0.	4
2	910300.	913400.	952000.	872300.	939800.	968400.	9
3	0.	0.	0.	0.	0.	0.	15
4	997200.	1007000.	1035000.	996400.	993300.	1010000.	21
5	0.	0.	0.	0.	0.	0.	29
6	930500.	935500.	969400.	925500.	956400.	953100.	33
7	0.	0.	0.	0.	0.	0.	39
8	900800.	892300.	914200.	892900.	909800.	919200.	45
9	0.	0.	0.	0.	0.	0.	50
10	850400.	861500.	899000.	870900.	872000.	897700.	57
11	0.	0.	0.	0.	0.	0.	63
12	863900.	882600.	896300.	877100.	880800.	903900.	69
13	0.	0.	0.	0.	0.	0.	75
14	875900.	867900.	894300.	854000.	893100.	897600.	81
15	0.	0.	0.	0.	0.	0.	87
16	919900.	932400.	965800.	942500.	951900.	981400.	93
17	0.	0.	0.	0.	0.	0.	99
18	952500.	966600.	1004000.	947700.	976900.	988700.	103
19	0.	0.	0.	0.	0.	0.	111
20	1179000.	1146000.	1163000.	1105000.	1152000.	1181000.	117
21	0.	0.	0.	0.	0.	0.	123
22	1173000.	1162000.	1163000.	1047000.	1152000.	1142000.	129
23	0.	0.	0.	0.	0.	0.	135
24	723700.	710100.	630000.	617100.	615900.	627600.	141
Integral	945442.	945478.	965298.	918817.	949293.	964396.	

ASSEMBLY NORMALIZED NODAL INTENSITIES

Node	A03	A23	A01	A22	A31	A43	Inches
1	0.	0.	0.	0.	0.	0.	4
2	0.9686	0.9719	0.9946	0.9561	0.9986	1.0130	9
3	0.	0.	0.	0.	0.	0.	15
4	1.0610	1.0720	1.0810	1.0920	1.0550	1.0570	21
5	0.	0.	0.	0.	0.	0.	29
6	0.9901	0.9955	1.0130	1.0140	1.0160	0.9970	33
7	0.	0.	0.	0.	0.	0.	39
8	0.9586	0.9495	0.9551	0.9787	0.9667	0.9616	45
9	0.	0.	0.	0.	0.	0.	50
10	0.9049	0.9167	0.9392	0.9546	0.9265	0.9391	57
11	0.	0.	0.	0.	0.	0.	63
12	0.9193	0.9392	0.9363	0.9614	0.9359	0.9456	69
13	0.	0.	0.	0.	0.	0.	75
14	0.9321	0.9235	0.9343	0.9360	0.9489	0.9390	81
15	0.	0.	0.	0.	0.	0.	87
16	0.9789	0.9921	1.0090	1.0330	1.0110	1.0270	93
17	0.	0.	0.	0.	0.	0.	99
18	1.0140	1.0290	1.0490	1.0390	1.0380	1.0340	103
19	0.	0.	0.	0.	0.	0.	111
20	1.2550	1.2190	1.2150	1.2120	1.2240	1.2360	117
21	0.	0.	0.	0.	0.	0.	123
22	1.2480	1.2360	1.2150	1.1470	1.2240	1.1940	129
23	0.	0.	0.	0.	0.	0.	135
24	0.7701	0.7556	0.6582	0.6764	0.6544	0.6565	141